Synthesis and Characterization of Cation-Containing and Hydrogen Bonding Supramolecular Polymers

Shijing Cheng

Dissertation submitted to the faculty of the Virginia Polytechnic Institute and State University in partial fulfillment of the requirements for the degree of
Doctor of Philosophy
in
Chemistry

Timothy E. Long, Chair
Richey M. Davis
Robert B. Moore
Judy S. Riffle
S. Richard Turner

August 26, 2011
Blacksburg, Virginia

Keywords: phosphonium, ammonium, nucleobase, reversible addition-fragmentation chain transfer polymerization, nitroxide mediated polymerization, ionomers, hydrogen bonding, molecular recognition, non-covalent interactions, Michael addition, ionic liquids, polyacrylates

Synthesis and Characterization of Cation-Containing and Hydrogen Bonding Supramolecular Polymers

Shijing Cheng

Abstract

Non-covalent interactions including nucleobase hydrogen bonding and phosphonium/ammonium ionic aggregation were studied in block and random polymers synthesized using controlled radical polymerization techniques such as nitroxide mediated polymerization (NMP) and reversible addition-fragmentation chain transfer polymerization (RAFT). Non-covalent interactions were expected to increase the effective molecular weight of the polymeric precursors through intermolecular associations and to induce microphase separation. The influence of non-covalent association on the structure/property relationships of these materials were studied in terms of physical properties (tensile, DMA, rheology) as well as morphological studies (AFM, SAXS).

Ionic interactions, which possess stronger interaction energies than hydrogen bonds (~150 kJ/mol) were studied in the context of phosphonium-containing acrylate triblock (ABA) copolymers and random copolymers. Phosphonium-containing ionic liquid monomers with different alkyl substituent lengths and counterions enabled an investigation of the effects of ionic aggregation of phosphonium cations on the polymer physical properties. The polymerization of styrenic phosphonium-containing ionic liquid monomers using a difunctional alkoxyamine initiator, $DEPN_2$, afforded an ABA triblock copolymer with an *n*-butyl acrylate soft center block and symmetric phosphonium-containing external reinforcing blocks. Small-angle X-ray scattering (SAXS) and transmission electron microscopy (TEM) of triblock copolymers revealed pronounced

microphase separation at the nanoscale. Phosphonium aggregation governed block copolymer flow activation energies. In random copolymers, the phosphonium cations only weakly aggregated, which strongly depended on the length of alkyl substituents and the type of counterions. Acrylate random copolymers consisting of quaternary ammonium functionalities were synthesized using reversible addition-fragmentation chain transfer polymerization (RAFT). The obtained copolymers possessed controlled compositions and narrow molecular weight distributions with molecular weights ranging from M_n =50,000 to 170,000 g/mol. DMA evidenced the weak aggregation of ammonium cations in the solid state. Additionally, this ionomer was salt-responsive in NaCl aqueous solutions.

Hydrogen bonding, a dynamic interaction with intermediate enthalpies (10-40 kJ/mol) was introduced through complementary heterocyclic DNA nucleobases such as adenine, thymine and uracil. Our investigations in this field have focused on the use of DNA nucleobase pair interactions to control polymer self-assembly and rheological behavior. Novel acrylic adenine- and thymine-containing monomers were synthesized from aza-Michael addition reaction. The long alkyl spacers between nucleobase and polymer backbone afforded structural flexibility in self-assembly process. Adenine-containing polyacrylates exhibited unique morphologies due to adenine-adenine π-π interactions. The complementary hydrogen bonding of adenine and thymine resulted in disruption of adenine-adenine π-π interactions, leading to lower plateau modulus and lower softening temperatures. Moreover, hydrogen bonding interactions enabled the compatibilization of complementary hydrogen bonding guest molecules such as uracil phosphonium chloride.

Acknowledgements

First, I would like to thank my advisor, Prof. Timothy E. Long, for his tireless guidance and inspiration over the course of my graduate career. I am very fortunate to work under your supervision and I have learned a lot from you, not only polymer science, but also presentation skills, teaching, and most importantly, how to be a good researcher. I really appreciate all the opportunities that I have been given. Without your patience and guidance, this work is impossible.

I also I would also like to thank my committee members. I would like to express my special thanks to Prof. Robert B. Moore for his constant guidance and close research collaboration. He has been an insightful and helpful committee member and teacher during my graduate career. I would also like to thank Prof. S. Richard Turner for his helpful discussions and his very practical class on the transition to industry. I would like to thank Prof. Judy S. Riffle, for being a great teacher in both presentation skills and technical writing skills courses and Prof. Richey M. Davis, who was always willing to share his wisdom and technical expertise. I would also like to thank Prof. Garth L. Wilkes and Prof. Eugene Joseph for lots of helpful research discussions. I would like to thank Laurie Good, Valerie Owens, and Tammy Jo Hiner, who have truly been lifesavers. I would like to thank Vicki Long, who has helped me many times in both technical work and organizing travel.

I would like to thank ACS Petroleum Research Fund (PRF), which has provided funding for my research. I would also like to thank Kimberly Clark for supporting my research both financially and through collaborations. I would also like to thank Dr. Peter Eliker and Dr. Clay Bunyard with whom I spent an exciting summer at Kimberly Clark in Neenah, WI in 2010. The internship was an excellent opportunity to learn about the industrial side of polymer research. I would like to thank Dr. Rick Beyer at the Army Research Laboratories in Aberdeen, MD who has been an excellent collaborator and has always been willing to share his expertise in X-ray scattering analysis of polymers. The staffs at Virginia Tech have been a great resource. I would especially like to acknowledge Steve McCartney and John McIntosh for their help with AFM and TEM imaging. Geno, Hugo, and Sharelle have also been a great help.

I would also like to thank those that I worked with during undergraduate research. My first research experience was with Prof. Jian Xu and Prof. Shuguang Yang at the Institute of Chemistry the Chinese Academy of Sciences (ICCAS). I would also like to thank my undergraduate mentor Prof. Wenbing Hu at Nanjing University.

I would especially like to thank my research group including post-docs and graduates, whom I have enjoyed interacting with. You have been good friends and I really enjoyed the good times working together. Brian, Rebecca, Matthew Cashion, Matt Hunley, Tomonori, Sharlene, Gozde, Andy, Takeo, Emily, Akshay, Funda, Erin, Sean Ramerize, Daisuke, Philippe, Steve, Renlong, Tianyu, and Mana. I can't recall how many times I bothered you with writing and experimental issues. I really enjoy working with you. Matt G, Sean Hemp, Nancy, David, Ali, Eva, and Mike were fun people to interact with and always inspiring. I would like to especially thank Mingqiang for lots of research discussions and constant help. Lucy, Julie, Xu, Bin, Yanpeng, and Ming Ma also gave me lots of good suggestions. Wan and Xiaojun were the best roommates, who provided me with great support. Thank all my friends at Blacksburg. I look forward to my new adventure in Minnesota after graduation.

Finally, I would like to thank my family. Thanks dad and mom for constant support and encouragement during my entire graduate life and long absence from home. I would not be where I am today without them.
Lastly, but not the least, this work is also dedicated to the brilliant researchers in the field of polymer science, who explored me to the exciting world of sciences and technologies. This work is impossible without their invention, discovery and hard work.

Attribution

Several colleagues and coworkers aided in the writing and research behind several of the chapters of this dissertation. A brief description of their background and their contributions are included here.

Prof. Timothy E. Long - Ph.D. (Department of Chemistry, Virginia Tech) is the primary research advisor.

Prof. Robert B. Moore - Ph.D. (Department of Chemistry, Virginia Tech) conducted all SAXS and WAXD experiments in chapter 6.

Mingqiang Zhang - Ph.D. candidate (Department of Chemistry, Virginia Tech) conducted all SAXS and WAXD experiments in chapter 6.

Frederick L. Beyer - Ph.D. (Polymer Science and Engineering, University of Massachusetts in Amherst) is a researcher at the Army Research Laboratory in Abderdeen, MD. Rick contributed to this work by carrying out extensive SAXS analysis and through editing the chapters.

Clay Bunyard - Ph.D. (Polymer Science and Engineering, UNC) is a researcher at Kimberly-Clark Co. Clay contributed to chapter 5 through scientific discussions.

Steve McCartney - technician (Virginia Tech) aided in TEM and AFM experiments in chapter 6 and 7.

John McIntosh - technician (Virginia Tech) aided in TEM and AFM experiments in chapter 6 and 7.

Tianyu Wu - Ph.D. candidate (Department of Chemistry, Virginia Tech), conducted all SEC analysis.

Gozde Ozturk - Ph.D. (Department of Chemistry, Virginia Tech), aided peel test.

Brian D. Mather - Ph.D. (Department of Chemistry, Virginia Tech), mentored nitroxide mediated polymerization technique.

Ninad Dixit - MS (Department of Chemistry, Virginia Tech), conducted IR measurement in chapter 6.

Sean T. Hemp - Ph.D. candidate (Department of Chemistry, Virginia Tech), conducted anion exchange reactions in chapter 4.

Table of Contents

List of Figures

List of Schemes

List of Tables

Chapter 1: Introduction

Non-covalent interactions including nucleobase hydrogen bonding and ionic interaction were studied in block and random copolymers synthesized using controlled radical polymerization techniques such as nitroxide mediated polymerization and reversible addition-fragmentation chain transfer polymerization. Non-covalent interactions were expected to increase the effective molecular weight of the polymeric precursors through intermolecular associations and to enhance microphase separation. The influence of non-covalent association on the structure/property relationships of these polymers were studied in terms of physical properties (tensile, DSC, DMA, and rheology) as well as morphological studies (AFM, TEM, SAXS, WAXD).

Phosphonium ion-containing acrylate triblock (ABA) copolymers were synthesized using nitroxide mediated radical polymerization. The polymerization of styrenic phosphonium-containing ionic liquid monomers using a difunctional alkoxyamine initiator, $DEPN_2$, afforded an ABA triblock copolymer with an *n*-butyl acrylate soft center block (DP~400) and symmetric phosphonium-containing external reinforcing blocks (DP<30). Two phosphonium monomers with different alkyl substituent lengths enabled an investigation of the effects of ionic aggregation of phosphonium cations on the physical properties of ABA block copolymer ionomers. Shortening the alkyl substituents on the phosphonium cation enhanced the hydrophilicity of tributyl-4-vinylbenzyl phosphonium chloride (BPCl) relative to trioctyl-4-vinylbenzyl phosphonium chloride (OPCl). In both cases, phosphonium cations promoted microphase-separation and thermoplastic elastomer performance for the OPCl- and BPCl-containing triblock copolymers compared to a less well-defined, microphase

segregated morphology for the styrene analog. The solid state morphologies of the block copolymers were studied using small-angle X-ray scattering (SAXS) and transmission electron microscopy (TEM), and both techniques revealed phase separation at the nanoscale. DMA studies indicated that phosphonium aggregation governed flow activation energies.

Phosphonium functionalities can be reversibly attached to polyacrylates through complementary hydrogen bonding. Hydrogen bonding, a dynamic interaction with intermediate enthalpies (10-40 kJ/mol) was introduced through complementary heterocyclic DNA nucleobases such as adenine, thymine, uracil, and cytosine. Novel adenine- and thymine-functionalized acrylate monomers were synthesized using aza-Michael addition and randomly copolymerized with *n*-butyl acrylate. At a content of 7 mol%, adenine-functionalized polyacrylates self assembled into needle-like nanostructures as shown under atomic force microscopy (AFM), small-angle X-ray scattering (SAXS), and wide-angle X-ray diffraction (WAXD); but thymine-functionalized polyacrylates did not microphase separate even at a level of 30 mol%. When mixed together, the complementary hydrogen bonds of adenine and thymine base pairs drove the random copolymers fused into thermodynamically stable hydrogen bonding polymer complex. The polymer complex exhibited higher glass transition temperature and enhanced melt viscosity than the precursors based on the results of DSC and rheological studies. The hydrogen bonding content, stacking capability, and hydrogen bonding strength were the parameters that principally influence self-assembly. Additionally, the nucleobase-functionalized polyacrylates exhibited stronger adhesive and cohesive strength in comparison to the electrostatic polymer analogues.

Chapter 2: Recent Advances in the Synthesis and Structure-Property Relationships of Self-Healing Polymers

2.1. Introduction-Scientific Rationale and Potential Impact

Polymers are susceptible to damage from external factors, which can lead to microscopic crack formation, propagation of the crack, and failure of the material. Therefore, the inherent ability of polymers to recover their strength after damage and extend their service lifetime is especially attractive for conservation reasons, because materials will not require replacement after damage or wear.

Different strategies and approaches to devise self-healing materials have been intensely investigated over the last 10 years, accompanied with a significant increase in the number of scientific publications[1-5] (from < 5 in 2000 to 162 in 2010). As a result of the multitude of different approaches used and materials studied, self-healing materials can be divided into two different classes depending on the chemical nature of the self-healing process: covalent interactions and non-covalent interactions. Self-healing based on covalent interactions requires carbon-carbon bond formation, whereas self-healing driven by non-covalent interactions requires heat or light to stimulate polymer viscoelastic response.

2.2. Self-Healing Technologies

2.2.1 Self-Healing Based on Covalent Interaction

2.2.1.1 Automatic Healing Driven by Healing Monomers

Many species in nature have the ability to self-heal and self-repair upon injury. The

efficiency of wound repair in biological systems is facilitated with the circulatory system, which can carry vital reagents throughout the organism. Relying on this extensive transport network, the system recovers itself essentially anywhere, and the repair is repeatable.

Inspired from this, in 1993, Dry and Sottos et al. first developed a biomimetic approach to perform self-repair on a fiber-reinforced epoxy resin through a bleeding action of filled hollow fibers.[6-8] Hollow fibers containing healing monomers were dispersed in the polymer matrix. Controlled tensile or flexural loading broke the hollow fibers to release repair chemicals that reacted with the damaged surface. After sealing the cracked matrix, material restored the strength in damaged areas. This approach to self-heal requires a load to release the repairing chemical, suggesting a passive self-healing process. In 2001, White and Sottos et al. discovered automatic healing through incorporating microcapsules to epoxy resin.[9-11] Catalysts and microcapsulated monomers (dicyclopentadiene) were dispersed throughout epoxy. When a crack formed, the propagation of the crack ruptured the microcapsules and through capillary action drew them into the crack plane, where released monomers were polymerized through ring-opening polymerization (ROMP) in contact with the catalysts to fill the crack (Figure 1). Healing occurred at room temperature and yielded a tough and highly crosslinked polymer network. The fractured matrix recovered over 90% of its original fracture toughness. The damage-induced triggering mechanism provided site-specific automatic control of repair. Computational simulation on microcapsule motion showed that the high

strength of the capsule-surface adhesive and low particle release rate are required to obtain optimal surface coverage and repair of the crack.[12] Additionally, the size of capsules[13] and catalyst concentration[14] influenced the sensibility of microcapsules to damage.

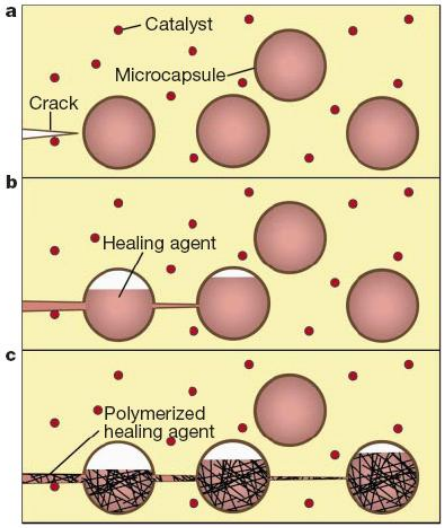

Figure 2.1. Automatic healing concept.

Besides microcapsules, nanoparticles[15] and single walled carbon nanotubes (SWCNTs) were also used as nanoreservoirs for healing agents where the catalytic trigger molecules are either wrapped around or dispersed in the matrix (Figure 2). The advantage of using the SWCNTs in comparison to nanocapsules is that they also bring an additional mechanical strength to the material. However, there are several factors, such as SWCNTs diameter, length, orientation, dispersion, and loading density in the matrix which limits the amount of healing agent that can be stored in SWCNTs.

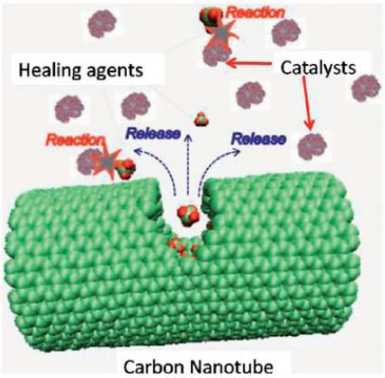

Figure 2.2. Molecular model of carbon nanotube and organic molecules for self-healing.

Beside ROMP, atom transfer radical polymerization (ATRP)[16] and condensation of isocyanates[17] also meet automatic healing requirements on long shelf life and rapid polymerization at ambient conditions. White et al. recently investigated the feasibility of using non-covalent adhesion to improve the healing performance of ROMP based systems.[18] They synthesized a comonomer capable of hydrogen bonding to the matrix, which improved the adhesion at interface and hence the healing efficiency.

For covalent approaches, the bulk material contains functionalities which react together to form new covalent bonds and thereby bridge a damaged zone. The new crosslinks are as thermodynamically stable as the covalent bonds present in the bulk material from which they originate, but the chemical composition of the healed zone may be distinct from that found in the bulk material. Overall, the limited ability of the material to self-heal multiple times is an unavoidable drawback.

2.2.1.2 Self-healing Driven by Reversible Reactions

Another covalent self-healing method is based on dynamic covalent chemistry,[19-20] which offers an appealing prospect of constructing healable materials through the

thermodynamic controlled reactions involving reversible covalent bonds. Recent covalent polymers investigated for their reversible properties are based on various reactions, such as Diels-Alder reaction,[21-25] photodimerization,[26-28] radical reaction,[29-30] and boronate ester formation.[31] The reversible covalent bonds offer the dynamic features of a supramolecular polymeric system as opposed to the much weaker non-covalent bonds used in the supramolecular systems.

The DA reaction for crosslinking linear polymers was studied over the past two decades.[32-33] Researchers used side-chain intermolecular DA reactions to generate thermo-reversible networks, which were gel-like[34], elastomeric[21] or thermoset.[35] These thermo-reversible networks are ideal for polymer recycling.[21] Wudl and coworkers extended the application of the thermo-reversible networks to the field of self-healing.[36-37] They preformed the DA reaction on two types of multifunctional monomers and successfully formed a macromolecular network (Scheme 1). When a film sample was cut into two pieces and the cut surfaces were kept in contact with each other at 120 ^{o}C, the cut pieces rejoined. The reversible crosslinking reaction bridged the cut surfaces. Compact tension tests and fracture tests showed 50% to 80% recovery of the original fracture load after repeated mending. Yoshie et al. reported the self-healing of furyl-telechelic poly(ethylene adipate) crosslinked with a tris-maleimide through a DA reaction and proposed the following healing mechanism (Figure 3).[38] The "weak" DA adducts are sacrificially dissociated to release the stress in order to protect the prepolymers and linkers from the scission or degradation. Since the DA reaction is an equilibrium reaction,

the dissociation and addition of furan and maleimide groups continually occur to mend the material. Additionally, the mending is additionally driven through chemical exchange between furan and maleimide groups as well as the entanglement of dangling chains at the cut surfaces.

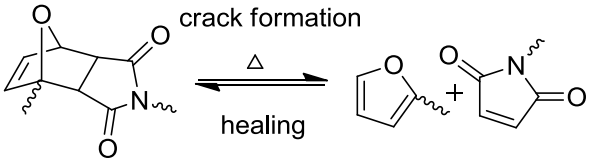

Scheme 2.1. Thermally reversible DA cycloaddition of a multi-diene and multi-dienophile

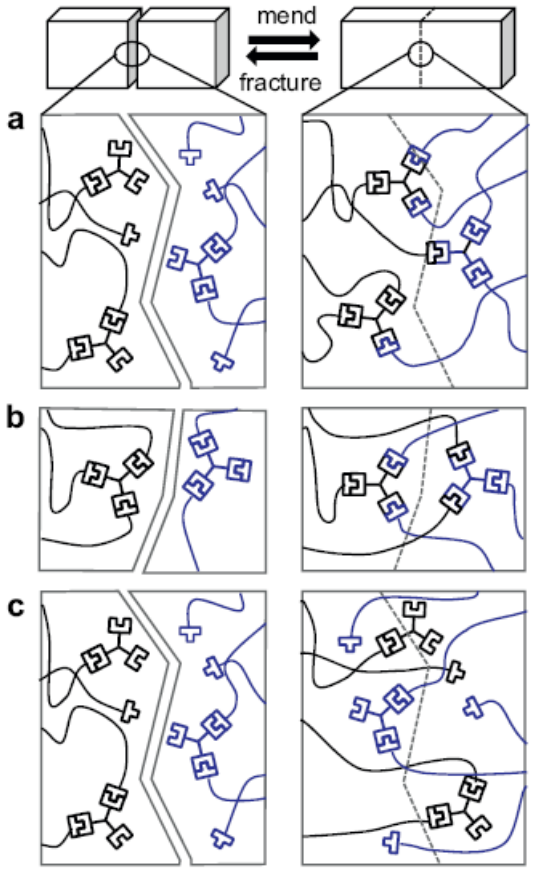

Figure 2.3. Schematic representation of the possible mending mechanism. Mending promoted by (a) sacrificed dissociation of DA adducts, (b) exchanging furan (maleimide)

groups between DA adducts, and (c) chain entanglement.

In addition to thermal reversible DA reaction, reversible [2+2] cycloaddition was also applied for self-healing application.[26-28] External stress ring-opened the highly strained cyclobutanediyl crosslinks (strain energy of 26.4 kcal mol/1), resulting in the corresponding cinnamoyl precursor. Irradiation of the damaged material with UV light promoted the [2+2] cycloaddition reaction to reheal (Scheme 2).

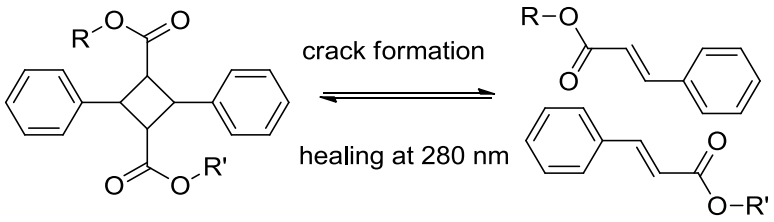

Scheme 2.2. Photo-reversible network formed with the reversible [2+2] cycloaddition

It is well known that disulfide bridges can be ruptured to form two thiol groups upon reduction. Thus, a variety of polymers can be reversibly crosslinked using this system under redox conditions. Chujo et al. first applied the thiol groups for reversible crosslinking application.[39] In their report, a redox-reversible hydrogel system based on thiol-modified poly(N-acetylethyleneimine) was designed, exploiting the reversible interconversion between disulfide (SS) groups and thiols (SH). The introduction of exchangeable disulfide groups in the network leads to renewal of crosslinks across the damaged surfaces. Takata and coworkers introduced thiol-disulfide bridges to a polyrotaxane network.[40] Two or three coupled crown ether rings were assembled with a disulfide-bridged ammonium salt threads which were easily cleaved in the presence of an appropriate thiol at 60 ^{o}C, enabling the recycling of the polymeric material. Tsarevsky

and Matyjaszewsky employed atom transfer radical polymerization (ATRP) in the preparation of well defined polystyrene ‘‘blocks’’, bridged with disulfide bonds (Scheme 3).[41] The reaction of internal disulfide bond with dithiothreitol yielded the corresponding thiol end groups, which could be efficiently coupled back to the starting disulfide through oxidation with $FeCl_3$. Furthermore, trithiocarbonate (TTC), the chain transfer agent in RAFT polymerization also demonstrated the ability to undergo photo-stimulated reshuffling reactions. Recently, Matyjaszewski et al. reported the use of dimethacrylate trithiocarbonate as a dynamic covalent crosslinker to prepare PMMA and PS gels and crosslink poly(*n*-butyl acrylate) which underwent self-repair based on reshuffling reactions (Scheme 4).[42] Bowman and coworkers utilized that photoinduced reversible chain rearrangements of allyl sulfide groups (Scheme 5) to release accumulated stress in a crosslinked elastomer at room temperature.[43]

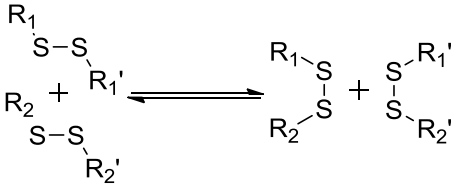

Scheme 2.3. Disulfide interchange reaction

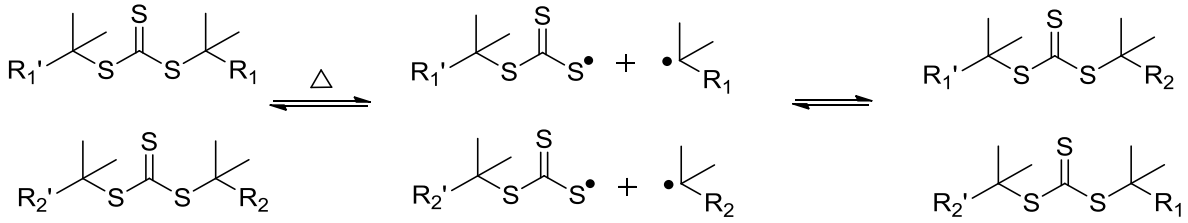

Scheme 2.4. TTC reshuffling reactions

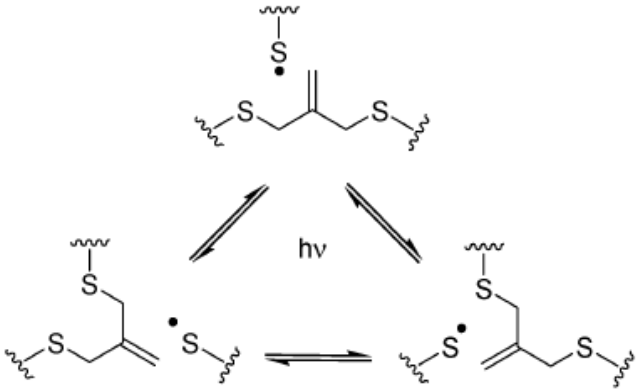

Scheme 2.5. Mechanism for photo-activated reversible formation of allyl sulfide bonds

Stable organic radicals similar to the thiol-based systems have received considerable attention over the past few years.[44-45] The C-O bond reforms quite easily upon cleavage and thus in principle, this process can be used to effectively mend cracks in polymers. Alkoxyamines used in nitroxide mediated polymerization also enabled the dynamic crosslinking through the radical exchange reactions.[29] Otsuka et al. introduced thermally reversible alkoxyamine units in the polymer main chain.[46] The exchange reaction between the derivatives occurred above 60 ^{o}C. Radical copolymerization of alkoxyamine functionalized monomers formed side-chain crosslinked polymer networks (Scheme 6).[30, 47] The crosslinks were cleaved upon heating the crosslinked polymer in the presence of an excess amount of alkoxyamine.

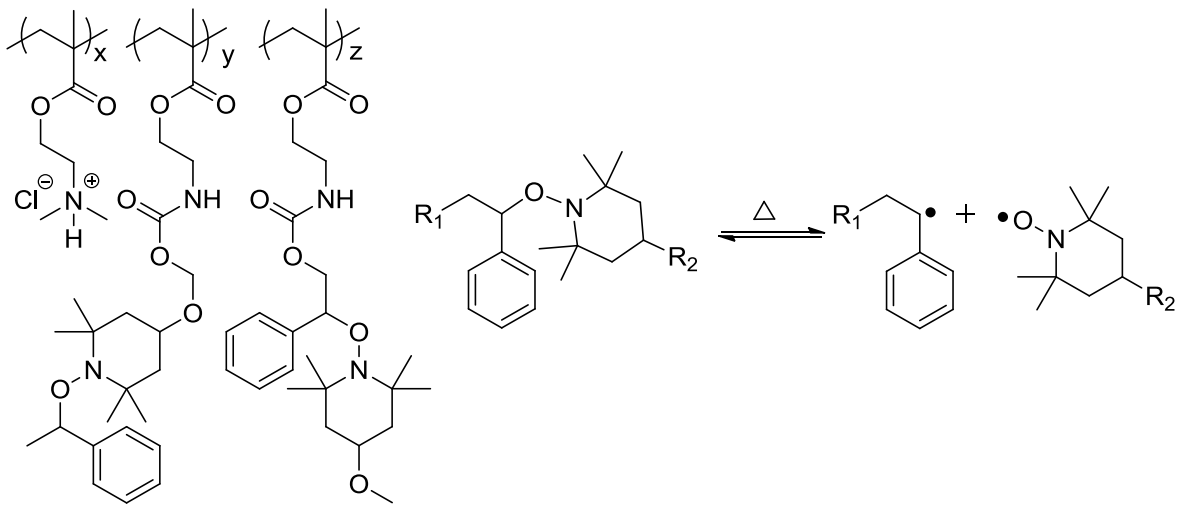

Scheme 2.6. Crosslinking and de-crosslinking reactions of water-soluble dynamic covalent polymers through radical exchange reaction of alkoxyamines

Among the known reversible covalent reactions, amino-carbonyl condensations, which yield C=N products, such as imines, hydrazones, and oximes, are particularly attractive. Acylhydrazone bonds are covalent in nature, and the acylhydrazone formation displays reversibility under mild conditions in the presence of acid catalysis. Lehn and coworkers successfully prepared the dynamic covalent polyacylhydrazones.[48-49] Recently Deng and Chen et al. reported a strategy of constructing healable chemical gels based on reversible condensation of acylhydrazine-telechelic poly(ethylene oxide) (PEO) with aldehyde groups (Scheme 7).[50] Upon adjusting the acidity of the system, this chemical gel exhibited reversible sol-gel phase transitions and self-healing properties.

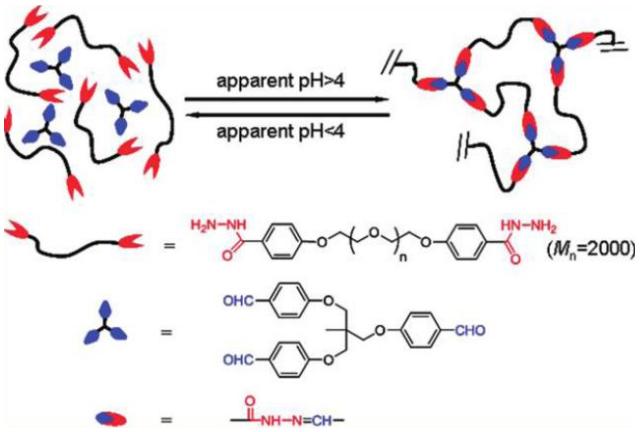

Scheme 2.7. Construction of covalent crosslinked polymer gel based on reversible condensation of dihydrazide with a trialdehyde

Boronate ester formation provides another covalent alternative that can be synthesized and repaired under mild conditions without the need for additives. Poly(dioxaborolane)s degrade upon exposure to water and repair upon removal of the solvent under reduced pressure.[31] However, the moisture is usually present in the air; the moisture-sensitivity makes the polymer undesirable for many commercial applications.

In general, the healing behavior of a structurally dynamic polymer depends on the nature of the dynamic bonds. The thermodynamic parameter, such as the equilibrium/association constant (K) describes the relative stability of the resulting dynamic bonds, which plays an integral role in healing efficiency, since the bond dissociation also results in crack propagation. The kinetic parameters describe the formation or dissociation rate of the dynamic bonds, which determine the healing speed. The self-healing of reversible covalent polymers is stimulated with temperature, pH, light, and redox reaction. Among all, photo-stimulation is a relatively powerful technique

because the stimulation can occur at room temperature, it is easy to handle, and exposure can be limited to targeted areas. Additionally, due to the stronger nature of the reversible covalent bonds, the products are relatively more stable than supramolecular self-healings.[48, 51] The combination of the unique self-healing properties and applicability for a large variety of polymers makes this approach ideal for applications such as coatings.[52]

2.2.2 Self-Healing based on Non-Covalent Interactions

Covalent bonds (~360 kJ/mol)[53] require a large amount of energy (heat or light) to break and reform, which is a major drawback for covalent self-healing mechanisms. Non-covalent bonds use molecules and ions to form assemblies with low kinetic stability and reversible association. The healing of elastomers or thermosets through non-covalent interactions has been reported extensively in the literature.[54-55] The most conventional healing methodology is based on hot-plate welding and solvent softening of polymer chains at fracture interfaces.[56] The dynamic nature of non-covalent interactions endows polymers with improved properties such as tailored thermal, mechanical,[57-59] and stimuli responsive properties.[60-62] Over the past decade, reversible self-healing materials based on non-covalent interactions such as electrostatic interactions,[62-63] hydrogen bonding,[57] and metal-ligand coordination[64-65] have been designed successfully.

2.2.2.1 Self-Healing Hydrogels based on Reversible Solid-Gel Transition

The supramolecular networks based on non-covalent interactions in physical gels are able to perform a sol-gel transition in response to temperature, pH and solvent. Copolypeptide hydrogels[66] are early examples of self-healing hydrogels, but they are

mechanically weak (G' <1 KPa) and require long time to recover. A recent report of a hydrogel prepared from a mixture of water, clay, dendritic macromolecule, and sodium polyacrylate revealed better mechanical strength and a fast-recovery capability.[67]

2.2.2.2 Self-Healing of Ion-Containing Polymers

Ionomers are macromolecules that contain less than 15 mol% of ionic groups.[68-69] The ionic interaction within one ion pair is approximately 100 kJ/mol; the forces are reduced considerably less in further aggregation between ion pairs (dipole-dipole interactions), but remain in 0.5-2 kJ/mol.[70-71] The incompatibility between ions and organic polymer backbones drives the ions together and separates them from the polymer backbones causing ionic aggregation. Eisenberg, Hird, and Moore proposed a model describing the structure of ionic aggregates (Figure 4).[72-73] The small, tightly bonded, isolated groups are called multiplets with a diameter of 5-10 Å containing a few ions or ion pairs. Multiplets act as moderately strong and temporary ionic crosslinks and restrict the mobility of surrounding hydrocarbon polymer chains. As the ion content increases, the region of restricted mobility surrounding each multiplet overlaps into continuous phases known as clusters. The structure of ionic aggregates in ionomers was evidenced from small-angle X-ray scattering (SAXS) studies. Ionomers give rise to characteristic SAXS peaks that are attributed to low-level ion aggregations within the non-polar, low-dielectric-constant polymer matrix. Ionic aggregates provide unique properties such as improved tensile strength,[74] impact resistance,[75] and optical properties.[76] The application of ionomers in self-healing materials has only recently been explored. Ionomers used for

self-healing purposes are generally copolymers of ethylene and methacrylic acid (EMAA) neutralized to their respective sodium salt form, known as Surlyn® and React-A-Seal®. Surlyn® recovers into its original shape following a high impact puncture at velocities ranging from 300 to 1200 ft/s (Figure 4).[62-63]

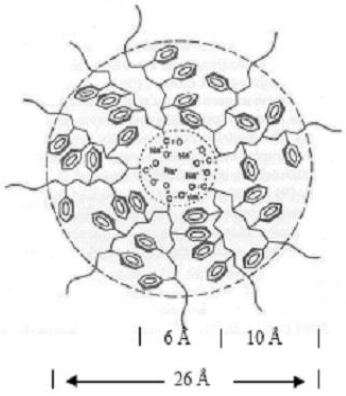

Figure 2.4. A multiplet in poly(styrene-co-methacrylate) ionomer neutralized with NaOH.

Surlyn® is a semicrystalline polymer, produced from the free radical copolymerization of ethylene and methacrylic acid under high pressure similar to the production of low density polyethylene. It is now believed Surlyn® heals through a viscoelastic healing process.[77] Upon puncture, corrosion-generated heat passed around the broken area and melted the crystallites. The ionic clusters disordered but persisted, and provided the molten polymer with sufficient strength to bounce back. Then, polymer chains interdiffused together to completely reseal or heal the cavity (Figure 5). The surrounding polymers remained at around room temperature and provided a stable framework or "anchor" for the elastomeric material to "pull against". Unlike many of the systems already discussed, the viscoelastic healing process arises from the inherent

chemical structure and morphology of the ionomer and the process can in principle be repeated many times.

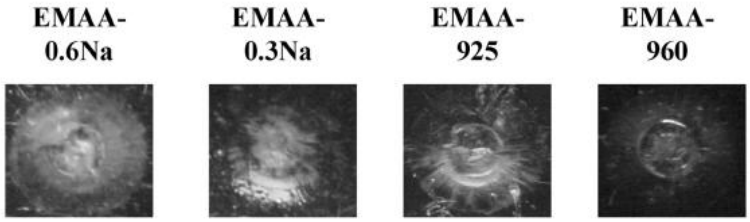

Figure 2.5. Films following puncture of the four EMAA materials at room temperature.

2.2.2.3 Self-Healing of Multiple Hydrogen Bonding Polymers

Self-healing hydrogen bonding polymers such as Nucrel®, the fully acidic form of Surlyn®, are also commercially available, in which the carboxylic acid groups weakly aggregated through hydrogen bonds. Pellethane® 2102-65D, a polyurethane thermoplastic elastomer, was able to self heal as well.[78] Although it was crosslinked through urethane hydrogen-bonded hard segments (in contrast to Surlyn®'s crystallites and ion clusters), the mechanical properties and the ability to heal the impression and ballistic impacts were similar to Surlyn®.

Relative to ionic interaction, hydrogen bonding is weak with a bond energy of 10-80 kJ/mol.[79] Hydrogen bonds that naturally occur in polypeptides and nucleic acids determine the three-dimensional folding of biological macromolecules due to their specificity and directionality. Lehn and coworkers exploited hydrogen bonds as the driving force for polymer assembly.[80] In 1997, Meijer and Sijbesma et al. used a quadruple hydrogen-bonded, self-complementary unit (2-ureido-4-pyrimidone, UPy) in chain extension of telechelic oligodimethylsiloxane (Figure 5).[81] UPy end groups

dimerized (K_a>6×10^7 M^{-1}in $CHCl_3$)[82-83] through the self-complementary donor-donor-acceptor-acceptor (DDAA) hydrogen bonding array which led to a high degree of polymerization. Monomers containing two and three binding sites formed linear and crosslinked polymers, respectively. Heat readily disrupted hydrogen bonding and therefore the bulk viscosity of the supramolecular polymers was low at high temperature. As a result, these polymeric systems can undergo thermal mending. SupraB®, an UPy-functional polysiloxane, repaired itself rapidly at 140 °C and restored the smooth coating existing at room temperature. The UPy based materials represent the first example of a truly reversible supramolecular polymer network that can be easily synthesized from commercially available starting materials, where the UPy dimerization is strong enough to construct supramolecular materials possessing acceptable mechanical properties. Similarly, Chino et al. used amide trazole-caroxylic acid units to vulcanize polyisoprene.[84] The thermoreversibly crosslinked network had similar mechanical properties to chemically vulcanized rubber and the rubber reformation could be repeated more than 10 times without changing its various properties, suggesting a practical application in recycling. Interest from industry in this reversible polymeric system also includes the non-linear concentration dependence of melt viscosity. The incorporation of even a small amount of UPy in existing plastics dramatically simplifies the processing of the material.[85]

Besides UPy, researchers also looked into other self- or hetero-complementary multiple hydrogen bonding units which strongly dimerize to build supramolecular

polymers or polymer networks, such as nucleobases (adenine, thymine, cytosine, guanine),[86-88] diamidopyridine,[89] ureidoguanosine,[90] and diamidonaphthyridine[91] building blocks. The degree of polymerization depends on the bond strength, concentration, and the stoichiometry of the building blocks in the mixture. These hydrogen bonding building blocks can be incorporated into a polymer chain using various techniques, such as functional initiators[92] or monomers,[61, 93-94] and post-polymerization modifications.[81, 95-96]

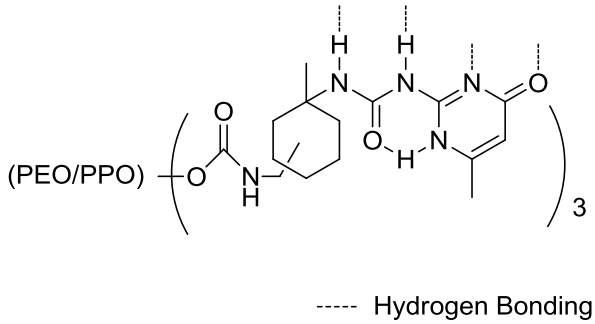

Scheme 2.8. UPy trifunctional copolymers forming thermally reversible polymer networks

Another approach has been demonstrated by Leibler et al. using a variety of hydrogen bonding units to construct self-healing elastomers without applying heat or catalyst.[97] They avoided the usage of two or three identical molecules that assemble into a rigid supramolecular network, and instead employed a mixture of randomly branched oligomers based on dimers and trimers of fatty acids from bio-renewable resources. The polymers equipped with a variety of hydrogen bonding groups, such as amides, 1,3-dialkyl-ureas, 1,1- dialkyl-ureas, and imidazolidones which strongly associated with each other. When the polymer was broken or cut, it was simply repaired at ambient temperature through bringing the fractured ends together to self-heal autonomously

(Figure 6). This process was reproducible and the healed materials showed reasonably conserved mechanical properties after several repetitions. The second-generation supramolecular polymer network showed essentially instant and quantitative recovery of tensile modulus at 80 ^{o}C. However, it is crucial to bring the ends of the material together as quick as possible to obtain sufficient self-healing as the hydrogen bonding units may react with the closest ones in their section.

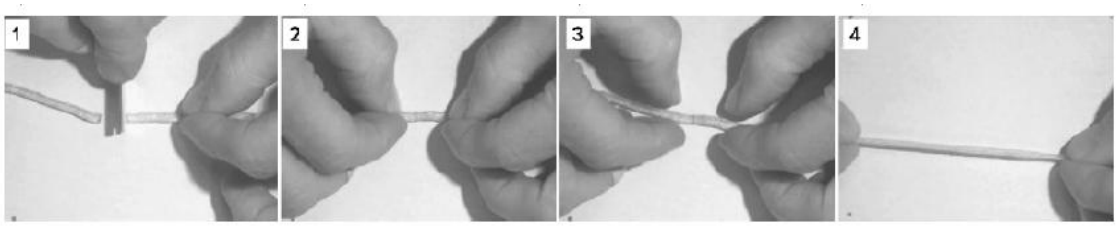

Figure 2.6. Self-healing supramolecular rubber: a) cutting, b) mending, c) healing, and d) stretching.

2.2.2.4 Self-Healing of π-π Stacked Polymers

π-π Stacking, another non-covalent interaction, has been used in the synthesis of self-healing smart materials. Colquhoun and Hayes et al. reported a series of novel, rehealable, non-covalent networks based on complementary aromatic π-π stacking interactions (Figure 7).[98] The first system of this type consisted of a low molecular weight polyimide containing multiple π-electron deficient receptor sites. This polyimide proved capable of chain-folding around the π-electron rich pyrenyl chain ends of a telechelic polysiloxane to form a complementary, π-π stacked, non-covalent polymer complex. The polymer network demonstrated rapid re-healing at temperatures higher than 90 ^{o}C. It was proposed that the healing process of this supramolecular network was

initiated from partial dissociation of the complementary π-π stacking interactions as the temperature increased. The melt viscosity exhibited strong temperature dependence similar to hydrogen bonded systems. On cooling, the non-covalent π-π stacking interactions were progressively reestablished, regenerating the pristine structures. A second-generation healable supramolecular network featured different polymer backbones, including a double pyrenyl end-capped polyamide and a chain-folding co-polyimide which exploited the same supramolecular π-π stacking motif.[99] The healable supramolecular network was found to fully regain its tensile modulus (ca. 1 MPa) over three cycles of breaking and healing. Unlike the healable hydrogen bonding elastomer reported by Leibler et al.,[97] separation of the fractured parts for up to 24 hours did not result in any loss of healing efficiency.

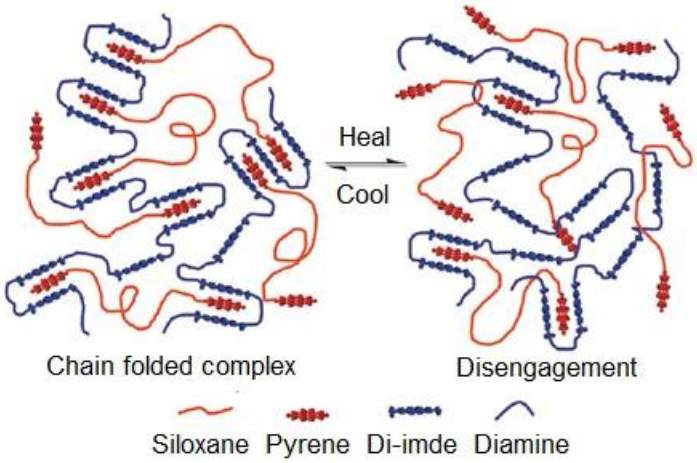

Figure 2.7. The proposed self-healing mechanism for the polymer blend comprising a chain-folding polydiimide and bis-pyrenyl end-capped polysiloxane.

2.2.2.5 Self-Healing of Metal-Coordinated Polymers

Another way to form supramolecular polymers is to exploit metal-ligand coordination to introduce polymer assembly.[64-65] Rowan and coworkers prepared gel-like, elastomeric metallo-supramolecular polymers from a monomer unit which consisted of a 2,6-bis-(benzimidazolyl)-4-hydroxypyridine unit attached to either end of a polyether chain, mixed with a transition metal ion (e.g., Co(II) or Zn(II)) and a small percentage of a lanthanoid metal (e.g., La(III), Eu(III)).[64] Such materials show dramatic reversible responses to a variety of stimuli, including heat, force, chemicals, and light. Varghese et al. showed that the amino acid based hydrogel possessing flexible hydrophobic side chains and terminal carboxyl groups underwent healing at ambient temperature mediated with transition-metal ions.[100] Healing occurred through the formation of coordination complexes that were much stronger than other non-covalent interactions such as chain entanglements and hydrogen bonding. Holten et al. developed a catechol-Fe^{3+} crosslinked polymer gel, which exhibited pH-responsiveness similar to the native mussel thread cuticle. The gels displayed elastic moduli (G′) that approached covalently crosslinked gels as well as self-healing properties.[101]

2.2.2.6 Role of Rheology in Design of Self-Healing Supramolecular Polymers

Polymer viscoelastic properties are crucial for self-healing processes, especially for supramolecular polymer system. Rheological measurement performed on the self-healing ionomer, Surlyn®, showed as the temperature increased from 90 ºC to 150 ºC, the

viscosity of the ionomers decreased by up to two orders of magnitude, indicating a strong temperature dependence of viscosity. However, the ionic aggregates persisted in the melt polymer, enabling the rapid polymer recrystallization after bullet penetration. Varley and van der Zwaag compared the self-healing behavior of Surlyn® with polyethylene and polypropylene, the non-ionic polymer analogues.[102-103] Although the non-ionic analogues exhibited higher levels of viscous healing (chain diffusion), they had negligible elastic rebound, and therefore displayed little capacity to self heal at similar temperatures. Therefore, it is important to recognize that the hole-closure arise from the elastic response.

The hydrogen bonding supramolecular polymers also exhibited a strong temperature and concentration dependence of viscosity.[81] The hydrogen bonding self-healing rubbers described by Leibler et al. possessed a room-temperature T_g and achieved flow above 180 ^oC.[104] The relaxation time, extrapolated from the time-temperature superposition was actually quite large ($>3\times10^6$ s, a few weeks, at 50 ^oC). The slow relaxation process possibly arises from the nature of hydrogen bond, which is directional and produces interatomic distances shorter than the sum of van der Waals radii, and usually involves a limited number of bonding partners. Therefore, the bonding pair will break and reform many times before finally separating, leading to an overall bond lifetime greater than the bare bond lifetime. It was reported that the lifetime of the UPy dimers increased from 170 ms in $CDCl_3$ to 1.7 s in toluene-d_8, a more nonpolar solvent.[83] Therefore, some of the

strong complementary hydrogen bonding motifs might remain associated in nonpolar polymer matrix even at elevated temperature.[105]

2.2.3 Evaluation of Self-Healing Efficiency

Microscopy such as optical microscopy[106] and scanning electron microscopy (SEM)[10] is the most common method for visualizing effective healing. Spectroscopy such as infrared[97] and ultra-violet spectra[107] has been used for imaging the bond dissociation/reformation during healing process as well. Pang and Bond utilized an ultra-violet mapping technique (UVMT) to observe the damage and healing of microcapsule-embedded polymer composites through incorporating a UV fluorescent dye into the healing chemicals.[107] As the healing chemicals transmitted to the cracks, damage was successfully highlighted under UV.

White et al. proposed the protocol to evaluate self-healing ability using fracture toughness.[10, 108] A natural precrack on the specimen was created upon inserting a fresh razor blade and gently tapping into the molded notch starter. Subsequently, the specimen was pin-loaded and tested to failure, while compliance and peak load were determined to estimate the virgin fracture toughness. Load was then removed, allowing the crack faces to come back into contact and to be self-healed at certain time and temperature. Finally, the healed specimens were tested again following the above procedure. Efficiency of healing was defined as the ratio of fracture toughness of healed and virgin materials.

2.3. Conclusions and Future Outlook

This literature review discussed two types of polymer self-healing mechanisms: covalent and non-covalent interactions. In comparison to the covalent bonds, the bond strength of non-covalent interactions is relatively low. Polymers containing hydrogen bonding and ionic functionalities are dynamic in nature and have unique thermal and rheological properties which lead to the potential application as multi-responsive self-healing materials which self-heal under different stimuli.

2.4 References

1. Bergman, S. D.; Wudl, F. *J. Mater. Chem.* **2008,** 18, (1), 41-62.
2. Mauldin, T. C.; Kessler, M. R. *Int. Mater. Rev.* **2010,** 55, (6), 317-346.
3. Wool, R. P. *Soft Matter* **2008,** 4, (3), 400-418.
4. Syrett, J. A.; Becer, C. R.; Haddleton, D. M. *Polym. Chem.* **2010,** 1, (7), 978-987.
5. Burattini, S.; Greenland, B. W.; Chappell, D.; Colquhoun, H. M.; Hayes, W. *Chem. Soc. Rev.* **2010,** 39, (6), 1973-1985.
6. Dry, C. *Composites Structures* **1996,** 35, 263-269.
7. Dry, C., Sottos, N.R. *In Smart Structures and Materials 1995: Smart Materials, Proc. SPIE* **1993,** 1916, 438-441.
8. Dry, C. *Proc. SPIE- Int Soc Opt Eng* **1994**, (2189), 62.
9. Brown, E. N.; White, S. R.; Sottos, N. R. *J. Mater. Sci.* **2004,** 39, (5), 1703-1710.
10. White, S. R.; Sottos, N. R.; Geubelle, P. H.; Moore, J. S.; Kessler, M. R.; Sriram, S. R.; Brown, E. N.; Viswanathan, S. *Nature* **2001,** 409, (6822), 794-797.
11. Cho, S. H.; Andersson, H. M.; White, S. R.; Sottos, N. R.; Braun, P. V. *Adv. Mater.* **2006,** 18, (8), 997-1000.
12. Verberg, R., et al. *J. R. Soc. Interface* **2007,** 4, 349.
13. Kessler, M. R.; Sottos, N. R.; White, S. R. *Composites A* **2003,** 34, (8), :743–53.
14. Brown, E. N.; Kessler, M. R.; Sottos, N. R.; White, S. R. *J Microencapsul* **2003,** 20, (6), 719–30.

15. Gupta, S.; Zhang, Q.; Emrick, T.; Balazs, A. C.; Russell, T. P. *Nat. Mater.* **2006,** 5, (3), 229-233.
16. Wang, H. P.; Yuan, Y. C.; Rong, M. Z.; Zhang, M. Q. *Macromolecules* **2010,** 43, (2), 595-598.
17. Wilson, G. O.; Caruso, M. M.; Schelkopf, S. R.; Sottos, N. R.; White, S. R.; Moore, J. S. *ACS Appl. Mater. Interfaces, Articles ASAP* **2011**.
18. Yang, J.; Keller, M. W.; Moore, J. S.; White, S. R.; Sottos, N. R. *Macromolecules* **2008,** 41, (24), 9650-9655.
19. Rowan, S. J.; Cantrill, S. J.; Cousins, G. R. L.; Sanders, J. K. M.; Stoddart, J. F. *Angew. Chem., Int. Ed.* **2002,** 41, (6), 899-952.
20. Wojtecki, R. J.; Meador, M. A.; Rowan, S. J. *Nat. Mater.* **2011,** 10, (1), 14-27.
21. Gousse, C.; Gandini, A.; Hodge, P. *Macromolecules* **1998,** 31, (2), 314-321.
22. Inglis, A. J.; Nebhani, L.; Altintas, O.; Schmidt, F. G.; Barner-Kowollik, C. *Macromolecules* **2010,** 43, (13), 5515-5520.
23. Zhang, Y.; Broekhuis, A. A.; Picchioni, F. *Macromolecules* **2009,** 42, (6), 1906-1912.
24. Tian, Q.; Rong, M. Z.; Zhang, M. Q.; Yuan, Y. C. *Polym. Int.* **2010,** 59, (10), 1339-1345.
25. Syrett, J. A.; Mantovani, G.; Barton, W. R. S.; Price, D.; Haddleton, D. M. *Polym. Chem.* **2010,** 1, (1), 102-106.
26. Chujo, Y.; Sada, K.; Saegusa, T. *Macromolecules* **1990,** 23, 2693.
27. Zheng, Y.; Micic, M.; Mello, S. V.; Mabrouki, M.; Andreopoulos, F. M.; Konka, V.; Pham, S. M.; Leblanc, R. M. *Macromolecules* **2002,** 35, 5228.
28. Chujo, Y.; Sada, K.; Nomura, R.; Naka, A.; Saegusa, T. *Macromolecules* **1993,** 26, 5611.
29. Otsuka, H.; Aotani, K.; Higaki, Y.; Takahara, A. *J. Am. Chem. Soc.* **2003,** 125, 4064-4065.
30. Higaki, Y.; Otsuka, H.; Takahara, A. *Macromolecules* **2006,** 39, 2121.
31. Niu, W.; O'Sullivan, C.; Rambo, B. M.; Smith, M. D.; Lavigne, J. J. *Chem. Commun.* **2005**, 4342–4344.
32. Kennedy, J. P.; Castner, K. F. *J. Polym. Sci., Polym. Chem. Ed.* **1979,** 17, 2039.
33. Engle, L. P.; Wagener, K. B. *J. Macromol. Sci. Rev. Macromol. Chem.* **1993,** C33(3), 239.
34. Chujo, Y.; Sada, K.; Saegusa, T. *Macromolecules* **1990,** 23, 2636
35. Jones, J. R.; Liotta, C. L.; Collard, D. M.; Schiraldi, D. A. *Macromolecules* **1999,** 32, 5786.
36. Chen, X.; Dam, M. A.; Ono, K.; Mal, A.; Shen, H.; Nutt, S. R.; Sheran, K.; Wudl, F. *Science* **2002,** 295, 1698-1702.
37. Murphy, E. B.; Bolanos, E.; Schaffner-Hamann, C.; Wudl, F.; Nutt, S. R.; Auad, M. L. *Macromolecules* **2008,** 41, 5203-5209.

38. Yoshie, N.; Watanabe, M.; Araki, H.; Ishida, K. *Polym. Degrad. Stab.* **2010,** 95, (5), 826-829.
39. Chujo, Y.; Sada, K.; Naka, A.; Nomura, R.; Saegusa, T. *Macromolecules* **1993,** 26, 883.
40. Oku, T.; Furusho, Y.; Takata, T. *Angew. Chem., Int. Ed.* **2004,** 43, 966.
41. Tsarevsky, N. V.; Matyjaszewsky, K. *Macromolecules* **2002,** 35, 9009.
42. Ran, R.; Yu, Y.; Wan, T. *J. Appl. Polym. Sci.* **2007,** 105 398-404.
43. Scott, T. F.; Schneider, A. D.; Cook, W. D.; Bowman, C. N. *Science* **2005,** 308, 1615–1617.
44. Hawker, C. J.; Bosman, A. W.; Harth, E. *Chem. Rev.* **2001,** 101, (12), 3661-3688.
45. Lutz, J.-F.; Neugebauer, D.; Matyjaszewski, K. *J. Am. Chem. Soc.* **2003,** 125, (23), 6986-6993.
46. Otsuka, H.; Aotani, K.; Higaki, Y.; Amamoto, Y.; Takahara, A. *Macromolecules* **2007,** 40, 1429.
47. Su, J.; Amamoto, Y.; Nishihara, M.; Takahara, A.; Otsuka, H. *Polymer Chemistry* **2011**.
48. Lehn, J. M. *Chem. Soc. Rev.* **2007,** 36, 151-160.
49. Skene, W. G.; Lehn, J.-M. P. *PNAS* **2004,** 101, (22), 8270-8275.
50. Deng, G.; Tang, C.; Li, F.; Jiang, H.; Chen, Y. *Macromolecules* **2010,** 43, (3), 1191-1194.
51. Lehn, J. M. *Prog. Polym. Sci.* **2005,** 30, 814-831.
52. Canadell, J.; Goossens, H.; Klumperman, B. *Macromolecules* **2011,** 44, 2536–2541.
53. Weinhold, F.; Landis, C. *Valency and bonding, Cambridge* **2005**, 96-100.
54. Wool, R. P.; O'Connor, K. M. *J. Polym. Sci., Polym. Lett. Ed.* **1982,** 20, 7.
55. Outwater, J. O.; Gerry, D. J. *J. Adhes.* **1969,** 10, 290.
56. Wool, R. P., In *Polymer Interfaces: Structure and Strength*, Hanser/Gardner, Munich: 1995; pp 209-267.
57. Sijbesma, R. P.; Beijer, F. H.; Brunsveld, L.; Folmer, B. J. B.; Hirschberg, J.; Lange, R. F. M.; Lowe, J. K. L.; Meijer, E. W. *Science* **1997,** 278, (5343), 1601-1604.
58. McKee, M. G.; Elkins, C. L.; Long, T. E. *Polymer* **2004,** 45, (26), 8705-8715.
59. Mather, B. D.; Baker, M. B.; Beyer, F. L.; Green, M. D.; Berg, M. A. G.; Long, T. E. *Macromolecules* **2007,** 40, 4396-4398.
60. Gong M., L. C.-W., Joo S-W. *Jounal Of Materials Science* **2002** 37 4615 – 4620.
61. Yamauchi, K.; Lizotte, J. R.; Long, T. E. *Macromolecules* **2003,** 36, (4), 1083-1088.
62. Kalista, J. J. S., Ward, C.T., Oyetunji, Z. *Mechanicals of Advanced Materials and Structures* **2007,** 14, 391.

63. Stephen, J.; Kalista, J.; Ward, T. C. *J. R. Soc. Interface* **2007,** 4, 405.
64. Beck, J. B.; Rowan, S. J. *J. Am. Chem. Soc.* **2003,** 125, 13922–13923.
65. Weng, W.; Beck, J. B.; Jamieson, A. M.; Rowan, S. J. *J. Am. Chem. Soc.* **2006,** 128, 11663–11672.
66. Nowak, A. P.; Breedveld, V.; Pakstis, L.; Ozbas, B.; Pine, D. J.; Pochan, D.; Deming, T. J. *Nature* **2002,** 417, 424-428.
67. Wang, Q.; Mynar, J. L.; Yoshida, M.; Lee, E.; Lee, M.; Okuro, K.; Kinbara, K.; Aida, T. *Nature* **2010,** 463, (7279), 339-343.
68. Eisenberg, A.; Hird, B.; Moore, R. B. *Macromolecules* **1990,** 23, (18), 4098-4107.
69. Tant, M. R.; Mauritz, K. A.; Wilkes, G. L., *Ionomers*. Blackie, London, UK: 1997.
70. Miles, I. S., Rostami,S. *Multicomponent Polymer Systems (Longman Scientific & Technical.)* **1992**, 187-206.
71. Ege, S. N., Organic Chemistry: Structure and Reactivity. In 2003; pp 30-33, 67.
72. Eisenberg, A.; Hird, B.; Moore, R. B. *Macromolecules* **1990,** 23, 4098-4107.
73. Marx, C. L.; Caulfield, D. F.; Cooper, S. L. *Macromolecules* **1973,** 6, 344.
74. Luo, J. L.; Liou, Y. J.; Chin, T. M.; Kuo, Y. M.; Chao, D. Y. *Journal of Applied Polymer Science* **2006,** 101, (6), 3767-3773.
75. Rengarajan, R.; Kesavan, S. K.; Fullerton, K. L.; Lee, S. *Journal of Applied Polymer Science* **1992,** 45, (2), 317-31.
76. Ghannam, L.; Garay, H.; Francois, J.; Billon, L. *Macromolecular Chemistry and Physics* **2007,** 208, (13), 1469-1479.
77. Varley, R. J.; Shen, S.; van der Zwaag, S. *Polymer* **2010,** 51, (3), 679-686.
78. Huber, A.; Hinckley, J. *NASA Technical Memorandum* **2005,** NASA/TM-2005-213532.
79. Pimentel, G. C.; McClellan, A. L., *The Hydrogen Bond*. 1960; p 1-9.
80. Berl, V.; Schmutz, M.; Krische, M. J.; Khoury, R. G.; Lehn, J.-M. *Chem. Eur. J.* **2002,** 8, 1227-1244.
81. Sijbesma, R. P.; Beijer, F. H.; Brunsveld, L.; Folmer, B. J. B.; Hirschberg, J. H. K. K.; Lange, R. F. M.; Lowe, J. K. L.; Meijer, E. W. *Science* **1997,** 278, (5343), 1601-1604.
82. Beijer, F. H.; Sijbesma, R. P.; Kooijman, H.; Spek, A. L.; Meijer, E. W. *J. Am. Chem. Soc.* **1998,** 120, (27), 6761-6769.
83. Soentjens, S. H. M.; Sijbesma, R. P.; van Genderen, M. H. P.; Meijer, E. W. *J. Am. Chem. Soc.* **2000,** 122, (31), 7487-7493.
84. Chino, K.; Ashiura, M. *Macromolecules* **2001,** 34, (26), 9201-9204.
85. http://www.suprapolix.com/index.php?page=supramolecular.
86. Lutz, J.-F.; Nehring, R.; Pfeifer, S. *ACS Symp. Ser.* **2006,** 944, (Controlled/Living Radical Polymerization), 185-197.

87. Lo, P. K.; Sleiman, H. F. *J. Am. Chem. Soc.* **2009,** 131, 4182-4183.
88. Sivakova, S.; Rowan, S. J. *Chem. Soc. Rev.* **2005,** 34, (1), 9-21.
89. Ilhan, F.; Gray, M.; Rotello, V. M. *Macromolecules* **2001,** 34, 2597-2601.
90. Wilson, A. J. *Nature Chemistry* **2011,** 3, 193-194.
91. de Greef, T. F. A.; Ligthart, G. B. W. L.; Lutz, M.; Spek, A. L.; Meijer, E. W.; Sijbesma, R. P. *J. Am. Chem. Soc.* **2008,** 130, (16), 5479-5486.
92. Mather, B. D.; Lizotte, J. R.; Long, T. E. *Macromolecules* **2004,** 37, (25), 9331-9337.
93. Mather, B. D.; Baker, M. B.; Beyer, F. L.; Berg, M. A. G.; Green, M. D.; Long, T. E. *Macromolecules* **2007,** 40, (19), 6834-6845.
94. Spijker, H. J.; van Delft, F. L.; van Hest, J. C. M. *Macromolecules* **2007,** 40, (1), 12-18.
95. Sivakova, S.; Bohnsack, D. A.; Mackay, M. E.; Suwanmala, P.; Rowan, S. J. *J. Am. Chem. Soc.* **2005,** 127, (51), 18202-18211.
96. Karikari, A. S.; Mather, B. D.; Long, T. E. *Biomacromolecules* **2007,** 8, 302-308.
97. Cordier, P.; Tournilhac, F.; Soulie-Ziakovic, C.; Leibler, L. *Nature* **2008,** 451, (7181), 977-980.
98. Burattini, S.; Greenland, B. W.; Hayes, W.; Mackay, M. E.; Rowan, S. J.; Colquhoun, H. M. *Chem. Mater.* **2011,** 23, (1), 6-8.
99. Jones, J. R.; Liotta, C. L.; Collard, D. M.; Schiraldi, D. A. *Macromolecules* **1999,** 32, 5786.
100. Varghese, S.; Lele, A.; Mashelkar, R. *J. Polym. Sci., Part A: Polym.Chem.* **2006,** 44, 666-670.
101. Holten-Andersen, N.; Harrington, M. J.; Birkedal, H.; Lee, B. P.; Messersmith, P. B.; Lee, K. Y. C.; Waite, J. H. *PNAS* **2010,** 108, (7), 2651-2655.
102. Varley, R. J.; van der Zwaag, S. *Polym. Test.* **2008,** 27, (1), 11-19.
103. Varley, R. *Springer Ser. Mater. Sci.* **2007,** 100, (Self Healing Materials), 95-114.
104. Tournilhac, F.; Cordier, P.; Montarnal, D.; Soulie-Ziakovic, C.; Leibler, L. *Macromol. Symp.* **2010,** 291-292, (Polymer Networks), 84-88.
105. Feldman, K. E.; Kade, M. J.; Meijer, E. W.; Hawker, C. J.; Kramer, E. J. *Macromolecules* **2009,** 42, (22), 9072-9081.
106. Kalista, S. J., Jr.; Ward, T. C.; Oyetunji, Z. *Mech. Adv. Mater. Struct.* **2007,** 14, (5), 391-397.
107. Pang, J. W. C.; Bond, I. P. *Compos. Sci. Technol.* **2005,** 65, (11-12), 1791-1799.
108. Brown, E. N.; Sottos, N. R.; White, S. R. *Exp. Mech.* **2002,** 42, (4), 372-379.

Chapter 3: Ionic Aggregation in Phosphonium-Containing ABA Triblock Copolymers: Controlled Radical Polymerization of Phosphonium Ionic Liquids

(Shijing Cheng, Frederick L. Beyer, Brian D. Mather, Robert B. Moore, and Timothy E. Long*, Macromolecules, *published*) Reproduced in part with permission from Macromolecules.

3.1 Abstract

Phosphonium ion-containing acrylate triblock (ABA) copolymers were synthesized using nitroxide mediated radical polymerization. The polymerization of styrenic phosphonium-containing ionic liquid monomers using a difunctional alkoxyamine initiator, $DEPN_2$, afforded an ABA triblock copolymer with an *n*-butyl acrylate soft center block (DP~400) and symmetric phosphonium-containing external reinforcing blocks (DP<30). Two phosphonium monomers with different alkyl substituent lengths enabled an investigation of the effects of ionic aggregation of phosphonium cations on the physical properties of ABA block copolymer ionomers. Subsequently, the thermomechanical properties and morphologies of these materials were compared to a noncharged triblock copolymer analog with neutral polystyrene external blocks. Shortening the alkyl substituents on the phosphonium cation enhanced the hydrophilicity of tributyl-4-vinylbenzyl phosphonium chloride (BPCl) relative to trioctyl-4-vinylbenzyl phosphonium chloride (OPCl). In both cases, phosphonium cations promoted microphase-separation and thermoplastic elastomer performance for the OPCl- and BPCl-containing triblock copolymers compared to a less well-defined, microphase

segregated morphology for the styrene analog. Dynamic mechanical analysis (DMA) of phosphonium-containing triblock copolymers exhibited well-defined rubbery plateau regions, whereas the plateau was shortened for the non-ionic analog. The solid state morphologies of the block copolymers were studied using small-angle X-ray scattering (SAXS) and transmission electron microscopy (TEM), and both techniques revealed phase separation at the nanoscale. DMA studies indicated that phosphonium aggregation governed flow activation energies.

3.2 Introduction

As a result of the development of new synthetic methods for producing charged block copolymers,[1-2] there is a growing interest in microphase-separated ion-containing block copolymers as membranes for the next generation of batteries, water purification membranes, and fuel cells.[3] For these applications, ionic species are often mixed with block copolymers, such as lithium salts blended with poly(ethylene oxide)-containing copolymers;[4-5] alternatively, ionic sites are covalently attached to the block copolymer, e.g., sodium styrene sulfonate-containing block copolymers.[6-9] Due to the fact that most organic polymers are incompatible with ionic species, charged block copolymers may selectively restrict ion transport through one microphase and enable the formation of well-defined, ionic pathways for conduction.

Cation-containing polymers, which possess positively-charged ammonium or phosphonium atoms, are particularly important because of their technological importance as phase-transfer catalysts,[10] antistatic agents,[11] biocides,[12] humidity sensors,[13] and water filtration membranes.[14] Polymers functionalized with amphiphilic phosphonium or ammonium units are also good candidates for alkaline fuel cell membranes.[15-16] Minteer

et al. reported that the alkaline anion-exchange capacity of tetraalkylphosphonium bromide treated membranes was larger than the ammonium analogs.[15] In addition, a widely described concern with ammonium-based polymers is their chemical instability in alkaline environments, especially at elevated temperatures, which is mainly due to the reactivity of ammonium cations with hydroxide anions in a nucleophilic substitution and/or a Hofmann-type elimination. Thus, the thermal stability and chemical resistance of phosphonium salts suggest a potentially superior alternative.

By varying the alkyl groups and mobile counterions it is possible to tailor the amphiphilicity of phosphonium units for self-assembly.[17] A special class of phosphonium salts comprises low melting ionic liquids (mp<100 °C).[18] Polymers with phosphonium units randomly distributed along the polymer main-chain are well documented. For example, McGrath et al. reported the synthesis of poly(arylene ether) main-chain phosphonium-containing ionomers for high-performance applications, such as ion-exchange membranes.[19] The phosphonium ionomers were prepared through the reduction of poly(arylene ether phosphine oxide) to phosphine/phosphine oxide copolymers with phenylsilane and subsequent quaternization of phosphines with alkyl halides. In addition, quaternization of polyamides with phosphines yielded polymers bearing quaternary phosphonium cations along the polymer backbone.[20] Yan et al. recently synthesized a phosphonium-containing polysulfone that offered high alkaline conductivity, good solubility in low-boiling-point water-miscible solvents, and outstanding alkaline stability.[16] In addition, our research group recently synthesized a novel phosphonium diol as a chain extender to form polyurethane, main-chain, phosphonium ionomers, which demonstrated a facile strategy for phosphonium-containing step-growth polymers.[21]

Chain-growth polymerization represents a versatile strategy for the synthesis of phosphonium ionomers through either post-polymerization modification[22-23] or the polymerization of styrenic,[24] acrylate,[25] or methacrylate[26] phosphonium-containing monomers. Compared to the synthesis of other ionomers such as sodium styrene sulfonate, direct polymerization of phosphonium-containing monomers is attractive due to the moderate amphiphilicity of phosphonium compounds, which renders them miscible with most hydrocarbons and prevents insolubility during polymerization. Lowe et al. first demonstrated the controlled reversible addition-fragmentation chain transfer (RAFT) radical homo- and copolymerization of phosphonium-based styrenic monomers in aqueous media, and they qualitatively confirmed the pH-responsive aggregation of phosphonium-based hydrophilic diblock copolymers in aqueous solutions.[24] Yoshida et al. also found that phosphonium-containing amphiphilic diblock copolymers formed reversible spherical micelles in organic solvents.[27] Parent et al. synthesized poly(isobutylene-*co*-isoprene) phosphonium and ammonium ionomers with thermomechanical behavior comparable to vulcanized thermosets due to ionic aggregation of the phosphonium cations.[22] Matyjaszewski and coworkers reported the synthesis of phosphonium-based telechelic polystyrene and poly(methyl methacrylate) using atom transfer radical polymerization (ATRP).[23]

Our research group previously reported the noncovalent attachment of phosphonium cations to ABA block copolymers using complementary multiple hydrogen bonds.[28] These thermally reversible hydrogen bonds introduced strong temperature-dependent properties to the ionomers, which were melt processible above the hydrogen bond dissociation temperature. The present work demonstrates nitroxide mediated radical

polymerization (NMP) of styrenic phosphonium ionic liquid monomers with a difunctional alkoxyamine initiator ($DEPN_2$), which results in an ABA triblock copolymer with symmetrically-charged external blocks. NMP is a well-established controlled free radical polymerization methodology that facilitates block copolymer formation with a wide range of acrylic and styrenic monomers. Moreover, NMP is particularly suited for fundamental studies of ion-containing block copolymers, due to high tolerance to ionic functionalities and the absence of residual metal catalysts.[29-30] In this study, we utilized NMP and successfully synthesized a series of phosphonium-containing triblock copolymers, varying the ionic content and the lengths of the hydrophobic alkyl substituents on the phosphonium cations. We studied the influence of phosphonium cations on the thermomechanical behavior of phosphonium-containing triblock copolymers. Complementary studies of the microphase separation and structure-property relationships of the block copolymers with regards to the tunable electrostatic interactions and self-assembly of phosphonium cations were also performed using differential scanning calorimetry (DSC), dynamic mechanical analysis (DMA), transmission electron microscopy (TEM), and small-angle X-ray scattering (SAXS). The resulting materials offer promise as thermally stable thermoplastic elastomers with tunable morphology.

3.3 Experimental

3.3.1 Materials

n-Butyl acrylate (99%) was purchased from Aldrich and purified using an neutral alumina column and subsequent distillation at reduced pressure from calcium hydride. 4-Vinylbenzylchloride (90%) was purchased from Aldrich and purified with an alumina column. 2,2'-Azobis(isobutyronitrile) (AIBN) (98%), 2,6-di-*tert*-butyl-4-methylphenol

(99%), diethyl-*meso*-2,5-dibromoadipate (98%), copper(I) bromide (99.999%), copper powder (45 *u*m, 99%), and *N,N,N',N'',N''*-pentamethyldiethylenetriamine (PMDETA) (98%) were purchased from Aldrich and used without further purification. Cytec Industries kindly donated trioctylphosphine (≥95%) and tributylphosphine (≥95%). DEPN,[31] $DEPN_2$,[32] trioctyl-4-vinylbenzyl phosphonium chloride[33] (OPCl) (Figure 3.1), and tributyl-4-vinylbenzyl phosphonium chloride[33] (BPCl) (Figure 3.2) were synthesized according to previous literature. Hexanes (Fisher Scientific, HPLC grade), tetrahydrofuran (THF) (Fisher Scientific, HPLC grade), and *N*,*N*-dimethylformamide (DMF) (Fisher Scientific, HPLC grade, anhydrous) were used as received.

3.3.2 Polymerization of *n*-Butyl Acrylate with $DEPN_2$

$DEPN_2$ (78 mg, 0.10 mmol) and DEPN (6 mg, 0.20 mmol) were weighed into a 100-mL, round-bottomed flask containing a magnetic stirbar. The flask was sealed with a three-way joint allowing the application of vacuum or nitrogen and the introduction of reagents using a syringe. The flask was evacuated to 60 mmHg and refilled with high-purity nitrogen three times. Purified *n*-butyl acrylate (30 mL, 210 mmol) was added and the mixture was degassed with three freeze-pump thaw cycles. Finally, the flask was immersed in an oil bath maintained at 120 °C for 2 h. After polymerization, residual monomer was removed at reduced pressure (60 mmHg, 40 °C, 6 h). SEC analysis in THF revealed a typical number-average molecular weight of 53,600 g/mol, M_w/M_n =1.17. Yield: 31%

3.3.3 Synthesis of Phosphonium-Containing Triblock Copolymers

DEPN-terminated poly(*n*-butyl acrylate) homopolymer (500 mg, M_n=53,600 g/mol) and OPCl (900 mg, 3.6 mmol) were added to a 50-mL, round-bottomed flask with a

magnetic stirbar. The flask was sealed with a three-way joint and evacuated to 60 mmHg and refilled with high-purity nitrogen three times. DMF (15 mL) was syringed into the flask and the mixture was degassed repeatedly with freeze-pump-thaw cycles. The flask was then immersed in an oil bath at 120 °C for 2 h. After polymerization, DMF was removed upon distillation at reduced pressure. The polymer was redissolved in THF and precipitated into methanol/water mixture and finally dried at 50 °C under reduced pressure (0.5 mmHg) for 24 h. ^{1}H NMR (CD_2Cl_2) revealed block molecular weights 29.7K-53.6K-29.7K (OPCl: 21.3 mol%). BPCl-containing triblock copolymers were synthesized in a similar fashion. After polymerization, DMF was removed at reduced pressure. The polymer was redissolved in $CHCl_3$ and then precipitated into warm DI water. Yield: 56%. ^{1}H NMR (400 MHz, CD_2Cl_2, 25 ^{o}C) (δ, ppm): 0.86 (t, CH_3, 3H), 1.2-1.5 (br, COO $CH_2CH_2CH_2CH_3$, CH_2-CH-COO-, CH_2-CH-Ph-), 1.7 (br, CH_2-CH-Ph-, 1H), 2.1 (br, CH_2-CH-COO-, CH_2-CH-Ph-, 1H), 3.9 (br, $COOCH_2$, 2H), 4.7 (br, Ph-CH_2-P, 2H), 6.5 (br, Ph, 2H), 7.3 (br, Ph, 2H).

3.3.4 Synthesis of Phosphonium-Containing Homopolymer

OPCl or BPCl (3.7 g) was weighed into a 100-mL, round-bottomed flask containing a magnetic stirbar. The flask was sealed and purged with N_2 for 20 min. Anhydrous DMF (25 wt%) was added to the flask to dissolve the phosphonium-containing monomers. Finally, AIBN (0.58 mol%) was dissolved in 10 mL of anhydrous DMF and sparged with dry nitrogen for 10 min and added to the reaction mixture. The reaction flask was placed in an oil bath at 60 °C for 24 h with constant stirring. For OPCl homopolymerization, DMF was removed at reduced pressure after the reaction was completed. The crude product was redissolved in THF and precipitated into a methanol-water mixture. For

BPCl homopolymerization, the reaction solution was directly precipitated into THF and filtered. The final products were dried at 50 °C under reduced pressure (0.5 mmHg) for 24 h. Yield: 91% for BPCl; 73% for OPCl. ^{1}H NMR for BPCl homopolymer (400MHz, D_2O, 25 ^oC) (δ, ppm): 0.86 (t, C*H*$_3$, 3H) 1.2-1.5 (br, P-CH$_2$-C*H*$_2$-C*H*$_2$-CH$_3$, 4H), 1.7 (br, C*H*$_2$-CH-Ph-, 2H), 2.1 (br, C*H*-Ph-, 1H), 4.7 (br, Ph-C*H*$_2$-P, 2H), 6.5 (br, Ph, 2H), 7.3 (br, Ph, 2H).

3.3.5 Synthesis of Poly(styrene-*b*-*n*-butyl acrylate-*b*-styrene)

DEPN-terminated poly(*n*-butyl acrylate) homopolymer (1.0 g, M_n = 53,200 g/mol), styrene (3.5 g, 33.6 mmol), and DMF (13 mL) were added to a 50-mL, round-bottomed flask with a magnetic stir bar. The flask was sealed with a three-way joint and evacuated to 60 mmHg and refilled with high-purity nitrogen three times repeatedly with freeze-pump-thaw cycles. The flask was then immersed in an oil bath at 120 °C for 2 h. After polymerization, DMF was removed with reduced pressure. The polymer was dissolved in THF and precipitated into a methanol/water mixture. ^{1}H NMR ($CDCl_3$) revealed block molecular weights 21.6K-53.2K-21.6K (Styrene: 50 mol%). SEC analysis in THF revealed molecular weight data M_n = 99.1K g/mol, M_w/M_n =1.34. ^{1}H NMR (400MHz, $CDCl_3$, 25 ^oC) (δ, ppm): 0.86 (t, C*H*$_3$, 3H) 1.2-1.5 (br, CH$_2$C*H*$_2$CH$_3$-, CH$_2$C*H*$_2$CH$_2$-, 2H), 1.7 (br, C*H*$_2$-CH-Ph-, 1H), 2.1 (br, C*H*-Ph-, 1H), 6.5 (br, Ph, 2H), 7.3 (br, Ph, 2H).

3.3.6 Polymer Characterization

Size exclusion chromatography (SEC) was performed in THF using a Waters size exclusion chromatograph. The instrument was equipped with an autosampler, three 5 μm PLgel Mixed-C columns, a Waters 2410 refractive index (RI) detector operating at 880 nm, a Wyatt Technologies miniDAWN multi-angle laser light scattering (MALLS)

detector operating at 690 nm, and a Viscotek 270 viscosity detector at 40 °C at a flow rate of 1 mL/min. ^{1}H NMR and ^{31}P NMR spectroscopies were performed in CD_2Cl_2 on a 400 MHz Varian Inova spectrometer at 23 °C. FAB-MS was conducted in positive ion mode on a JEOL HX110 Dual Focusing Mass spectrometer. Differential scanning calorimetry (DSC) was performed using a TA Instruments Q2000 differential scanning calorimeter under a nitrogen flow of 50 mL/min with a heating rate of 10 or 20 °C/min. Glass transition temperatures were measured at the midpoint of the transition in the second heat. Dynamic mechanical analysis (DMA) was conducted on a TA Instruments Q800 Dynamic Mechanical Analyzer in tension mode at a frequency of 1 Hz, an oscillatory amplitude of 15 μm, and a static force of 0.01 N. The temperature ramp was 3 °C/min. The glass-transition temperature (T_g) was determined at the peak maximum of the tanδ curve. Tensile experiments employed an Instron at 13 mm/min strain rate.

3.3.7 Sample Preparation and Morphological Characterization

Solution cast films of OPCl and BPCl-containing block copolymer were prepared for SAXS and TEM study of the bulk ionomer morphology. Solutions of 5 wt% OPCl and BPCl-containing block copolymer in $CHCl_3$ were prepared at room temperature and the solvent was allowed to evaporate slowly over a period of 2 d. The resulting films were annealed for 2 d at reduced pressure at 120 °C and 170 °C, respectively.

SAXS data were collected on a customized, 3 m pinhole-collimated camera. Characteristic $Cu_{K\alpha}$ X-rays (λ = 1.542 Å) were generated with a Rigaku Ultrax18 rotating anode generator operated at 4.5 kW and filtered using Ni foil. A 120 mm Molecular Metrology multiwire area detector collected two-dimensional data sets for samples characterized at two sample-to-detector distances (50 cm and 150 cm). Camera length

was calibrated using silver behenate. The raw data were corrected for background noise and placed on an absolute scale (cm^{-1}) using a glassy carbon secondary standard. Using Wavemetrics Igor Pro software and procedures available from Argonne National Laboratory, the data were corrected and then azimuthally averaged for analysis as intensity, *I*, as a function of *q*, the magnitude of the scattering vector, where $q = 4\pi \cdot \sin(\theta)/\lambda$, in which 2θ is the scattering angle and λ is wavelength.[34] Finally, for each sample, the 1D data from the two camera lengths were combined into one data set spanning an angular range 0.007 $Å^{-1}$ to 0.45 $Å^{-1}$. Peak positions were determined by fitting Lorentzian distributions, along with a power-law background and a constant, to the data and minimizing error using least squares analysis. A helium pycnometer (AccuPyc 1330 Pycnometer) was used to determine the volume, and thus density, of 100 mol% BPCl and 100 mol% OPCl. This is a non-invasive procedure using purified helium as the displaced medium. After calibration, the specimens were placed in the measurement cell and purged with helium for 5-10 min. At least three experiments were conducted on each sample. The densities reported are the averages and standard deviations of these repeated experiments are below 2‰.

TEM specimens approximately 100 nm thick were dry sectioned from the solvent-cast and annealed films using a Reichert-Jung ultramicrotome equipped with a cryo unit operated at -75 ^{o}C. The microtomed sections were stored in desiccators at room temperature prior to imaging. TEM experiments were performed using a Philips EM-420 scanning transmission electron microscope operated at 100 kV. Images were collected with a charge-coupled device (CCD) camera.

3.4 Results and Discussion

3.4.1 Monomer and Polymer Synthesis

Introducing ionic functionalities to block copolymers is often challenging using post-polymerization modification or functional group protection/deprotection strategies due to limited accessibility of the functional sites.[35] In contrast, controlled radical polymerization of monomers bearing anionic, cationic, zwitterionic, and neutral functionalities is readily achieved in organic and aqueous environments under both homogeneous and heterogeneous conditions. Currently, there are only reports in the literature detailing the direct polymerization of phosphonium-containing monomers using RAFT polymerization.[24, 36] In fact, to the best of our knowledge this is the first report of the synthesis of phosphonium-containing triblock copolymers using nitroxide-mediated polymerization (Scheme 3.1). DEPN-terminated poly(*n*-butyl acrylate) prepared with a difunctional nitroxide initiator ($DEPN_2$)[37] reinitiated phosphonium functional monomers (OPCl and BPCl) and afforded symmetrical outer blocks at each chain end. Both OPCl and BPCl monomers were soluble in most organic solvents. OPCl had a melting point of 87 ^{o}C, which classified this compound as a polymerizable phosphonium ionic liquid. In contrast, BPCl, which possesses shorter butyl substituents, had a higher melting point of 125 °C and dissolved readily in water. Copolymerization of the difunctional poly(*n*-butyl acrylate) precursor and phosphonium-containing monomers using a variety of feed ratios afforded triblock copolymers with various outer block lengths and similar center block lengths. Tables 3.1 and 3.2 summarize the monomer feed ratios, compositions, molecular weights, and glass transition temperatures. All polymerizations remained homogeneous in DMF. However, significant copolymer aggregation in organic solvents prevented SEC

molecular weight characterization of the phosphonium-containing triblock copolymers. Thus, the block copolymer molecular weights were determined indirectly using SEC data of the central P*n*BA blocks and ^{1}H NMR spectroscopic data of the block copolymers. Comparison of the integration of ^{1}H NMR resonances at 6.0-8.0 ppm and 3.5-5.0 ppm, which corresponded to the chemical shift of four aromatic protons in one phosphonium-containing repeat unit and two protons from both *n*-butyl acrylate (-O-CH_2-) and phosphonium monomer (-phenyl-CH_2-P^+-), respectively (Figure 3.3), revealed the ionic concentration of the triblock copolymer. ^{31}P NMR spectra of the phosphonium monomers and block copolymers revealed a single peak at 32 ppm, which corresponded to the quaternary phosphonium cation, suggesting the absence of degradation of phosphonium cations during polymerization (Figure 3.4). The copolymerization of the OPCl and BPCl monomers was stopped at moderate conversion (50%~60%) in order to control polydispersibility. All copolymers investigated were optically clear, suggesting the absence of macrophase separation.

Scheme 3.1. Synthesis of phosphonium-containing triblock copolymers.

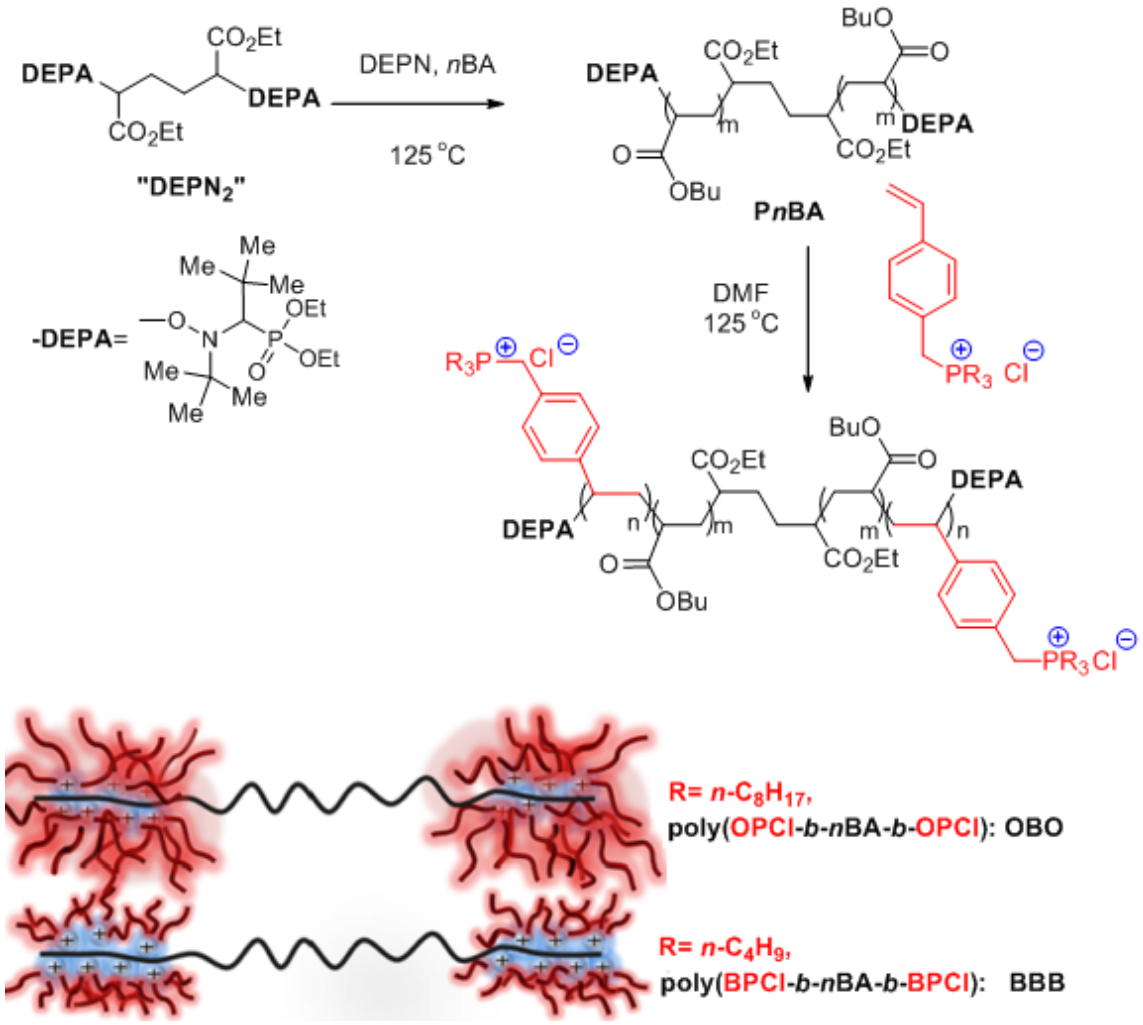

Table 3.1. Molecular characterization of poly(OPCl-*b*-*n*BA-*b*-OPCl) with identical molecular weight of the center block (M_n= 53.6 K, M_w /M_n=1.17).

Sample Name	OPCl in feed (mol%)	OPCl in polymer (mol%)	OPCl in polymer (wt%)	$M_{n,NMR}$(g/mol)	$T_{g,DSC}$ (^oC)*	$T_{g,DMA}$ (^oC)*
OBO6	12	6	21	7.4K-53.6K-7.4K	-47	N/A
OBO10	20	10	31	12.2K-53.6K-12.2K	-45	-37
OBO21	31	21	53	29.7K-53.6K-29.7K	-43	-36
-	100	100	100	N/A	82	N/A

*Only one T_g observed in DSC and DMA

Table 3.2. Molecular characterization of poly(BPCl-*b*-*n*BA-*b*-BPCl) with the same center block (M_n= 52.7 K, M_w /M_n=1.20).

Sample Name	BPCl in feed (mol%)	BPCl in polymer (mol%)	BPCl in polymer (wt%)	$M_{n,NMR}$(g/mol)	$T_{g,DSC}$ (^oC)	$T_{g,DMA}$ (^oC)
BBB6	11	6	15	4.5K-52.7K-4.5K	-49	N/A
BBB9	19	9	22	7.6K-52.7K-7.6K	-48	-25,-[a]
BBB15	27	15	33	12.9K-52.7K-12.9K	-49,140	-24,49
BBB33	65	33	58	35.9K-52.7K-35.9K	-49,142	-26,190
-	100	100	100	N/A	176	N/A

a: broad transition

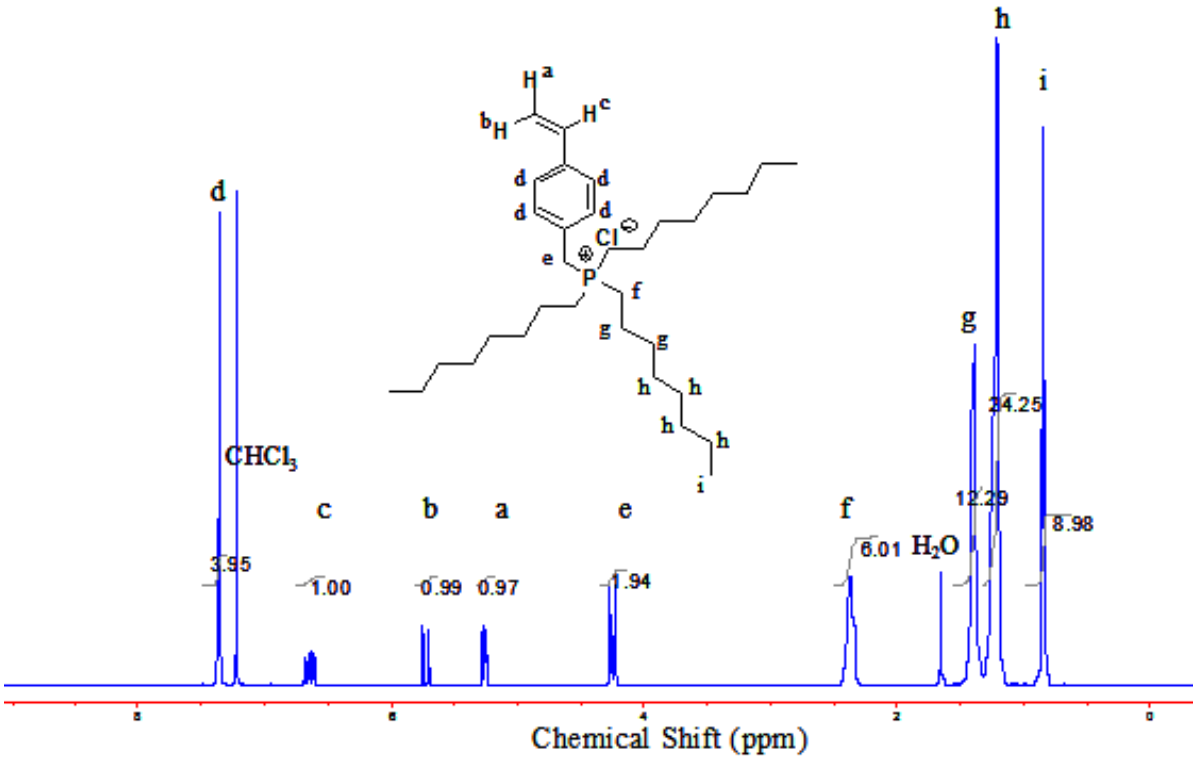

Figure 3.1 ^{1}H NMR spectra of trioctyl-4-vinylbenzyl phosphonium chloride

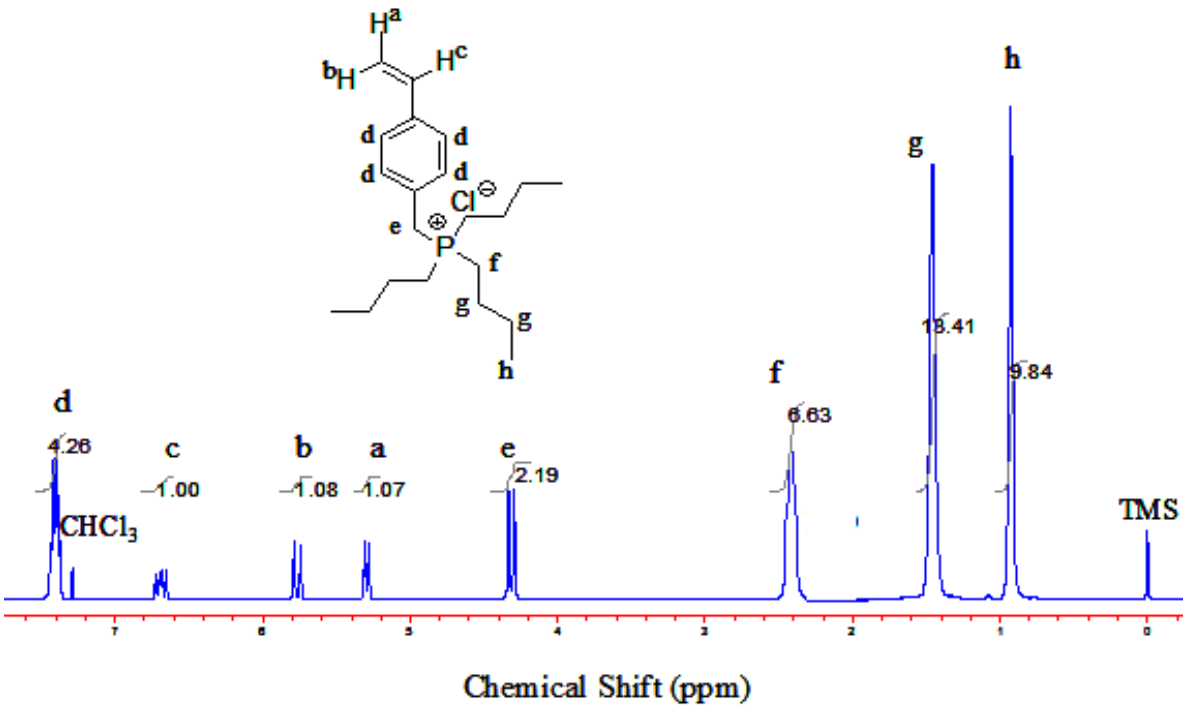

Figure 3.2. [1]H NMR spectra of tributyl-4-vinylbenzyl phosphonium chloride

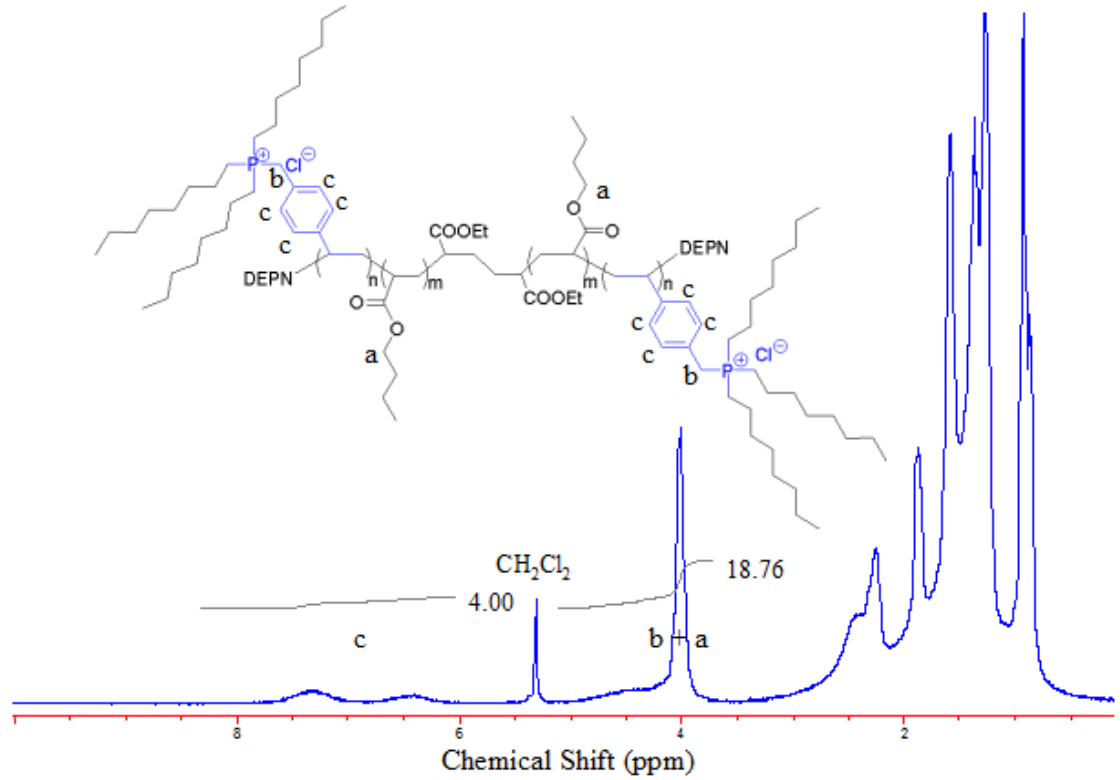

Figure 3.3. [1]H NMR spectrum of phosphonium-containing triblock copolymers

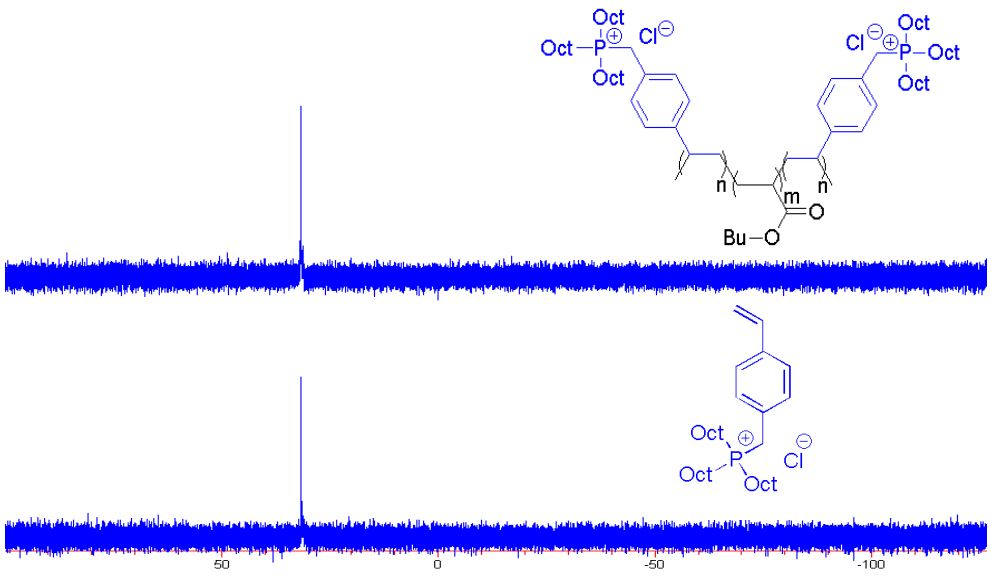

Figure 3.4. ^{31}P NMR spectrum of phosphonium-containing triblock copolymers

3.4.2 Thermal Properties

The glass transition temperatures of OPCl and BPCl homopolymers were 82 ^{o}C and 176 ^{o}C respectively (Table 3.1 and 3.2). The bulky trioctyl groups in OPCl plasticized the polymer matrix, reducing the glass transition temperature lower than polystyrene. In contrast, BPCl homopolymer bearing tributyl groups had a much higher glass transition temperature, indicating strong ion association. DSC analysis of poly(OPCl-*b*-*n*BA-*b*-OPCl)s with ionic concentration varying from 6 to 21 mol% exhibited a single glass transition around -40 °C, which was associated with the glass transition of P*n*BA. The absence of a glass transition temperature of OPCl is not surprising in view of the relatively small amount of OPCl present in these samples that the heat capacity change at the glass transition may be below the detection limit of the instrument. This independence of T_g with copolymer composition suggested OPCl units did not restrict segmental

motion in the P*n*BA phase and OPCl-containing triblock copolymers were microphase separated. Similarly, glass transition temperatures of poly(BPCl-*b*-*n*BA-*b*-BPCl) were in the range of -50 °C to -45 °C. At higher ionic concentrations of 15 and 33 mol%, a second glass transition temperature appeared near 140 °C, approaching the glass transition of BPCl homopolymer at 176 °C. DSC results suggested both OPCl- and BPCl-containing triblock copolymers exhibited microphase separation into a P*n*BA soft phase and an ion-rich hard phase. The presence of the second glass transition temperature, as well as the higher T_g of the BPCl homopolymer compared to OPCl homopolymer, indicated stronger ionic interactions in BPCl-containing polymers. According to the molecular structure of OPCl and BPCl, both van der Waal forces between alkyl chains and ionic interactions were expected to influence the segmental motion in the ion rich phase. The trioctyl substituents may shield ionic aggregation of the phosphonium cations and contribute to a depressed T_g. On the other hand, short tributyl substituents result in more cationic character, and ionic interactions are presumed to be more significant than van der Waal forces.

3.4.3 Thermomechanical Behavior

Dynamic mechanical analysis (DMA) was used to study the thermal dynamic mechanical behavior of phosphonium-containing triblock copolymers. Temperature dependencies of lorgarithms of storage modulus (G') and loss tangent (tanδ) of poly(BPCl-*b*-*n*BA-*b*-BPCl)s are shown in Figure 3.5. Poly(BPCl-*b*-*n*BA-*b*-BPCl)s showed two distinctive tanδ peaks in all cases. The first tanδ peak at -37 °C corresponded to the T_g of poly(*n*-butyl acrylate) center block. The second relaxation peak presented at higher temperature, corresponding to the relaxation of BPCl-containing hard phase. This

peak shifted from 25 °C to 190 °C with increasing BPCl block molecular weights and the peak height increased with weight fraction of BPCl block as well. Additionally, for BBB-15 and BBB-33, plateau modulus significantly increased with hard phase weight fraction, indicating decreased mobility of the soft acrylate phase. The flatness of the rubbery plateau in BBB-33 also suggested a higher degree of microphase separation at higher ionic concentration and correlated well with DSC results.

DMA data including the storage modulus and tanδ behaviors of poly(OPCl-*b*-*n*BA-*b*-OPCl)s are shown in Figure 3.6. The tanδ curves exhibited maxima at -37 °C, close to the T_g of poly(*n*-butyl acrylate) (-40 °C). A rubbery plateau was evident above T_g, with an onset of flow near 100 °C. The second tanδ peaks were covered up by the whole flow up of the polymer and difficult to be distinguished. However, from the G' curve, the second transition presented at much lower temperature than BPCl-containing block copolymers. A similar trend was also demonstrated in ammonium neutralized sulfonated polystyrene by Weiss et al[38] and in phosphonium salts treated Nafion membranes by Moore et al.[39], i.e., relaxation temperature decreased with increasing alkyl substituent length. Additionally, G' spanned a 70 ^{o}C temperature window prior to viscous flow with a G' decrease of 12MPa, indicating a very gradual dissociation of the hard phase. In contrast, the onset of flow for BPCl-containing polymers resulted in a loss of storage modulus over a 20 °C temperature window with a 50 MPa decrease of G' (Figure 3.5). The dramatic difference in melt flow behavior points to the structural differences of the two types of block copolymers. More interestingly, when OPCl hard phase weight fraction increased from 31 wt% to 58 wt%, both the rubbery plateau height and length were close. The similar plateau length indicated that the molecular weights of outer blocks were close to

or above M_e and the second glass transition was molecular weight independent. The constant plateau modulus was attributed to bulky trioctyl substituents in the hard phase that weaken the aggregation of phosphonium cations and decreased the relaxation. Whereas, *n*-butyl substituents on the phosphonium centers permitted more efficient physical crosslinking of ionic sites, as observed in the higher second T_g. Einsenberg et al. reported the similar melt flow behavior in quaternized poly(4-vinylpyridinium-b-styrene-b-4-vinylpyridium) ABA triblock ionomers that water-plasticized ionic aggregates in ionic outer segments hindered the flow of the styrene middle blocks to a greater extent than would the well-defined domains.[40]

In a comparative study, DMA studies of the non-charged analog (poly(S-*b*-*n*BA-*b*-S)) with a similar weight fraction of the hard phase did not show a distinct rubbery plateau, and a higher glass transition temperature of the rubbery phase at -17 ^oC was indicative of the phase mixing (Figure 3.7). Similar results has been shown for quaternized styrene-butadiene-2-vinylpyridine block copolymers that upon quaternization the height of the rubbery plateau increased by 1 order of magnitude, which was attributed to an "ionomeric behavior".[41] McGrath et al. also found that neutralization promoted stronger phase separation of poly(tBMA-b-BD-b-tBMA) shown by DMA even when the morphology did not change.[42] DMA studies demonstrated that OPCl- and BPCl-containing triblock copolymers showed enhanced microphase separation compared to the neutral block copolymers. The charged block copolymers also exhibited thermoplastic elastomer behavior.

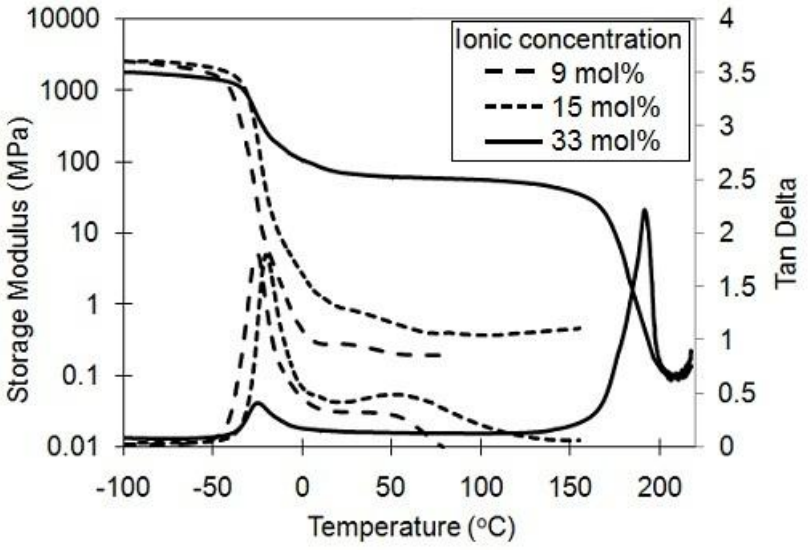

Figure 3.5. Dynamic mechanical temperature sweep for poly(BPCl-*b*-*n*BA-*b*-BPCl)s with 9 mo%, 15 mol%, and 33 mol% of BPCl respectively

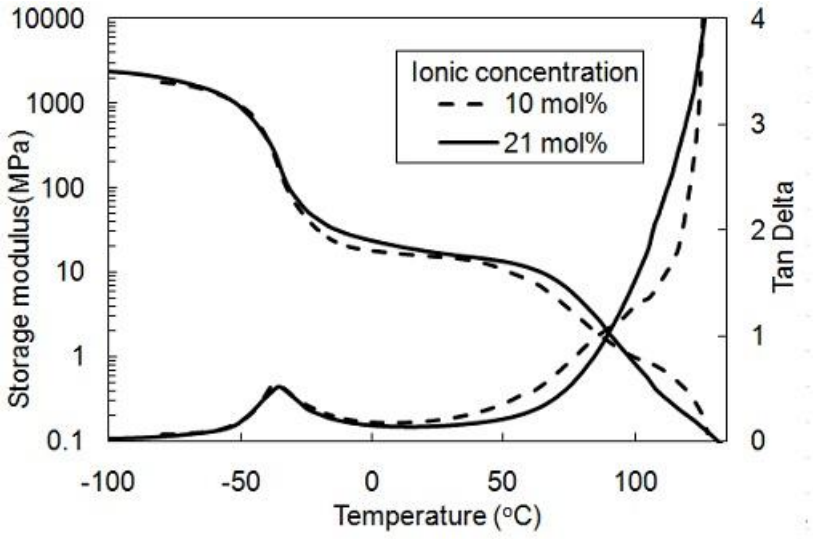

Figure 3.6. Dynamic mechanical temperature sweep for poly(OPCl-*b*-*n*BA-*b*-OPCl) with 10 mol% and 21 mol% of OPCl respectively

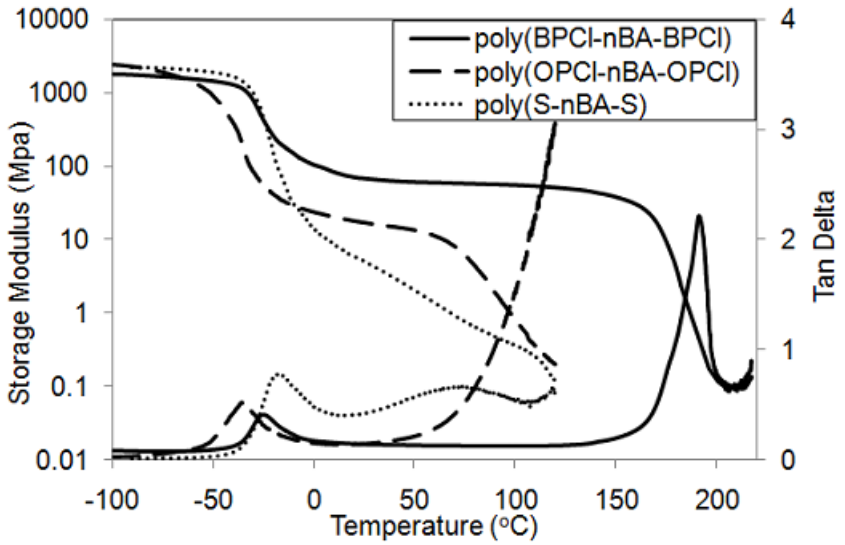

Figure 3.7. Dynamic mechanical temperature sweep for 1) poly(BPCl-*b*-*n*BA-*b*-BPCl) with 58 wt% of BPCl 2) poly(OPCl-*b*-*n*BA-*b*-OPCl) with 53 wt% of OPCl 3) poly(S-*b*-*n*BA-*b*-S) with 50 wt% of styrene

3.4.4 DMA at Multiple Frequencies

In order to gain more insight into the kinetics of ionic dissociation, DMA experiments were performed over multiple frequencies varying from 0.1 to 20 Hz. The transition temperature was defined as the temperature where a maximum in the loss modulus G" occurred. Plotting the logarithm of frequency versus the inverse of transition temperature yielded a straight line in all cases, indicating Arrhenius behavior, as shown in Figure 3.8. The apparent flow activation energies (E_as) calculated from the slopes of the lines were 115±9 kJ/mol for OBO10, 182±10 kJ/mol for OBO21, and 791±29 kJ/mol for BBB33 respectively. We ascribed the different flow activation energies to the structural difference of phosphonium units, since molecular weights were close. To distinguish the influence between hydrophobic interaction from alkyl chains and ionic association from phosphonium cations, we plotted flow activation energies against phosphonium charge density (Figure 3.9). Phosphonium charge density was calculated based on the atomic

concentration of P. OBO exhibited a linear relationship and the slope was smaller than that of BBB, suggesting that the presence of long alkyl chains not only diluted charge density but also hindered the association between phosphonium cations. In conclusion, dissociation of the ionic rich phase was a thermally activated process with Arrhenius behavior, and E_a increased significantly with increasing ionic concentration and shortening *n*-alkyl chain length.

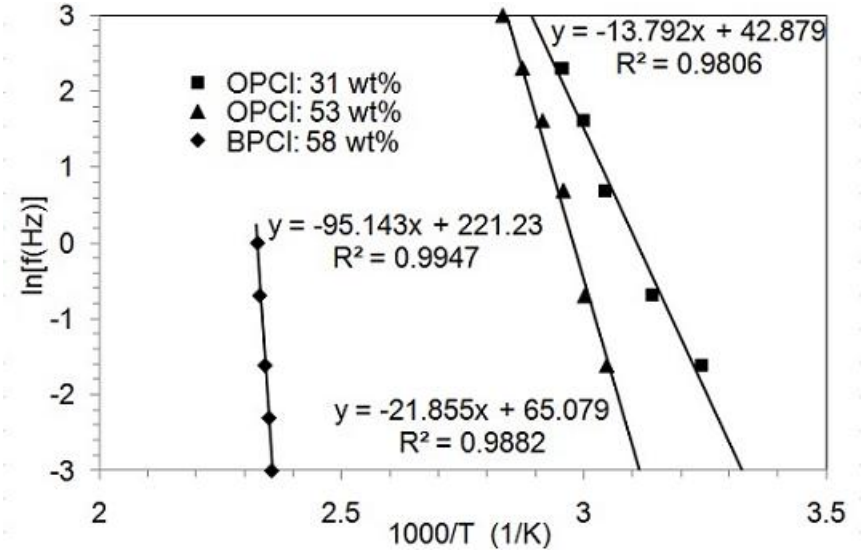

Figure 3.8. Influence of ionic content on flow activation energies (E_a) of phosphonium-containing triblock copolymers. E_as are 182±10 kJ/mol for 21 mol% OPCl and 115±9 kJ/mol for 10 mol% OPCl and 791±29 kJ/mol for 33 mol% BPCl.

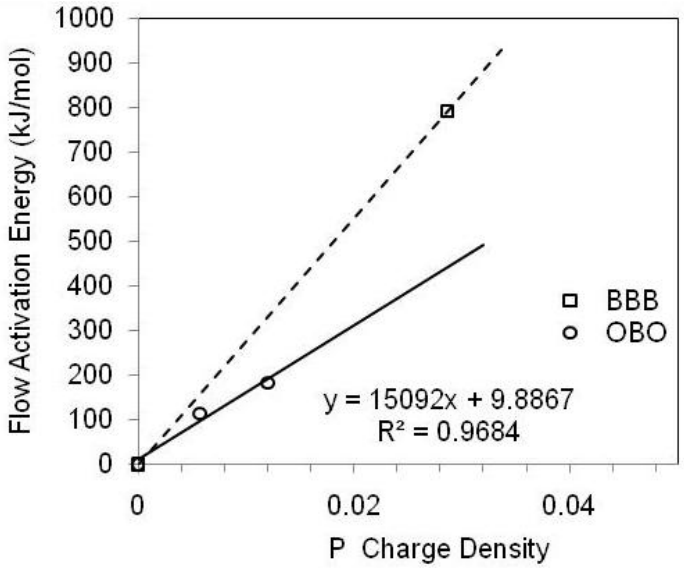

Figure 3.9. Influence of charge density on flow activation energies (E_as) of phosphonium-containing triblock copolymers.

3.4.5 Stress-Strain Experiments

Uniaxial stress-strain experiments were performed on rectangular tensile specimens punched from cast films of phosphonium-containing triblock copolymers and their non-ionic polymer analogs. Representative stress-strain curves are shown in Figure 3.10. Poly(BPCl-*b*-*n*BA-*b*-BPCl)s at low ionic concentrations exhibited behavior similar to covalently crosslinked rubbers with a relatively low modulus, substantial stress softening, and lack of yielding. The initial slopes of the curves increased with ionic concentration (curves A, B, and C) and the elongation at break was systematically reduced, which can be attributed to the fact that the rigid BPCl domains act as a "filler" in the rubbery acrylate matrix thereby leading to an increased value of the modulus. The enhancement of the strength at high elongations is often attributed to either strain-induced crystallization or finite extensibility of the polymer chains; the latter was assented to be operative for these polymers.[43] Increasing the ionic concentration resulted in significant

enhancements of Young's moduli, but the value of Young's moduli of phosphonium triblock copolymers are generally not comparable to styrene-butadiene triblock copolymers.[44] Additionally, with 50 wt% of hard phase, OPCl-containing triblock copolymers exhibited a lower modulus and a longer strain at break compared to the corresponding BPCl-containing polymers (Table 3.3), possibly due to smaller outer block lengths and stronger plasticization from alkyl substituents. The overall shape of the stress-strain curve of poly(OPCl-*b*-*n*BA-*b*-OPCl) exhibited a combination of elastomeric and yield behavior.

Table 3.3. Tensile properties of phosphonium-containing triblock copolymers and non-ionic analogs.

Sample	Calculated M_n from ^{1}H NMR(g/mol) (g/mol)	Hard Phase (wt%)	Tensile Strain at Break (%)	Tensile Stress at Break (25 °C, MPa)	Young's Modulus (25 °C, MPa)
BBB	7.6K-52.7K-7.6K	22	275±10	0.36±0.02	0.20±0.05
	12.9K-52.7K-12.9K	33	186±17	0.40±0.11	0.30±0.07
	35.9K-52.7K-35.9K	58	22.5±0.8	1.10±0.10	12.8±0.8
OBO	29.7K-53.6K-29.7K	53	103±18	0.48±0.12	15.1±2.0
Poly(S-*b*-*n*BA-*b*-S)	21.6K-53.2K-21.6K	45	147±7	0.85±0.33	2.5±0.4

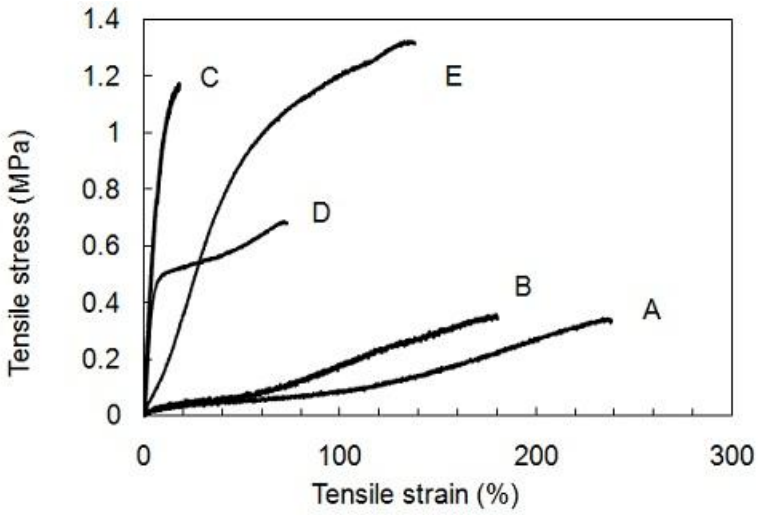

Figure 3.10. Engineering stress-strain curves of triblock copolymers. BBBs: (A) 9 mol%, (B) 15 mol%, (C) 33 mol% of BPCl; OBOs: (D) 21 mol% of OPCl; poly(S-*b*-*n*BA-*b*-S): (E) 50 mol% of styrene.

3.4.6 Morphology

Limited TEM was performed in order to obtain real-space information to complement SAXS experiments. The phosphonium cations with chloride counterions provided weak but sufficient contrast to image samples without use of a staining contrast agent. The morphology of BBB-15, shown in Figure 3.11, is indeterminate but clearly microphase separated. Figure 3.12 shows a lamellar structure of the OBO-21. SAXS was used to investigate microphase separation and to determine, where possible, morphological organization with respect to the degree of microphase separation of the phosphonium-containing block copolymers. X-ray scattering data are shown in Figure 3.12, plotted as intensity, I(q), versus scattering vector, q. Clear Bragg diffraction maxima were observed for the OBO-21 and BBB-15 triblock copolymers, denoting the presence of ordered morphologies. For OBO-21, the maxima were found at q^*, $2q^*$, and approximately $4q^*$, ratios typical of a lamellar morphology. The average lamellar period, $d = 2\pi/q^*$, was

calculated to be approximately 74 nm, which was larger than the expected spacing based on the volume fraction of the outerblocks, suggesting possible phase mixing or other interactions between the blocks. Sample BBB-15 exhibited maxima at q^* and roughly $2q^*$, but the number of Bragg maxima present was insufficient for the identification of an ordered morphology. A very weak feature was visible in the SAXS data for BBB-9, possibly indicating the presence of a disordered nanoscale structure.

The SAXS data provided information on microphase separation that was not wholly consistent with the physical and mechanical characterization data described above. For example, although all samples showed characteristics of microphase separation using DSC, the SAXS data for the OBO-10 and BBB-33 copolymers were featureless. BBB-33 also revealed a clear rubbery plateau in DMA behavior, indicative of the presence of physical crosslinks, and a much greater elastic modulus than the lower ion-content BBB materials.

This lack of clear evidence of microphase separation in the SAXS data, especially for the BBB samples, may be a result of the X-ray scattering characteristics. X-ray scattering contrast is given by the square of the difference of the X-ray scattering length density for each phase, $(\Delta\rho)^2(cm^{-4})$, where ρ is the scattering length density (cm^{-2}). Scattering length density is a function of both composition and mass density. Using density values of 1.0745 g/cm^3 for 100 mol% BPCl (measured), 1.0039 g/cm^3 for 100 mol% OPCl (measured), and 1.08 g/cm^3 for P*n*BA, the X-ray scattering contrast factor $(\Delta\rho)^2$ was calculated to be 8.95×10^{14} cm^{-4} for BPCl and *n*BA, while OPCl and *n*BA had an X-ray scattering contrast factor of 2.61×10^{19} cm^{-4}. For comparison, the X-ray scattering contrast factor for polyisoprene and PS, for which microphase separated block copolymers scatter

X-rays relatively well, is 8.19×10^{19} cm^{-4}, which is more than three times that of OPCl-*n*BA and several orders of magnitude greater than that calculated for BPCl-*n*BA. In addition, the solution casting process for film formation also influences microphase separation, and this may be more significant for the bulkier side groups.

The limited TEM data combined with the SAXS data indicated generally weak microphase separation in these materials. While a complete determination of the thermodynamics of microphase separation for these two sets of block copolymers is beyond the scope of this manuscript. Measurements of the actual functional form of χ for these two series of samples, as well as a more complete understanding of the effect of ionic interactions on morphological behavior in such materials,[45-46] would provide a clearer understanding of the morphological behaviors observed in this study.

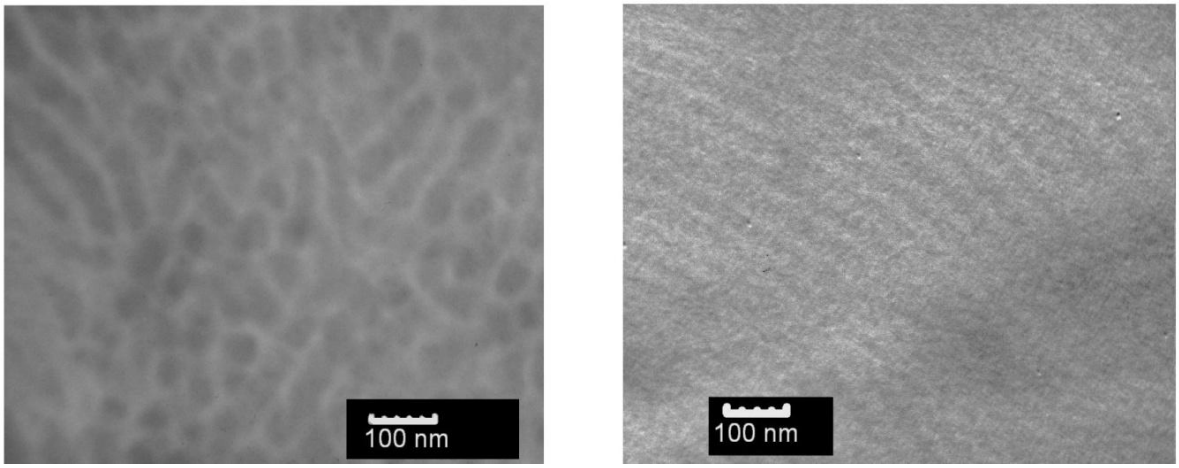

(1) (2)

Figure 3.11. Transmission electron microscopy image of (a) BBB (BPCl: 15 mol%) (b) OBO (OPCl: 21 mol%) without stain.

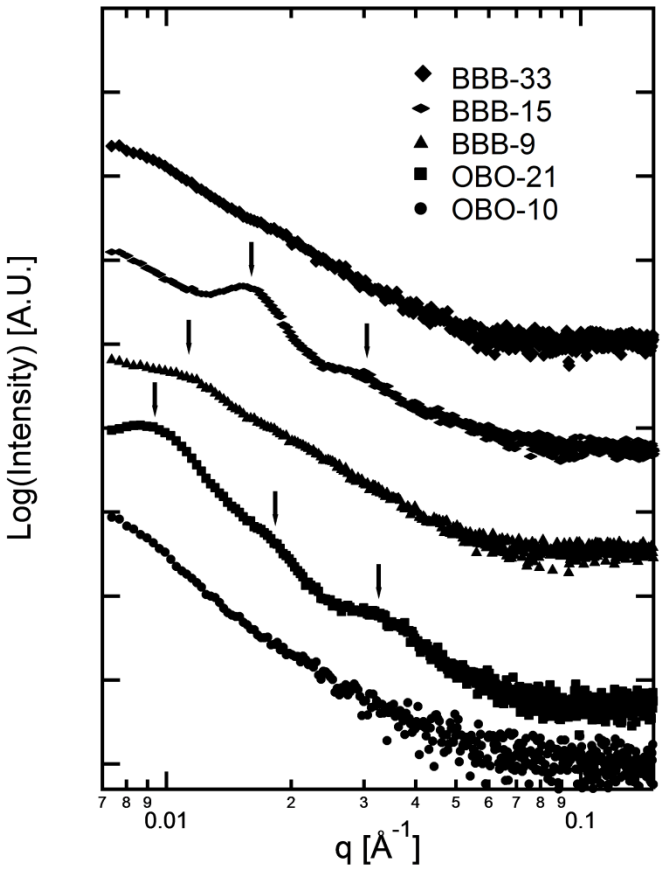

Figure 3.12. X-ray scattering intensity vs scattering vector (*q*) for (a) BBB and (b) OBO.

3.5 Conclusions

Phosphonium cation-containing ABA-type triblock copolymers were synthesized for the first time using nitroxide-mediated polymerization involving a difunctional initiator and a phosphonium ionic liquid monomer. For comparative purposes, phosphonium units with tributyl and trioctyl substituents (BPCl and OPCl) were incorporated into outer blocks respectively, and poly(S-*b*-*n*BA-*b*-S), a noncharged analog, was also synthesized. DMA analyses of phosphonium ion-containing block copolymers and the noncharged analog showed that incorporating phosphonium units afforded microphase separated polymers with a well-defined rubbery plateau. Phosphonium ion-rich domains

microphase separated from amorphous rubbery matrices and evolved to various morphologies clearly shown under TEM and SAXS. The block copolymer containing 15 mol% of BPCl self-assembled into hexagonal cylindrical structures, and the copolymer bearing 21 mol% of OPCl formed lamellae. Their corresponding SAXS peaks systematically shifted to lower q region, indicating an increase of ionic domain size with the length of alkyl substituents. Additionally, block copolymers with tributyl groups required significantly higher activation energy for flow compared to trioctyl groups. The presence of hydrophobic long alkyl chains diluted charge density and decreased the relaxation of the ionic phase. Tensile properties of BPCl-containing triblock copolymers showed an elastomeric behavior, and OPCl-containing triblock copolymers behaved with a combination of elastomeric and yield-like behavior. Polymerized phosphonium ionic liquids offer potential as polymer biocides and ion conductive membranes. The self-assembly of amphiphilic phosphonium units in block copolymer systems resulted in well-defined microphases and tuned flow behaviors, which provide potential routs for alkaline fuel cell membrane and melt processing applications.

3.6 Acknowledgements

Acknowledgment is made to the Donors of the American Chemical Society Petroleum Research Fund for partial support of this research. Parts of this work were carried out using instruments in the Nanoscale Characterization and Fabrication Laboratory, a Virginia Tech facility operated by the Institute for Critical Technology and Applied Science (ICTAS). The authors thank Steve McCartney and John McIntosh at Virginia Tech ICTAS for their help with TEM imaging. We also acknowledge funding from NSF (CHE-0722638) for the acquisition of our Agilent 6220 LC-TOF-MS. This

material is based upon work supported by the U.S. Army Research Laboratory and the U.S. Army Research Office under contract/grant number W911NF-07-1-0452 Ionic Liquids in Electro-Active Devices Multidisciplinary University Research Initiative (ILEAD MURI).

3.7 References

1. Mitsukami, Y.; Donovan, M. S.; Lowe, A. B.; McCormick, C. L. *Macromolecules* **2001,** 34, 2248-2256.
2. Lowe, A. B.; McCormick, C. L. *Prog. Polym. Sci.* **2007,** 32, 283-351.
3. Elabd, Y. A.; Hickner, M. A. *Macromolecules* **2010,** 44, (1), 1-11.
4. Singh, M.; Odusanya, O.; Wilmes, G. M.; Eitouni, H. B.; Gomez, E. D.; Patel, A. J.; Chen, V. L.; Park, M. J.; Fragouli, P.; Iatrou, H.; Hadjichristidis, N.; Cookson, D.; Balsara, N. P. *Macromolecules* **2007,** 40, (13), 4578-4585.
5. Floudas, G.; Vazaiou, B.; Schipper, F.; Ulrich, R.; Wiesner, U.; Iatrou, H.; Hadjichristidis, N. *Macromolecules* **2001,** 34, (9), 2947-2957.
6. Elabd, Y. A.; Napadensky, E.; Walker, C. W.; Winey, K. I. *Macromolecules* **2006,** 39, (1), 399-407.
7. Park, M. J.; Balsara, N. P. *Macromolecules* **2008,** 41, (10), 3678-3687.
8. Eisenberg, A.; Hird, B.; Moore, R. B. *Macromolecules* **1990,** 23, (18), 4098-4107.
9. Saito, T.; Mather, B. D.; Costanzo, P. J.; Beyer, F. L.; Long, T. E. *Macromolecules* **2008,** 41, (10), 3503-3512.
10. Bernard, M.; Ford, W. T.; Taylor, T. W. *Macromolecules* **1984,** 17, (9), 1812-1814.
11. Takeuchi, K.; Shimura, S.; Kanazawa, A.; Iijima, T. JP Patent 92-358552. 1994.

12. Kenawy, E. R.; Worley, S. D.; Broughton, R. *Biomacromolecules* **2007,** 8, 1359-1384.

13. Gong M., L. C.-W., Joo S-W. *J. Mater. Sci.* **2002,** 37, 4615-4620.

14. Hatakeyama, E. S.; Ju, H.; Gabriel, C. J.; Lohr, J. L.; Bara, J. E.; Noble, R. D.; Freeman, B. D.; Gin, D. L. *J. Membr. Sci.* **2009,** 330, 104-116.

15. Moore, C. M.; Hackman, S.; Brennan, T.; Minteer, S. D. *J. Membr. Sci.* **2005,** 254, 63-70.

16. Gu, S.; Cai, R.; Luo, T.; Chen, Z.; Sun, M.; Liu, Y.; He, G.; Yan, Y. *Angew. Chem., Int. Ed.* **2009,** 48, (35), 6499-6502.

17. Wathier, M.; Grinstaff, M. W. *J. Am. Chem. Soc.* **2008,** 130, (30), 9648-9649.

18. Bradaric, C. J.; Downard, A.; Kennedy, C.; Robertson, A. J.; Zhou, Y., Industrial Preparation of Phosphonium Ionic Liquids. In *ACS Symposium Series*, 2003; Vol. 856, pp 41-56.

19. Ghassemi, H.; Riley, D. J.; Curtis, M.; Bonaplata, E.; McGrath, J. E. *Appl. Organomet. Chem.* **1998,** 12, 781-785.

20. Kenawy, E.-R.; Abdel-Hay, F. I.; Shahada, L.; El-Raheem, A.; El-Shanshoury, R.; El-Newehy, M. H. *J. Appl. Polym. Sci.* **2006,** 102, (5), 4780-4790.

21. Williams, S. R.; Wang, W.; Winey, K. I.; Long, T. E. *Macromolecules* **2008,** 41, (23), 9072-9079.

22. Parent, J. S.; Penciu, A.; Guillen-Castellanos, S. A.; Liskova, A.; Whitney, R. A. *Macromolecules* **2004,** 37, (20), 7477-7483.

23. Coessens, V.; Matyjaszewski, K. *J. Macromol. Sci., Chem.* **1999,** 36, (5&6), 653-666.

24. Wang, R.; Lowe, A. B. *J. Polym. Sci., Part A: Polym. Chem.* **2007,** 45, (12), 2468-2483.

25. Nonaka, T.; Li, H.; Makinose, K.; Ogata, T.; Kurihara, S. *J. Appl. Polym. Sci.* **2003,** 90, (4), 1139-1147.

26. Nonaka, T.; Li, H.; Ogata, T.; Kurihara, S. *J. Appl. Polym. Sci.* **2003,** 87, (3), 386-393.

27. Yoshida, E.; Naito, T. *Colloid Polym. Sci.* **2008,** 286, 1203-1207.

28. Mather, B. D.; Baker, M. B.; Beyer, F. L.; Green, M. D.; Berg, M. A. G.; Long, T. E. *Macromolecules* **2007,** 40, (13), 4396-4398.

29. Moad, G.; Rizzardo, E.; Thang, S. H. *Accounts of Chemical Research* **2008,** 41, (9), 1133-1142.

30. Matyjaszewski, K.; Muller, A. H. E. *Prog. Polym. Sci.* **2006,** 31, 1039-1040.

31. Grimaldi, S.; Finet, J. P.; Le Moigne, F.; Zeghdaoui, A.; Tordo, P.; Benoit, D.; Fontanille, M.; Gnanou, Y. *Macromolecules* **2000,** 33, 1141-1147.

32. Mather, B. D.; Baker, M. B.; Beyer, F. L.; Berg, M. A. G.; Green, M. D.; Long, T. E. *Macromolecules* **2007,** 40, 6834-6845.

33. Kanazawa, A.; Ikeda, T.; Endo, T. *J. Polym. Sci., Part A: Polym. Chem.* **1993,** 31, (2), 335-43.

34. Ilavsky, J.; Jemian, P. R. *Journal of Applied Crystallography* **2009,** 42, 347-353.

35. Weiss, R. A.; Sen, A.; Willis, C. L.; Pottick, L. A. *Polymer* **1991,** 32, (10), 1867-1874.

36. Stokes, K. K.; Orlicki, J. A.; Beyer, F. L. *Polym. Chem.* **2011,** 2, 80-82.

37. Mather, B. D.; Baker, M. B.; Beyer, F. L.; Berg, M. A. G.; Green, M. D.; Long, T. E. *Macromolecules* **2007,** 40, 6834-6845.

38. Weiss, R. A. *J. Appl. Polym. Sci.* **1984,** 29, (9), 2719-2734.

39. Page, K. A.; Cable, K. M.; Moore, R. B. *Macromolecules* **2005,** 38, 6472-6484.

40. Gauthier;, S.; Eisenberg, A. *Macromolecules* **1987,** 20, 760-767.

41. Gielding-Russel, G. S.; Pillai, P. S. *Polymer* **1977,** 18, 859.

42. Loveday, D.; Wilkes, G. L.; Deporter, C. D.; McGrath, J. E. *Macromolecules* **1995,** 28, 7822-7830.

43. Noshay, A.; McGrath, J. E., *Block copolymers : overview and critical survey* Academic Press, New York 1977; p 516.

44. Bagrodia, S.; Wilkes, G. L. *J. Biomed. Mater. Res.* **1976,** 10, 101-111.

45. Zhou, N. C.; Burghardt, W. R.; Winey, K. I. *Macromolecules* **2007,** 40, 6401-6405.

46. Tan, N. C. B.; Liu, X.; Briber, R. M.; Peiffer, D. G. *Polymer* **1995,** 36, (10), 1969-1973.

Chapter 4: Conventional Free Radical Polymerization of Phosphonium Ionic Liquid Monomers

Shijing Cheng, Mingqiang Zhang, Tianyu Wu, Sean T. Hemp, Brian D. Mather, Robert B. Moore, and Timothy E. Long*

Journal of Polymer Science: Part A Polymer Chemistry, submitted

4.1 Abstract

Copolymers of *n*-butyl acrylate and phosphonium ionic liquid (IL) monomers possessing various alkyl substituents and counterions were synthesized through a combination of conventional free radical copolymerization and anion-exchange. Differential scanning calorimetry (DSC) and dynamic mechanical analysis (DMA) provided the thermal and mechanical properties of these phosphonium-cation containing random copolymers. Factors including alkyl chain length of phosphonium substituents, counterion type, as well as ionic concentration significantly influenced the association of phosphonium cations. Phosphonium ionomers with trialkyl substituents on phosphonium cations did not display the characteristic small-angle X-ray scattering (SAXS) peak, suggesting the absence of ionic clusters. However, low *q* peaks in wide-angle X-ray diffraction (WAXD) was indicative of significant concentration fluctuations wherein the ionic monomeric units associated.

4.2 Introduction

Ionic liquids (ILs) are typically organic salts chemically composed of an organic cation (e.g., imidazolium, pyridinium, quaternary ammonium and phosphonium) and an anion, such as halide, tetrafluoroborate, hexafluorophosphate, triflate, amidotriflate, and bis(trifluorosulfonyl)imide.[1-3] Due to their unique physicochemical properties, such as

low melting points, low vapor pressures, and high ion conductivities, ILs are currently receiving increased attention.[4-6] Polymeric ILs display structural and fluid dynamics that differ from low molar mass ionic liquids and offer broad potential applications as biosensors,[7-8] high CO_2-absorbing polymers,[9] solid-state polyelectrolytes,[10] and microwave absorbing materials.[11] Most research on polymerizable ILs has focused on imidazolium-based ionic liquid monomers,[12-18] and Ohno et al. have widely reported the synthesis of imidazolium polymerizable ionic liquids and related polycations.[19-22] In comparison to ILs where both cations and anions are mobile, constraining cationic or anionic centers in repeat units sacrifices ionic conductivity to some extent in polymerized ILs. Recent efforts on overcoming this drawback include incorporating flexible spacers in the monomers between the polymerizable site and ionic functionalities and/or anion-exchange reactions directly on the polymer to enhance counterion mobility. Winey and coworkers investigated the ionic conductivity-structure relationship of imidazolium ionic liquid random copolymers,[23] and they found the random copolymers of *n*-hexyl methacrylate and imidazolium-based methacrylate microphase separated; microphase separation as well as segmental motion both impacted ion mobility.

Phosphonium cation-based ILs potentially offer superior properties, such as higher thermal stabilities, higher conductivities, and lower viscosities compared to the corresponding ammonium ILs,[24] but this class of ILs has received less attention. The research interest of phosphonium-containing polymers particularly focused on for their antimicrobial property,[25] less humidity sensitivity,[26-27] and tunable hydrophilicity.[28-31] Varying counterions and chain lengths of alkyl substituents on phosphonium cations readily tailor polymer hydrophilicity and antimicrobial properties. For example, McGrath

et al. reported the synthesis of poly(arylene ether) main-chain phosphonium ionomers for high-performance applications including ion-exchange membranes and conductive polymers.[32] The synthesis of phosphonium-containing polymers utilizes either postpolymerization modification[33-34] or conventional radical polymerization of styrenic,[35] acrylate,[30] or methacrylate[29, 36] phosphonium-containing monomers. Parent et al. quaternized poly(isobutylene-*co*-isoprene) bromide with triphenylphosphine and first demonstrated ionic aggregation of phosphonium bromide units using dynamic mechanical and dilute solution viscosity analyses.[34] Our research group also recently reported that the presence of phosphonium cations interfered with hydrogen bonding association in poly(tetramethylene oxide)-based polyurethanes.[37]

In this study, phosphonium IL random copolymers were synthesized and their structure-property relationships were investigated as a function of copolymer composition. The random copolymers consisted of *n*-butyl acrylate with styrenic comonomers containing phosphonium cations bearing chlorine (Cl), tetrafluoroborate (BF_4), or bis(trifluoromethane sulfonyl)imide (TFSI) anions. Dynamic mechanical properties and morphologies of all copolymers were investigated as a function of ionic concentration to probe the effect of counterions and alkyl chain lengths on thermal and mechanical properties.

4.3 Experimental

4.3.1 Materials

Trioctylphosphine (90%), 4-vinylbenzyl chloride (90%), 2,6-di-*tert*-butyl-4-methylphenol (99%), sodium tetrafluoroborate ($NaBF_4$) (98%), and lithium bis(trifluoromethane sulfonyl)imide (LiTFSI) (99%) were purchased from Aldrich and

used without further purification. *n*-Butyl acrylate (99%) was purchased from Aldrich and was vacuum distilled from calcium hydride. α,α'-Azobis(isobutyronitrile) (AIBN) (from Fluka) was recrystallized from methanol. Hexanes (Fisher Scientific, HPLC grade), tetrahydrofuran (THF) (Fisher Scientific, HPLC grade), and *N*,*N*-dimethylformamide (DMF) (Fisher Scientific, HPLC grade, anhydrous) were used as received. Trioctyl-4-vinylbenzyl phosphonium chloride[38] (OPCl) and tributyl-4-vinylbenzyl phosphonium chloride[38] (BPCl) were synthesized according to the previous literature.

4.3.2 Instrumentation

^{1}H NMR and ^{31}P NMR spectra were collected in $CDCl_3$ or CD_2Cl_2 on a Varian INOVA spectrometer operating at 400 MHz 23 °C. Fast Atom Bombardment Mass Spectrometry (FAB-MS) was conducted in positive ion mode on a JEOL HX110 dual focusing mass spectrometer. Size exclusion chromatography (SEC) was used to determine the molecular weights of phosphonium-containing random copolymers at 50 °C in DMF with 0.05 M lithium bromide (LiBr) at 1 mL/min. DMF SEC was performed on a Waters SEC equipped with two Waters Styragel HR5E (DMF) columns, a Waters 717plus autosampler, and a Waters 2414 differential refractive index detector. Reported molecular weights are relative to polystyrene standards.

Differential scanning calorimetry (DSC) was performed under a nitrogen flush of 50 mL/min at a heating rate of 10 °C/min on a TA instruments Q1000^{TM} DSC, which was calibrated using indium (mp = 156.60 °C) and zinc (mp = 419.47 °C) standards. Glass transition temperatures were measured as the midpoint of the transition in the second heating scan. Dynamic mechanical analysis (DMA) was conducted on a TA Instruments Q800 Dynamic Mechanical Analyzer in tension mode at a frequency of 1 Hz, an

oscillatory amplitude of 15 μm, and a static force of 0.01 N. The temperature ramp was 3 °C/min. The glass transition temperature (T_g) was determined at the peak maximum of the tan δ curve. X-ray photoelectron spectroscopy (XPS) was performed using an XSAM-800 spectrometer. The spectrometer was equipped with a MgK_α achromatic X-ray source (20 kV, 10 mA), and a take-off angle of 30° was used.

WAXD was performed using Rigaku S-Max 3000 pinhole SAXS system. X-ray source was the Cu K_α radiation, and the wavelength was 0.154 nm. The sample-to-detector distance was 80 mm. A Fuji HR-V imaging plate was used to collect the two-dimensional images with an exposure time of 1 h. The imaging plate was scanned using a RAXIA-Di system, and Rigaku's SAXSGUI software package provided a plot of intensity versus scattering angle, 2θ.

4.3.3 Anion Exchange Reaction of Phosphonium Ionic Liquid

A typical synthesis of trioctyl-4-vinylbenzyl phosphonium tetrafluoroborate ($OPBF_4$) or trioctyl-4-vinylbenzyl phosphonium bis(trifluoromethane sulfonyl)imide (OPTFSI) was performed as follows. A solution of 6 g of sodium tetrafluoroborate in 200 mL of anhydrous acetone and a solution of 1 g of OPCl in 10 mL of anhydrous acetone was mixed in a 250-mL, round-bottomed flask. After stirring overnight at room temperature, the resulting cloudy solution was filtered and the filtrate was vacuum stripped and redissolved in 100 mL of dichloromethane and washed with DI H_2O (3×100 mL). The obtained ionic liquid was evaluated with silver nitrate and a silver chloride precipitate was not observed, indicating the absence of chloride anions. The product was dried under reduced pressure at 30 ^oC for 2 days until constant weight. (Yield of OPBF4: 68%; yield of OPTFSI: 71%) Tributyl-4-vinylbenzyl phosphonium tetrafluoroborate (BPBF4) and

tributyl-4-vinylbenzyl phosphonium bis(trifluoromethane sulfonyl)imide (BPTFSI) were synthesized according to the literature.[25]

4.3.4 Synthesis of Phosphonium-Containing Random Copolymers

Poly(*n*BA-*co*-OPCl) and poly(*n*BA-*co*-BPCl) random copolymers were synthesized using conventional free radical polymerization with AIBN as the initiator in DMF solution. A typical synthesis was performed as follows. OPCl (1 g, 1.91 mmol) was weighed into a 100-mL round-bottomed flask containing a magnetic stirbar. The flask was sealed with a rubber septum and purged with N_2 for 20 min. Then anhydrous DMF (20 mL, 20 wt% of solid) was added to the flask to dissolve the phosphonium-containing monomers. Purified *n*-butyl acrylate (4 mL, 28.0 mmol) was syringed into the reaction flask. Lastly, AIBN (10 mg, 0.22 wt%) was dissolved in 5 mL of anhydrous DMF and flushed with dry nitrogen for 10 min, and was then syringed into the reaction mixture. The reaction flask was placed in an oil bath at 60 °C for 24 h with constant stirring. After the polymerization, DMF was removed upon vacuum distillation. The product was redissolved in THF (25 mL) and precipitated into hexanes (800 mL). The final products were dried at 50 °C under reduced pressure (0.5 mm Hg) for 24 h. The product contained 4 mol% OPCl and 96 mol% *n*BA, with a yield of 82%.

4.3.5 Anion Exchange Reaction of Phosphonium-Containing Random Copolymers

A typical anion exchange of Cl with BF_4 or TFSI anions in phosphonium-containing polymers was conducted as follows. 6 g (excess) of sodium tetrafluoroborate was dissolved in 200 mL of dichloromethane; 1 g of phosphonium-containing polymer was dissolved in 10 mL of dichloromethane. The two solutions were then mixed in a 250-mL, round-bottomed flask and stirred overnight at room temperature. The resulting cloudy

solution was filtered and the filtrate was washed with DI H_2O (3×100 mL) and evaluated with silver nitrate. A silver chloride precipitate was not observed, indicating the absence of chloride anions. Finally, dichloromethane was removed with a roto-evaporator and the product was dried under reduced pressure at 30 °C for 2 d until constant weight. BPCl homopolymer was water soluble and the anion exchange reaction was carried out in DI water with the addition of sodium tetrafluoroborate aqueous solution. The resulting precipitates were isolated.

4.4 Results and Discussion

Phosphonium chloride monomers substituted with either trioctyl or tributyl groups were readily synthesized upon alkylation in a single step. Tributyl-4-vinylbenzyl phosphonium chloride (BPCl) was water soluble, whereas trioctyl-4-vinylbenzyl phosphonium chloride (OPCl) was soluble only in organic solvents. Thus, as expected, monomers possessing shorter hydrophobic alkyl chains were relatively more hydrophilic. A subsequent anion-exchange of OPCl with $NaBF_4$ generated a waxy solid with a melting point of 36 °C (OPBF4), and upon exchanging with TFSI, the resulting monomer was a liquid at room temperature (OPTFSI). XPS analyses (error 0.1%) of the anion-exchanged monomers confirmed the absence of chloride in all cases. The melting points of trioctylphosphonium monomers were all below 100 °C and decreased in the order of larger counterions: OPCl>OPBF4>OPTFSI (Table 4.1). Therefore, these monomers were classified as polymerizable ionic liquids, and the anion-exchanged monomers did not dissolve in non-polar solvents such as hexanes, in contrast to the precursor OPCl. This counterion-dependent solubility suggested that the association between the phosphonium cation and large anions, such as TFSI, was relatively weak. This observation also

correlated well with the change of chemical shift in ^{1}H NMR spectra (Figure 4.1), and the chemical shift of -CH_2 groups adjacent to the phosphonium cations showed an upfield shift upon anion exchange (OPCl>OPBF4>OPTFSI), indicating enhanced shielding effects of larger counterions.[39] In addition, large counterions also influenced the chemical shift of the aromatic protons, which split the peak into two equal intensities with upfield and downfield shift, respectively.

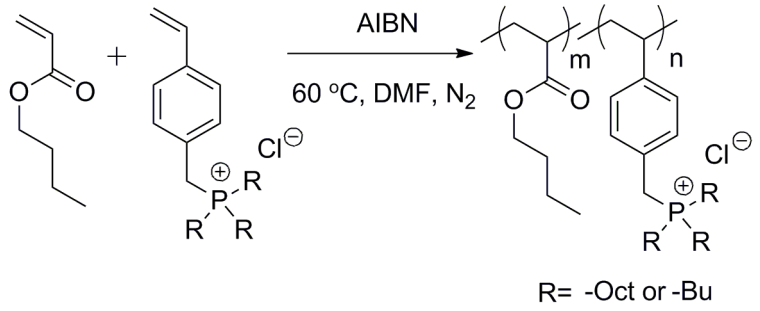

Scheme 4.1. Synthesis of phosphonium-containing random copolymers

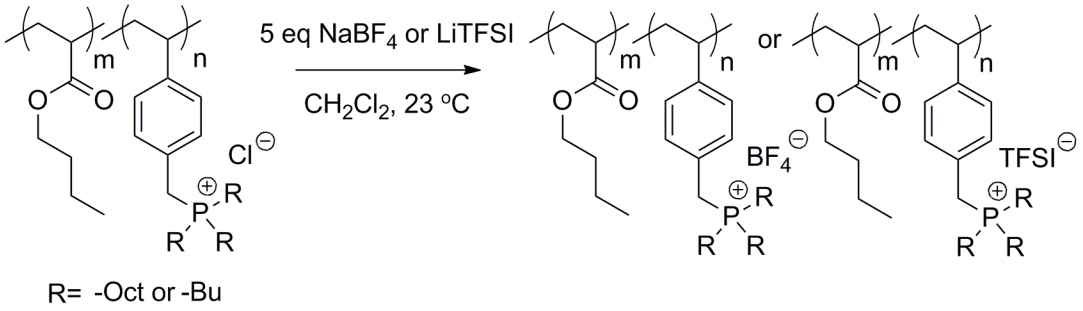

Scheme 4.2. Anion exchange of phosphonium-containing random copolymers

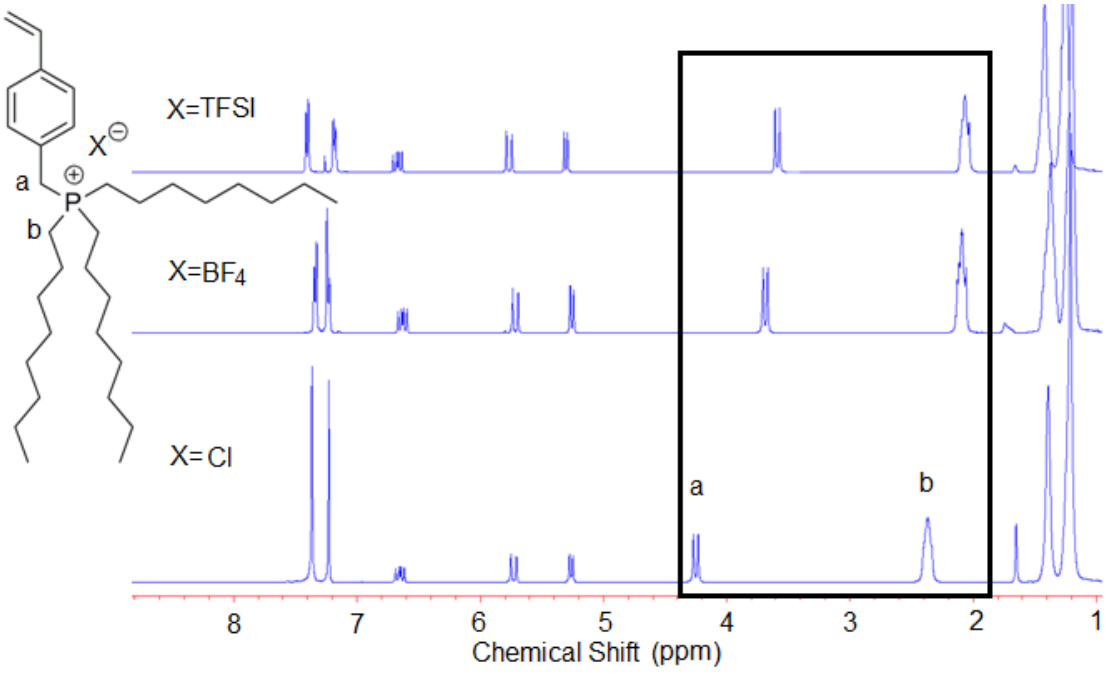

Figure 4.1. ^{1}H NMR spectra of polymerizable phosphonium ionic liquids with various counterions

Table 4.1. Thermal characterization of trialkyl-4-vinylbenzyl phosphonium monomers and homopolymers

Name	R	X	Monomer T_d (°C)[a]	Monomer T_m (°C)[b]	Homopolymer T_g (°C)[b]
BPCl	Butyl	Cl	363	125	176
BPBF4	Butyl	BF_4	ND	ND	145
BPTFSI	Butyl	TFSI	ND	ND	67
OPCl	Octyl	Cl	363	87	78
OPBF4	Octyl	BF_4	375	36	63
OPTFSI	Octyl	TFSI	426	<-90	30

a: TGA: 10 °C/min
b: DSC: 10 °C/min
ND= not determined

Table 4.2. Molecular weight characterization of poly(*n*BA-*co*-OPCl)s

OPCl in feed (mol%)	OPCl in polymer (mol%)	OPCl in polymer (wt%)	M_w by SEC ($g/mol \times 10^{-3}$)	M_w/M_n
3	4	14	146	1.72
12	17	45	137	1.67
26	30	63	126	2.42
38	45	77	80	1.75
100	100	100	118	2.62

Table 4.3. Molecular weight characterization of poly(*n*BA-*co*-BPCl)s

BPCl in feed (mol%)	BPCl in polymer (mol%)	BPCl in polymer (wt%)	M_w by SEC ($g/mol \times 10^{-3}$)	M_w/M_n
8	10	23	103	1.74
18	21	43	141	1.78
28	30	55	153	1.83
43	49	73	159	1.89
100	100	100	118	1.66

The thermal stabilities of the phosphonium IL monomers were investigated using TGA under N_2 atmosphere. OPCl decomposed in a single step at 363 °C. Replacing the Cl anion with BF_4 resulted in a slightly higher decomposition temperature at 375 °C, and OPTFSI exhibited the highest T_d (426 °C) (Table 4.1). Thermal degradation temperatures of phosphonium IL monomers increased with counterion size and decreased basicity, which was also reported for imidazolium ionic liquids. The improved thermal stability also suggested the potential for phosphonium polymers in high-temperature electrochemical devices.

Scheme 4.1 depicts the synthetic strategy for poly(OPCl), poly(OPBF4), poly(OPTFSI), poly(*n*BA-*co*-OPCl), and poly(*n*BA-*co*-BPCl) random copolymers. The mole fraction of phosphonium units in the copolymers was calculated by measuring the integral peak height of total aromatic protons to vinyl protons (2H, O-CH_2-; 2H, ϕ-CH_2-P). The copolymers had similar compositions to the feed, indicating successful copolymerization. In the anion-exchange of poly(*n*BA-*co*-OPCl) with $NaBF_4$ or LiTFSI, the concentrations of $NaBF_4$ or LiTFSI were in large excess in order to fully exchange the Cl anions (Scheme 4.2). Polymer solutions were subsequently filtered and extensively washed with DI water to remove the byproduct of NaCl or LiCl. XPS analysis of the anion-exchanged products showed that residual Cl concentration was below 0.1%. Anion-exchange of the copolymers afforded a series of polymers with an identical degree of polymerization (Tables 4.2 and 4.3). Although these polymers generally present difficulties in terms of molecular weight determination, size exclusion chromatography (SEC) using 0.05 M LiBr in DMF in a system calibrated with polystyrene standards afforded relative molecular weights as summarized in Table 4.1. Dynamic light scattering was performed prior to SEC to identify the optimal solvent composition and ensure minimal aggregation in DMF with LiBr.

The tensile storage modulus (G') and tanδ versus temperature from DMA for the phosphonium-containing polymers are depicted in Figures 4.2 and 4.3. For poly(*n*BA-*co*-OPCl)s with an ionic content of 17 and 30 mol%, the storage moduli gradually decreased from -60 °C. A sudden decrease of G' occurred at 20 °C with 17 mol% of OPCl, indicating polymer flow. When ionic concentration increased to 30 mol%, a very short rubbery plateau exhibited at 55 °C before complete flow occurred; the tanδ peak also

showed a shoulder at 30 °C. These results suggested that increasing ionic concentration led to an increase in G' and extended rubbery plateau due to ionic association. In comparison to poly(*n*BA-*co*-OPCl)s, shorter alkyl chains on phosphonium cations resulted in significantly different thermomechanical behavior. BPCl homopolymer had a glass transition at 176 °C by DSC, which was significantly higher than OPCl homopolymer (Table 4.1). This increase of T_g was ascribed to shortened alkyl substituents on phosphonium cations, which promoted electrostatic interactions of phosphonium ion pairs in relatively nonpolar polymer matrices. A similar trend was also observed in ammonium neutralized sulfonated polystyrene by Weiss et al[40] and in phosphonium-containing Nafion® membranes by Moore et al.,[41] i.e., relaxation temperature decreased with increasing alkyl substituent length. Poly(*n*BA-*co*-BPCl)s formed free-standing films with an ionic concentration as low as 10 mol%. The G' dependence on ionic concentration for poly(*n*BA-*co*-BPCl)s was similar to poly(*n*BA-*co*-OPCl)s and G' increased with ionic concentration, however, the flow temperature for poly(*n*BA-*co*-BPCl) was higher at similar ionic concentration. G' started to decrease at -22 °C, with a less-well defined rubbery plateau that extended to 50 °C for the sample containing 10 mol% of BPCl and 80 °C for 21 mol% of BPCl. The plateau was attributed to ionic association, while the second relaxation at 50~80 °C presumably corresponded to ion-pair dissociation upon heating. The microphase separation behavior was also observed in the tanδ behavior, which revealed two distinct maxima. The first peak corresponded to the glass transition of the matrix phase remained near -20 °C, and the second peak for ionic phase shifted to higher temperature with increasing ionic concentration. These results agreed with those observed in the previous mechanical

relaxation study of metal-salts neutralized poly(ethylene-*co*-methacrylic acid) ionomers.[42-43] Specifically, the β relaxation stayed at nearly the same temperature, and the α relaxation, associated with a glass-rubber transition of the ionic clusters,[43] shifted to higher temperatures with increasing neutralization. The presence of two distinct relaxation modes were unique for poly(*n*BA-*co*-BPCl)s, due to efficient association between tributyl phosphonium units in comparison to trioctyl phosphonium units.

Figure 4.4 reveals the counterion influence on DMA curves of poly(*n*BA-*co*-OPCl) at 30 mol% ionic concentration. After anion exchange, the tanδ peak at 60 °C shifted to 50 °C for BF_4 anion and 30 °C for TFSI anion. For the corresponding phosphonium-containing homopolymers, anion exchange of the Cl anion with BF_4 significantly reduced T_g from 87 °C to 63 °C; replacing the Cl anion with TFSI further reduced T_g to 30 °C and imparted the polymer with pronounced flow character (Table 4.1). This glass transition shifted toward lower temperatures possibly due to large delocalized counterions hindering ionic association and enhancing macromolecular mobility.[41] Poly(*n*BA-*co*-BPCl)s exhibited similar behavior, i.e. flow occurred earlier for larger counterions (Figure 4.5). However, interestingly, replacing Cl anions with either BF_4 or TFSI did not influence the first tanδ maximum at -20 °C for poly(*n*BA-*co*-BPCl)s, suggesting persistent microphase separation.

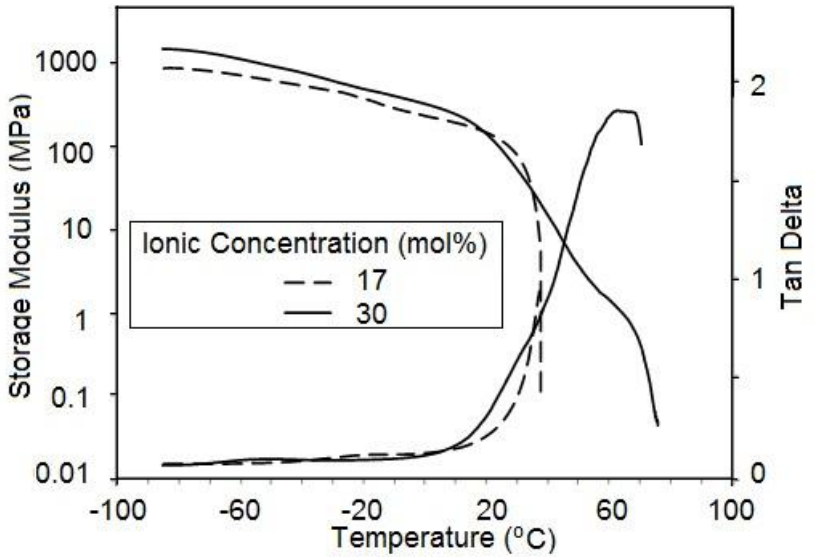

Figure 4.2. Dynamic mechanical temperature sweep for poly(*n*BA-*co*-OPCl)s with 17 mol% and 30 mol% of OPCl respectively

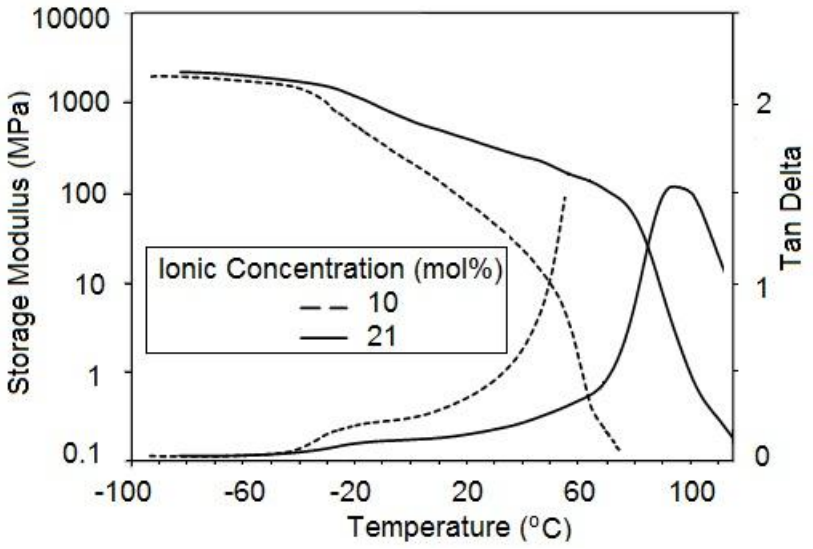

Figure 4.3. Dynamic mechanical temperature sweep for poly(*n*BA-*co*-BPCl)s with 10 mol% and 21 mol% of BPCl respectively

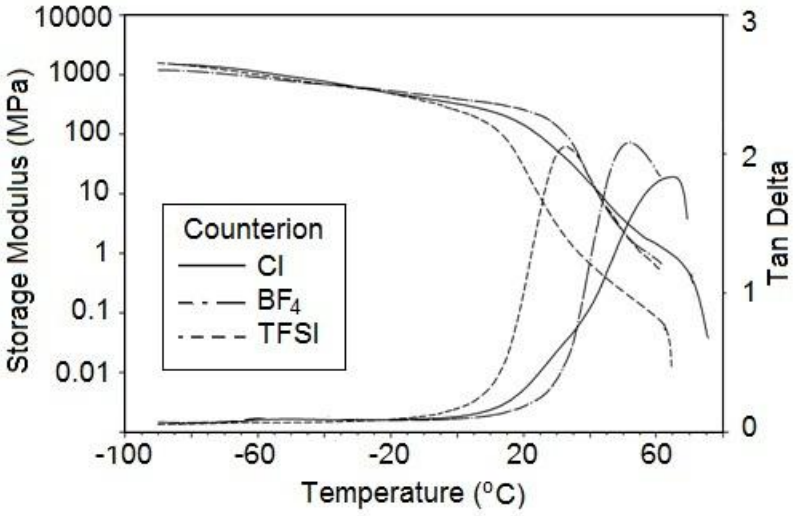

Figure 4.4. Dynamic mechanical temperature sweep for poly(*n*BA-*co*-OPCl)s with 30 mol% of OPCl after anion exchange reaction

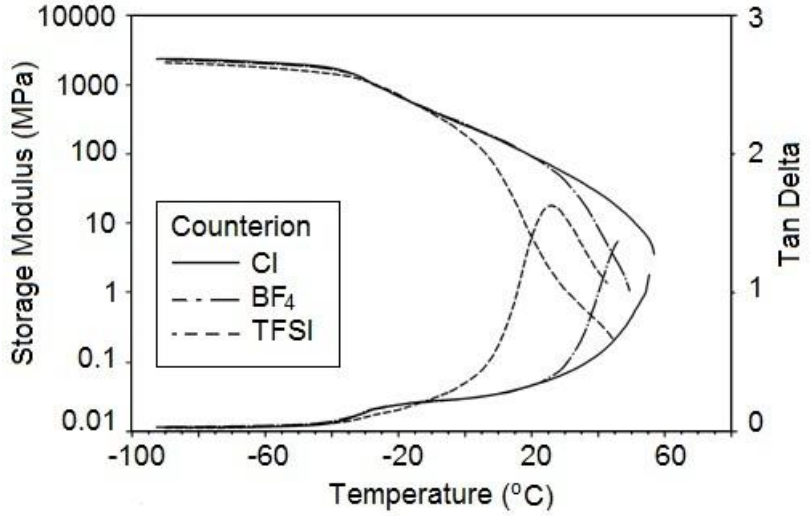

Figure 4.5. Dynamic mechanical temperature sweep for poly(*n*BA-*co*-BPCl)s with 10 mol% of BPCl after anion exchange reaction

WAXD measurements were performed at room temperature on the identical polymer films used for DMA analysis, which were slowly cast from dilute solution in order to achieve equilibrium or near-equilibrium morphologies. All of the diffraction profiles were shown in Figures 4.6 and 4.7. In comparison to polystyrene,[44] the diffraction

patterns of phosphonium-containing homopolymers displayed two new diffraction peaks at 2θ=3.76° and 5.81° for OPCl homopolymer, which corresponded to the non-interdigitated packing and interdigitated packing of octyl chains on phosphonium cations, respectively.[45] In comparison to the diffraction peaks of OPCl homopolymer, the non-interdigitated (2θ=4.79°) and interdigitated packing peaks (2θ=7.87°) for BPCl homopolymer were present at higher angles, due to shorter alkyl chain length. This ionic correlation length has been demonstrated in phosphonium and ammonium liquid crystallines.[45-47] In particular, Weiss et al. reported that an ammonium halide molecule with three equivalent long *n*-alkyl chains consisted of alternating interdigitated and non-interdigitated regions of alkyl chains separated by ionic planes.[47] Two alkyl substituents per molecule extended to one side in a non-interdigitated region. The third chain was located on the opposite side of the ionic plane and paired intermolecularly to form an adjacent, interdigitated region. A representative cartoon of the polymer morphology is shown in Figure 4.8. More interestingly, anion exchange of Cl with large counterions resulted in a higher angle shift of both non-interdigitated and interdigitated packing for the corresponding homopolymers (Table 4.4), presumably due to more chain tilting and shorter distance between ionic planes.[48]

The diffraction patterns of OPCl- and BPCl-containing random copolymers simply exhibited two diffraction peaks as shown in Figures 4.6.1 and 4.6.2. For poly(*n*BA-*co*-OPCl)s, the two peaks were observed at 2θ=5.0° and 20.0°, and for poly(*n*BA-*co*-BPCl)s, the two peaks were observed at 2θ=7.3° and 20.1°. The second diffraction peak (amorphous halo) at near 2θ=20° was attributed to van der Waals packing (VDW peak) of P*n*BA.[49] The first peak near 5.0° and 7.3° displayed in the intermediate spacing

corresponded to a combination of non-interdigitated packing and interdigitated packing of alkyl substituents on phosphonium cations. For poly(*n*BA-*co*-OPCl) possessing longer alkyl substituents, this peak displayed at a lower-angle region, which was consistent with the previous observation of BPCl and OPCl homopolymers. In addition, the peak shift dependence on counterions also correlated well with the results of the corresponding homopolymers (Table 4.4), indicating the association of phosphonium monomeric units and local heterogeneity within phosphonium-containing random copolymers.

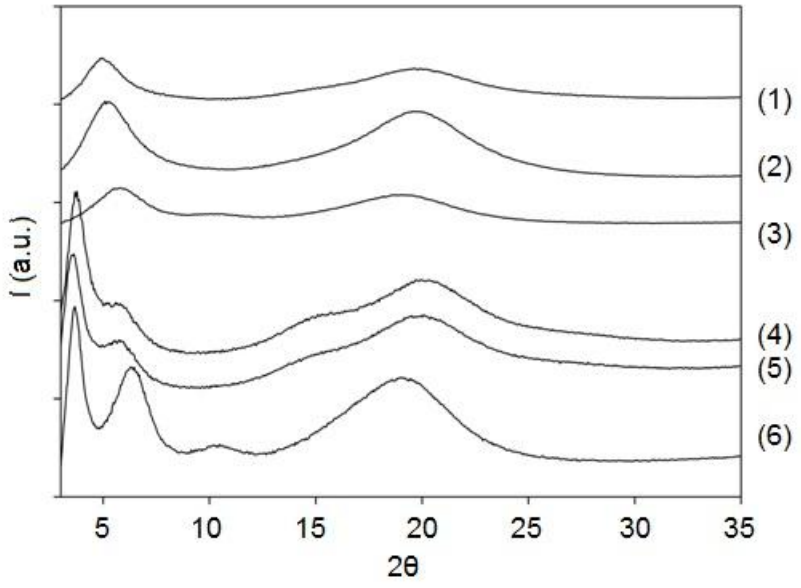

Figure 4.6. Wide angle X-ray diffraction profiles of poly(*n*BA-*co*-OPCl) (1) anion-exchanged with BF_4^- (2) and $TFSI^-$ (3) and OPCl homopolymer (4) anion-exchanged with BF_4^- (5) and $TFSI^-$ (6). The X-ray scattering intensity was shifted to display the influence of counterion type.

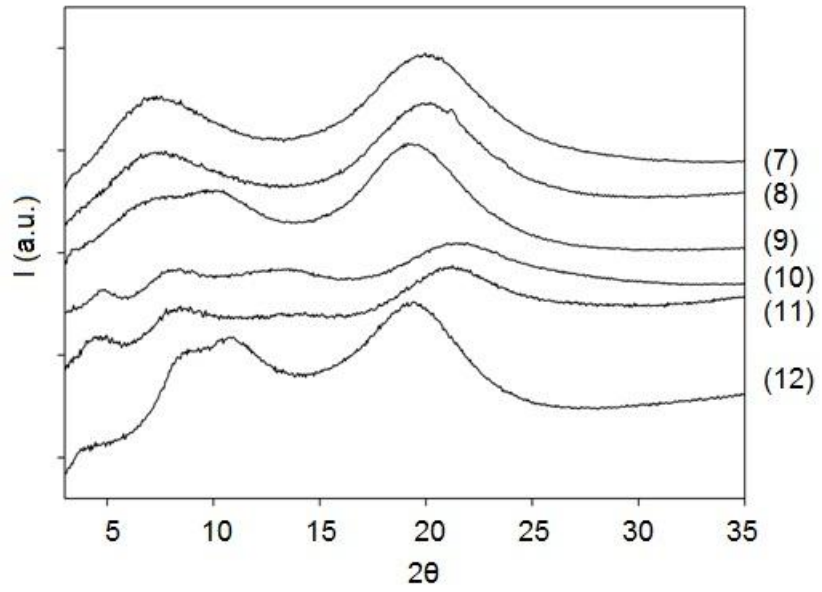

Figure 4.7. Wide angle X-ray diffraction profiles of poly(*n*BA-*co*-BPCl) (1) anion-exchanged with BF_4^- (2) and $TFSI^-$ (3) and BPCl homopolymer (4) anion-exchanged with BF_4^- (5) and $TFSI^-$ (6). The X-ray scattering intensity was shifted to display the influence of counterion type.

Table 4.4. Wide-angle X-ray scattering profiles of phosphonium-containing homopolymers

Homopolymer	1st peak (2θ)	d_1(Å)	d_1 (Number of C-C bond)	2nd peak (2θ)	d_2(Å)	d_2 (Number of C-C bond)
OPCl	3.76	23.5	15	5.81	15.2	10
OPBF4	3.62	24.4	16	5.86	15.1	10
OPTFSI	3.67	24.1	16	6.30	14.0	9
BPCl	4.79	18.4	12	7.87	11.2	7
BPBF4	4.45	19.8	13	8.45	10.5	7
BPTFSI	8.70	10.2	7	10.66	8.29	5

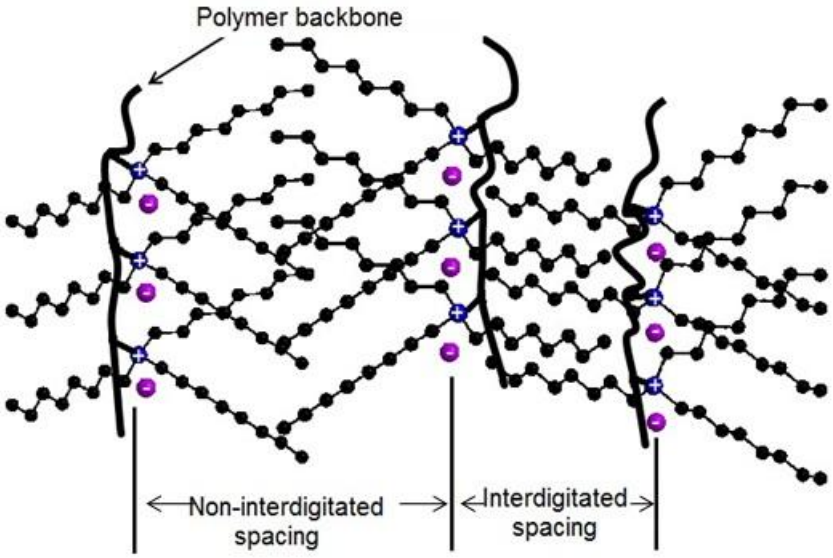

Figure 4.8. Schematic representation of alkyl chain packing of phosphonium-containing homopolymers

4.5 Conclusions

In this study, we synthesized a series of styrenic phosphonium ILs possessing various alkyl substituents and counterions and investigated the influence of chemical structure on the thermomechanical behaviors of phosphonium-containing random copolymers with *n*BA. DMA analyses of phosphonium ionomers possessing trioctyl substituents exhibited lower plateau moduli than analogs with tributyl substituents at identical ionic concentration, suggesting hindered association between phosphonium cations. Replacing Cl with large counterions, such as TFSI, also plasticized the polymer matrices and provided liquid-like behavior to certain extent after polymerization. Additionally, their corresponding WAXS peaks systematically shifted to lower q region, indicating an increase of ionic domain distance with the length of alkyl substituents.

4.6 Acknowledgements

Acknowledgment is made to the Donors of the American Chemical Society Petroleum Research Fund for partial support of this research. We also acknowledge funding from NSF (CHE-0722638) for the acquisition of our Agilent 6220 LC-TOF-MS. This material is based upon work supported by the U.S. Army Research Laboratory and the U.S. Army Research Office under contract/grant number W911NF-07-1-0452 Ionic Liquids in Electro-Active Devices Multidisciplinary University Research Initiative (ILEAD MURI). This material is partially based upon work supported by the National Science Foundation under Grant No. DMR-0923107.

4.7 References

1. Rogers, R. D.; Seddon, K. R., *Ionic Liquids as Green Solvents: Progress and Prospects*. American Chemical Society: Washington, D.C.: 2003.
2. Fraser, K. J.; MacFarlane, D. R. *Aust. J. Chem.* **2009,** 62, (4), 309-321.
3. Bradaric, C. J.; Downard, A.; Kennedy, C.; Robertson, A. J.; Zhou, Y. *ACS Symposium Series* **2003,** 856, (Ionic Liquids as Green Solvents), 41-56.
4. Welton, T. *Chem. Rev.* **1999,** 99, 2071-2083.
5. Dupont, J.; de Souza, R. F.; Suarez, P. A. Z. *Chem. Rev.* **2002,** 102, 3667-3691.
6. Wasserscheid, P.; Keim, W. *Angew. Chem., Int. Ed.* **2000,** 39, 3772-3789.
7. Marcilla, R.; Sanchez-Paniagua, M.; Lopez-Ruiz, B.; Lopez-Cabarcos, E.; Ochoteco, E.; Grande, H.; Mecerreyes, D. *J. Polym. Sci. Part A: Polym. Chem.* **2006,** 44, 3958–3965.

8. Marcilla, R.; Sanchez-Paniagua, M.; Lopez-Ruiz, B.; Lopez-Cabarcos, E.; Ochoteco, E.; Grande, H.; Mecerreyes, D. *J. Polym. Sci., Part A Polym. Chem.* **2006,** 44, (13), 3958-3965.

9. Tang, J.; Sun, W.; Tang, H.; Radosz, M.; Shen, Y. *Macromolecules* **2005,** 38, (6), 2037-2039.

10. Marcilla, R.; Alcaide, F.; Sardon, H.; Pomposo, J. A.; Pozo-Gonzalo, C.; Mecerreyes, D. *Electrochem. Commun.* **2006,** 8, 482-488.

11. Tang, J. R., M.; Shen, Y. Macromolecules 2008, 41, 493–496.

12. Chen, H.; Elabd, Y. A. *Macromolecules* **2009,** 42, (9), 3368-3373.

13. Tang, H.; Tang, J.; Ding, S.; Radosz, M.; Shen, Y. *J. Polym. Sci., Part A Polym. Chem.* **2005,** 43, (7), 1432-1443.

14. Mori, H.; Yahagi, M.; Endo, T. *Macromolecules* **2009,** 42, (21), 8082-8092.

15. Vijayakrishna, K.; Jewrajka, S. K.; Ruiz, A.; Marcilla, R.; Pomposo, J. A.; Mecerreyes, D.; Taton, D.; Gnanou, Y. *Macromolecules* **2008,** 41, (17), 6299-6308.

16. Lee, M.; Choi, U. H.; Salas-de la Cruz, D.; Mittal, A.; Winey, K. I.; Colby, R. H.; Gibson, H. W. *Adv. Funct. Mater.* **2011,** 21, (4), 708-717.

17. Anderson, E. B.; Long, T. E. *Polymer* **2010,** 51, (12), 2447-2454.

18. Green, M. D.; Long, T. E. *Polym. Rev.* **2009,** 49, (4), 291-314.

19. Ogihara, W.; Washiro, S.; Nakajima, H.; Ohno, H. *Electrochim. Acta* **2006,** 51, (13), 2614-2619.

20. Ohno, H.; Yoshizawa, M. *ACS Symp. Ser.* **2005,** 902, (Ionic Liquids IIIB: Fundamentals, Progress, Challenges, and Opportunities), 159-170.

21. Ohno, H.; Yoshizawa, M.; Ogihara, W. *Electrochim. Acta* **2004,** 50, (2-3), 255-261.

22. Ohno, H.; Washiro, S.; Yoshizawa, M. *ACS Symp. Ser.* **2005,** 913, (Ionic Liquids in Polymer Systems), 89-102.

23. Chen, H.; Choi, J.-H.; Salas-de la Cruz, D.; Winey, K. I.; Elabd, Y. A. *Macromolecules* **2009,** 42, (13), 4809-4816.

24. Tsunashima, K.; Sugiya, M. *Electrochemistry Communications* **2007,** 75, 734.

25. Kanazawa, A.; Ikeda, T.; Endo, T. *J. Polym. Sci., Part A Polym. Chem.* **1993,** 31, (6), 1441-7.

26. Gong M., L. C.-W., Joo S-W. *J. Mater. Sci.* **2002,** 37, 4615-4620.

27. Son, S.-Y.; Gong, M.-S. *Sens. Actuators, B* **2002,** B86, (2-3), 168-173.

28. Tomoi, M.; Ogawa, E.; Hosokama, Y.; Kakiuchi, H. *J. Polym. Sci., Polym. Chem. Ed.* **1982,** 20, (12), 3421-9.

29. Nonaka, T.; Li, H.; Ogata, T.; Kurihara, S. *J. Appl. Polym. Sci.* **2003,** 87, (3), 386-393.

30. Nonaka, T.; Li, H.; Makinose, K.; Ogata, T.; Kurihara, S. *J. Appl. Polym. Sci.* **2003,** 90, (4), 1139-1147.

31. Nonaka, T.; Yamada, K.; Watanabe, T.; Kurihara, S. *J. Appl. Polym. Sci.* **2000,** 78, (10), 1833-1844.

32. Ghassemi, H.; Riley, D. J.; Curtis, M.; Bonaplata, E.; McGrath, J. E. *Appl. Organomet. Chem.* **1998,** 12, 781-785.

33. Tomoi, M.; Hosokawa, Y.; Kakiuchi, H. *J. Polym. Sci., Polym. Chem. Ed.* **1984,** 22, (6), 1243-50.

34. Parent, J. S.; Penciu, A.; Guillen-Castellanos, S. A.; Liskova, A.; Whitney, R. A. *Macromolecules* **2004,** 37, (20), 7477-7483.

35. Wang, R.; Lowe, A. B. *J. Polym. Sci., Part A: Polym. Chem.* **2007,** 45, (12), 2468-2483.

36. Gupta, M. K.; Singh, R. P. *Polymer Bulletin* **2009,** 62, (3), 271-280.

37. Williams, S. R.; Wang, W.; Winey, K. I.; Long, T. E. *Macromolecules* **2008,** 41, (23), 9072-9079.

38. Kanazawa, A.; Ikeda, T.; Endo, T. *J. Polym. Sci., Part A: Polym. Chem.* **1993,** 31, (2), 335-43.

39. Tezuka, Y.; Goethals, E. J. *Mackromol. Chem.* **1987,** 188, 783-789.

40. Weiss, R. A. *J. Appl. Polym. Sci.* **1984,** 29, (9), 2719-2734.

41. Page, K. A.; Cable, K. M.; Moore, R. B. *Macromolecules* **2005,** 38, 6472-6484.

42. Tachino, H.; Hara, H.; Hirasawa, E.; Kutsumizu, S.; Tadano, K.; Yano, S. *Macromolecules* **1993,** 26, 752-757.

43. MacKnight, W. J.; Kajiyama, T.; McKenna, L. *Polym. Eng. Sci.* **1968,** 8, 267-271.

44. Hatakeyama, T. *J. Macromol. Sci.-Phys., B* **1982,** 21, (2), 299-305.

45. Abdallah, D. J.; Wauters, H. C.; Kwait, D. C.; Khetrapal, C. L.; Gowda, G. A. N.; Robertson, A.; Weiss, R. G. *ACS Symp. Ser.* **2005,** 902, (Ionic Liquids IIIB: Fundamentals, Progress, Challenges, and Opportunities), 303-320.

46. Gowda, G. A. N.; Chen, H.; Khetrapal, C. L.; Weiss, R. G. *Chem. Mater.* **2004,** 16, (11), 2101-2106.

47. Abdallah, D. J.; Lu, L.; Cocker, T. M.; Bachman, R. E.; Weiss, R. G. *Liq. Cryst.* **2000,** 27, (6), 831-837.

48. Abdallah, D. J.; Robertson, A.; Hsu, H.-F.; Weiss, R. G. *J. Am. Chem. Soc.* **2000,** 122, (13), 3053-3062.

49. Miller, R. L.; Boyer, R. F.; Heijboer, J. *J. Polym. Sci., Part B: Polym. Phys.* **1984,** 22, (12), 2021-2041.

Chapter 5: RAFT Polymerization and Characterization of Quaternary Ammonium-Containing Polymers

*Shijing Cheng, Mingqiang Zhang, Robert B. Moore, and Timothy E. Long**

5.1 Abstract

Salt-responsive acrylate random copolymers consisting of quaternary ammonium functionalities were synthesized using reversible addition-fragmentation chain transfer polymerization (RAFT). The obtained copolymers possessed controlled compositions and narrow molecular weight distributions with molecular weights ranging from M_n =50,000 to 170,000 g/mol. These ionomers exhibited salt concentration dependent solubility in water. This salt trigger ability was found to strongly depend on copolymer composition with little molecular weight effect. An ionomer morphology-dependent salt responsive mechanism has been proposed for the salt trigger ability based on the study of solution rheology and solution small-angle X-ray scattering. Furthermore, the thermoresponsive ethylene oxide acrylate monomer was introduced into the copolymers for doubly responsive terpolymer formation.

5.2 Introduction

Responsive polymeric structures with well-defined macromolecular composition, functionalities, and topology have become the interest of many researchers.[1-3] Temperature- and pH-responsive polymers are most frequently studied because these factors are variables that change in typical physiological, biological, and chemical systems.

Small polymeric structures can exhibit a phase transition from soluble to insoluble upon heating, called lower critical solution temperature (LCST) behavior, which is based on the existence of hydrogen bonding between the water molecules and the polymer chain. The polymers with LCST behavior show a sudden and (mostly) reversible change from hydrophilic to hydrophobic behavior that makes them attractive for usage as ‘‘smart’’ switchable materials in applications ranging from, i.e., drug delivery systems, soft actuators or valves, coatings and even in textile materials.[4-6] Poly(*N*-isopropyl acrylamide) (PNIPAm) is the most widely investigated thermoresponsive polymer because its LCST is close to physiological temperature and independent of concentration or ionic strength.[7-8] Alternatively, the comb shaped poly(oligoethylene glycol) acrylates (PEGMA) or methacrylates (PEGMMA) also display LCSTs which critically depends on the length of the PEG side-chains for homopolymers or in the case of copolymers, the monomer composition.[9-12] Alexander et al. have also reported a salt effect on the LCST behavior for linear PEGMA chains.[13] This tunable LCST behavior is typically not attainable with linear PEG.[9-12, 14] Moreover, the comb-shaped poly(ethylene glycol) (PEG) analogues are nontoxic, nonimmunogenic, low fouling, and biocompatible, similar to linear PEG.[15-17] These desirable properties make them especially useful in biological and pharmaceutical applications.[18-19]

The accuracy and the reproducibility of LCST transitions can be tailored by utilizing living and controlled polymerization techniques, such as anionic polymerization,[20-21] atom transfer radical polymerization (ATRP),[10, 12, 22] and reversible addition fragmentation chain transfer polymerization (RAFT).[23] These techniques have enabled the synthesis of advanced structures with a targeted length of the polymer. Moreover, the

architecture as well as the desired monomer composition and distribution along the backbone can be controlled in an excellent manner.

In this study we present results of utilizing RAFT to synthesize ammonium-containing random copolymers and terpolymers at relatively low temperatures since quaternary ammonium functionalities are known to become thermally unstable at high temperatures (>120 °C).[24-25] RAFT is presumably the most versatile controlled radical polymerization applicable to the widest range of monomers under a large number of experimental conditions because of its high tolerance to various functionalities and metal-free products.[26] The resulting ionomers exhibited water solubility dependent on salt concentration. This salt-responsive behavior has been reported previously for amphiphilic copolymers containing both hydrophilic and hydrophobic monomers, such as the terpolymer of acrylamide, *n*-decylacrylamide, and carboxylate or sulfonate acrylamido,[27] sodium 11-(acrylamido)undecanoate homopolymer and copolymers with acrylamide.[28-30] The salt-responsiveness was ascribed to the formation of micellar microdomains or interpolymer hydrophobic associations. In our case, the salt trigger ability was further investigated using solution rheology and small-angle X-ray scattering.

5.3 Experimental

5.3.1 Materials

Methyl acrylate (MA, 99+%) was purchased from Aldrich and passed through neutral alumina before use. α,α'-Azobis(isobutyronitrile) (AIBN, Fluka, 99%) was recrystallized from methanol. Cyanomethyl dodecyl trithiocarbonate (CDT), (2-(acryloyloxy)ethyl)trimethylammonium chloride (HQUAT), ethylene glycol methyl ether

acrylate(MEOMA), di(ethylene glycol) ethyl ether acrylate (MEO2A), poly(ethylene glycol) methyl ether acrylate (PEGA) were purchased from Aldrich and used without further purification. Hexane (HPLC grade), methanol (MeOH, HPLC grade), tetrahydrofuran (THF, HPLC grade), and *N*,*N*-dimethylformamide (DMF, HPLC grade, anhydrous) were purchased from Fisher Scientific and used as received.

5.3.2 Instrumentation

^{1}H NMR spectra were collected in D_2O or DMSO-d_6 on a Varian INOVA spectrometer operating at 400 MHz and 23 °C. Size exclusion chromatography (SEC) was used to determine the molecular weights of phosphonium-containing random copolymers at 50 °C in DMF with 0.05 M lithium bromide (LiBr) at 1 mL/min. DMF SEC was performed on a Waters SEC equipped with two Waters Styragel HR5E (DMF) columns, a Waters 717plus autosampler, and a Waters 2414 differential refractive index detector. Reported molecular weights are absolute molecular weights from MALLS.

Dynamic mechanical analysis (DMA) was conducted on a TA Instruments Q800 Dynamic Mechanical Analyzer in tension mode at a frequency of 1 Hz, an oscillatory amplitude of 15 μm, and a static force of 0.01 N. The temperature ramp was 3 °C/min. The glass transition temperature (T_g) was determined at the peak maximum of the tanδ curve. Tensile experiments employed an Instron equipped with a 500 Newton load cell and grips. A gauge length of 1 in. and a crosshead speed of 500 mm/min were employed. Typically 3-4 replicates were utilized and standard deviation calculated. Solutions for rheology were prepared by dissolving the desired amount of polymer in the NaCl aqueous solution. The solutions were allowed to stir magnetically for 3 d to ensure equilibration. Solution rheology was conducted on a TA Instruments AR-G2 strain-

controlled rheometer equipped with recessed concentric cylinder geometry. The solutions were allowed to equilibrate at 25 °C for 2 min prior to measurement. 15-20 wt% of polymer in methanol was cast on Teflon® molds and air-dried for 3 d. The air dried films were placed in vacuum ovens at 50 ^{o}C for 2 d to remove any residual solvent. Water uptake in these samples was determined by weight increase after hydration. Films were stored in NaCl aqueous solutions at room temperature for 4 d before tensile test. Water uptake ratio=$(M-M_0)/M_0$. Tensile tests were run under ambient humidity (40±5 % RH). The dehydration of swollen films after measurement was determined to be less than 10 wt%.

SAXS was performed using a Rigaku S-Max 3000 3 pinhole SAXS system. X-ray source was the Cu K_α radiation, and the wavelength was 0.154 nm. Silver behenate was used to calibrate the sample to detector distance and the sample-to-detector distance was 1600 mm. SAXS two-dimensional images were obtained using a fully integrated 2D multiwire proportional counting gas-filled detector, with an exposure time of 6 hours. SAXSGUI software package was used to obtain scattering intensity, $I(q)$, versus scattering wave vector $q=4\pi\sin(\theta)/\lambda$, where θ was half of scattering angle and λ was the wavelength of the incident beam. Solution samples were measured in a capillary with a diameter of 1.5 mm and wall thickness of 0.01 mm. The measured intensity had been corrected for sample transmission, solvent scattering and background scattering.

The scattering intensity, $I(q)$ was written as

$$I(q) = nV^2\Delta\rho^2 S(q)F(q)$$

where n is the particle concentration, V is the volume of a particle, $\Delta\rho$ is the scattering contrast, $S(q)$ is structure factor, and $F(q)$ is form factor. Since the concentration of the samples is only 0.1 wt%, the structure factor is equal to 1 and no longer affects the

scattering intensity. In this case, Guinier's Law was applied to calculate the radius of gyration R_g of a particle of unknown shape and size from SAXS measurement. Guinier's law is given as

$$I(q) = \rho^2 v^2 \exp\left(-\frac{1}{3} q^2 R_g^2\right)$$

where ρ is the electron density and v is the volume. R_g can be obtained from the slope of a ln $I(q)$ vs q^2 curve. Guinier's law can be used only at small q range, which should satisfy the relationship below:

$$q * R_g < 1$$

5.3.3 RAFT Polymerization

General Procedure. All polymerizations were performed in 250-mL round bottomed flasks. In all cases, CDT and AIBN were used as the CTA and initiator, respectively. For example, MA (25.88 g, 0.30 mol), HQUAT (3.03 g, 0.0125 mol), CDT (44 mg, 0.14 mmol) and AIBN (4 mg, 0.024 mmol) were dissolved in methanol (60 g). Degassing was achieved by purging the reaction solutions with nitrogen for 20 minutes. After degassing, the reaction flask was placed in an oil bath at 65 °C. The polymerizations were terminated by rapid cooling and freezing. The polymers were purified by precipitation into a THF/hexane mixture. ^{1}H NMR spectra was utilized to monitor RAFT polymerization process. The ratio of the vinyl peaks (CH2=CH-, 6 ppm) to the methylene peak (4 ppm) was used to roughly calculate the percent conversion of monomers as a function of reaction time. The small amount of HQUAT was neglected in the conversion calculation**.**

5.4 Results and Discussion

5.4.1 RAFT Copolymerization/Terpolymerization

The RAFT random copolymerization of MA and HQUAT and terpolymerization of MA, HQUAT, and MEOMA are shown in Schemes 5.1 and 5.2 respectively. In all cases cyanomethyl dodecyl trithiocarbonate was chosen as the CTA. [Monomer]:[CTA]:[AIBN] was chosen to be 1344/1/0.12 or 2250/1/0.175 as a parallel comparison. ^{1}H NMR spectra of poly(MA-*co*-HQUAT) and poly(MA-*co*-HQUAT-*co*-MEOMA) are shown in Figures 5.1 and 5.2. The mole fractions of ammonium unit and MEOMA in the co/terpolymers were calculated by measuring the integration of methylene protons (2H, O-C*H*$_2$-CH$_2$-N, 4.4 ppm; 2H, O-C*H*$_2$-CH$_2$-O, 4.15 ppm; 2H, -C*H*$_2$-CH-, 1.4-1.8 ppm). The polymer composition was very close to the monomer mixture in the feed. The characteristic RAFT ‘‘living’’ behavior is demonstrated in Figure 5.3. The reaction conversion was calculated based on the integration of the peak at 6.0 ppm (vinyl protons from unreacted monomers) and the peak at 1.4-1.8 ppm from -CH$_2$ at polymer backbone. Plotting the reaction conversion for a series of reaction solution extractions as a function of time generated a linear line, indicating that the polymerization proceeded in a controlled manner at conversion below 40% after 5 hours of polymerization. In all cases polymerizations were terminated at high conversions (>90%) and nearly monodisperse polymers with yields higher than 50% were obtained. The representative GPC traces are shown in Figure 5.4, which revealed a shift to lower retention times with higher [monomer]/[CTA]. It is evident that the random copolymer was prepared successfully (Tables 5.1 and 5.2).

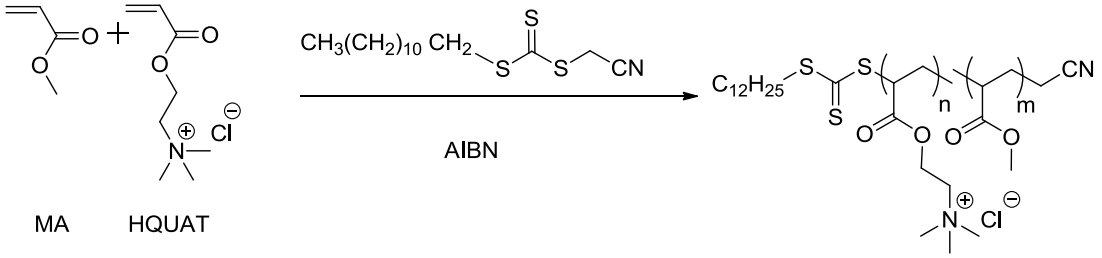

Scheme 5.1. RAFT copolymerization of MA and HQUAT

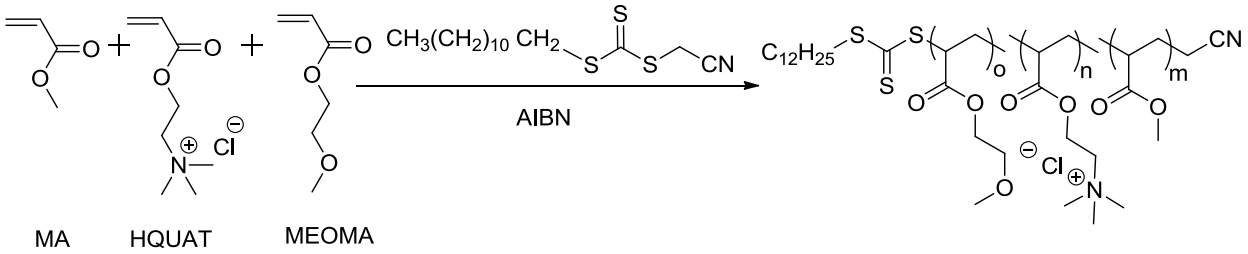

Scheme 5.2. RAFT terpolymerization of MA, HQUAT, and MEOMA

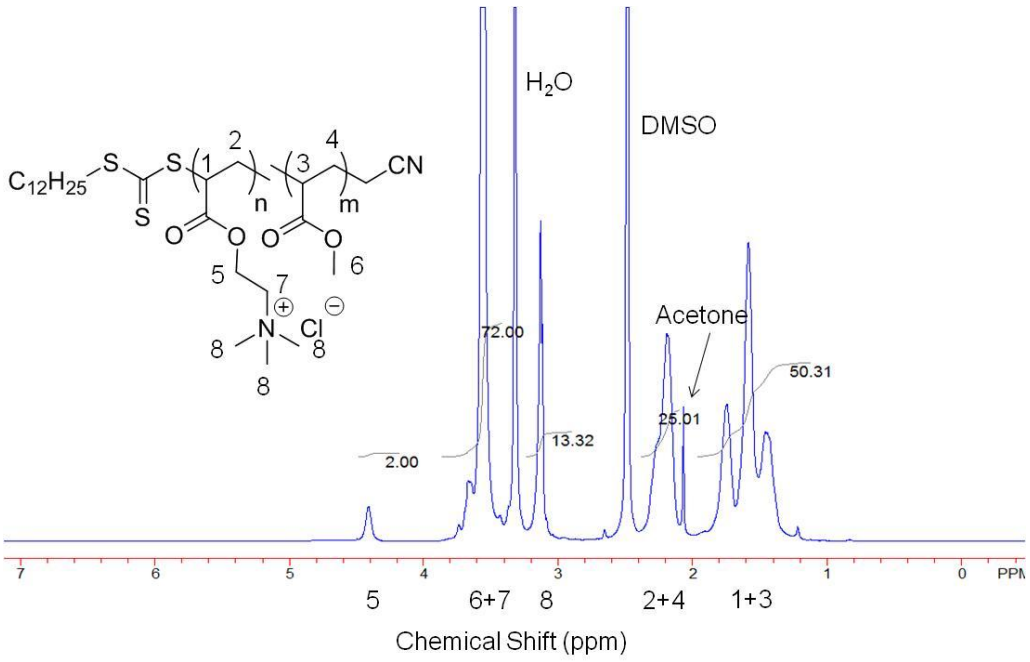

Figure 5.1. ^{1}H NMR spectra of poly(MA-*co*-HQUAT) in d_6-DMSO.

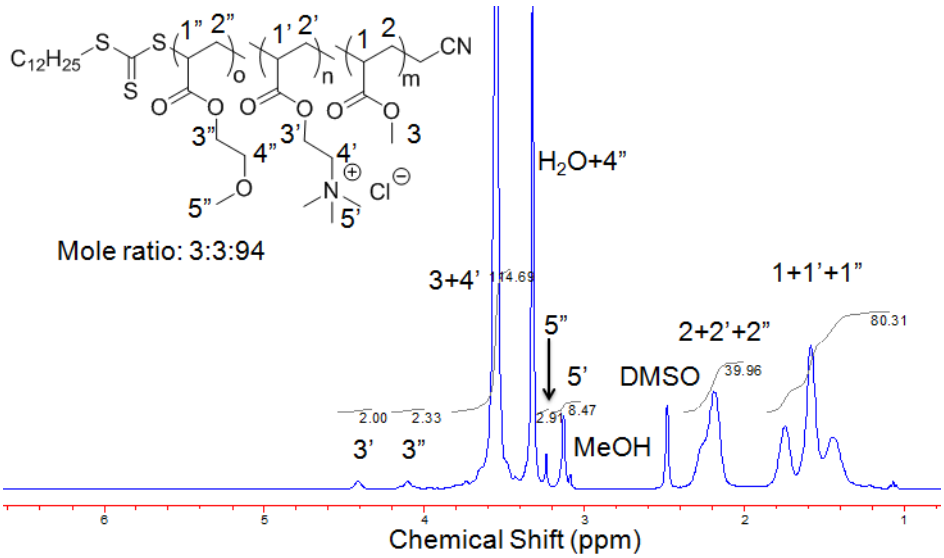

Figure 5.2. ^{1}H NMR spectra of poly(MA-*co*-HQUAT-*co*-MEOMA) in d_6-DMSO.

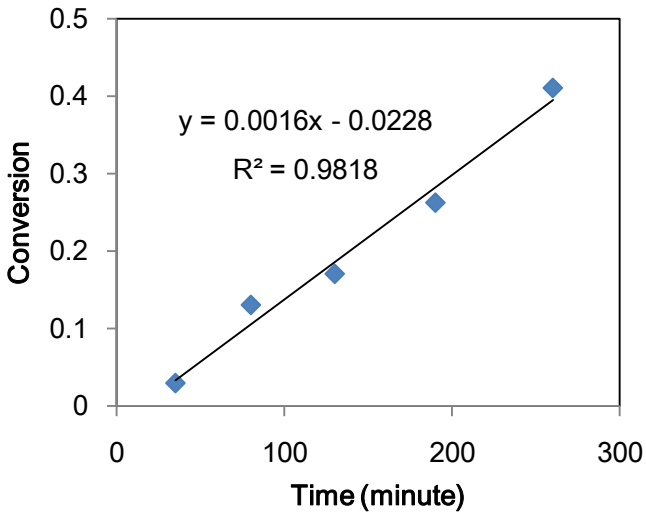

Figure 5.3. Reaction conversion of RAFT polymerization as a function of reaction time.

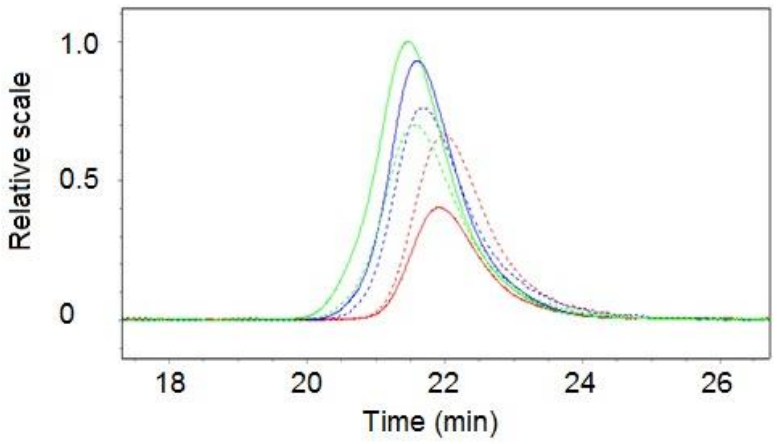

Figure 5.4. Representative SEC traces of ammonium-containing random copolymers. Light scattering traces are represented in the solid line. RI traces are drawn in dashed line.

Table 5.1. Molecular characteristics of ammonium-containing random copolymers

[MA+HQUAT]/ [CTA]/[AIBN]	[HQUAT] in feed (mol%)	[HQUAT] in polymer (mol%)	M_n (LS) (g/mol)	PDI
1400/1/0.12	6.0	6.2	-	-
1344/1/0.12	4.0	4.0	62.2K	1.21
1344/1/0.12	4.0	4.0	46.2K	1.31
2250/1/0.175	4.0	3.7	72.1K	1.03
2250/1/0.175	4.0	3.6	120K	1.02
2250/1/0.175	4.0	4.0	170K	1.07
2250/1/0.175	4.0	4.0	140K	1.07
2250/1/0.175	5.0	5.0	-	-

-: not soluble or filterable

Table 5.2. Chemical composition of ammonium-containing random terpolymers

[MA]:[HQUAT]:[MEOMA] feed	[MA]:[HQUAT]:[MEO MA] in polymer	M_n (LS) (g/mol)	PDI	Solubility in water
96:4:0	96:4:0	83.8K	1.06	Fall apart
92:3:5	90:4:6	117K	1.13	Fall apart
87:3:10	87:3:10	-	-	dissolve
93:2:5	92:2:6	102K	1.13	insoluble
96:2:2	94:3:3	100K	1.22	insoluble

5.4.2 Dynamic Mechanical Analysis

Poly(*M*A-*co*-HQUAT)s formed free-standing films with an ionic concentration as low as 4 mol%. The tensile storage modulus (G') and tanδ versus temperature from DMA for the ammonium-containing polymers with 4 mol% of HQUAT and various molecular weights are depicted in Figure 5.5. A decrease of G' occurred at -5 ℃, and then a very short rubbery plateau appeared before complete flow occurred. At similar ionic concentration the flow temperature decreased with molecular weights. These results suggested that increasing molecular weights led to an increase in G' and increased flow temperature due to chain entanglement. Additionally, for all the samples, the tanδ peak revealed a shoulder around 7 ℃, which corresponded to the glass transition of the matrix polymethylacrylate, and the second peak corresponded to the ionic phase. These results agreed well with those observed in the previous mechanical relaxation study of metal-salts neutralized poly(ethylene-*co*-methacrylic acid) ionomers.[31-32] Specifically, the β relaxation stayed at nearly the same temperature, and the α relaxation associated with a glass-rubber transition of the ionic clusters shifted to higher temperature with the increase of ionic concentration.[32] The presence of two distinct relaxation modes indicates sufficient association between ammonium units.

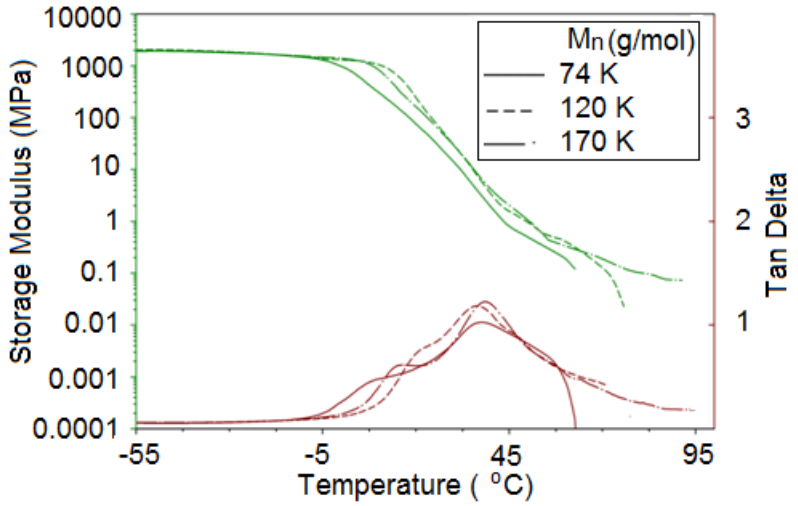

Figure 5.5. DMA traces of poly(MA-*co*-HQUAT).

5.4.3 Water Uptake

Figure 5.6 plots the polymer water uptake as a function of NaCl aqueous solution concentration. All of the curves presented sharp upturns at the low NaCl concentration. In general, compared to ionic concentration, molecular weight did not influence the swelling ratio of poly(MA-co-HQUAT) significantly. Replacing MA with hydrophilic MEOMA monomers enhanced the salt trigger ability by shifting the transition point to lower NaCl concentration.

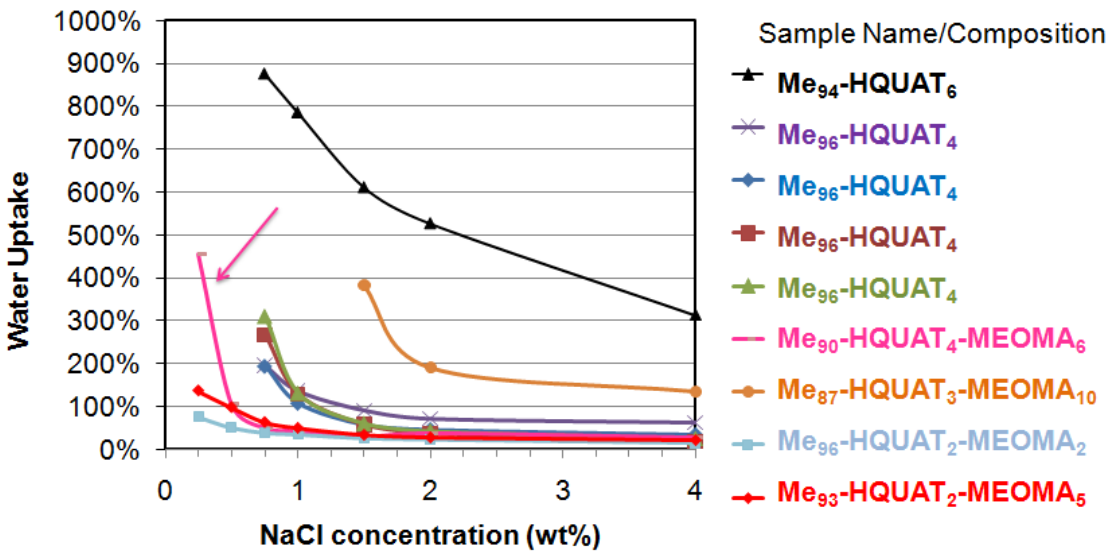

Figure 5.6. Swelling ratios of poly(MA-*co*-HQUAT) at various NaCl concentrations.

5.4.4 Wet Strength

Wet strength is normally considered in cosmetics and disposable diapers application, which generally demand good wet strength performance in water. Tensile test was performed on the identical films obtained from water uptake measurement. The typical stress-strain curves for the wet films are presented in Figure 5.7 and the corresponding date was summarized in Table 5.1. Tensile strengths of all samples at wet state are very low (0.4 MPa) and decreased with further increase of water uptake. The strong dependence of the tensile strength on the content of water is presumably related to the molecular-level dispersion of water and the ionic interactions. Water molecules strongly interacted with the ammonium groups and acted as a plasticizer resulting in swelling and weakening of ionic aggregates leading to decreased wet strength. Although a wet strength less than 1 MPa is much lower than the strength in the dry state, it is typically high enough in some nonstructural applications such as hygiene or biomedical products. The

addition of a small amount MEOMA increased the water uptake content slightly and decreased the stress at break significantly (Figure 5.8). Interestingly, at the same content of water uptake, the Young's modulus and strain at break for the terpolymer were very close to the copolymer, but the stress at break were much lower. With the presence of ethylene oxide along the pendant chains, the terpolymers in wet state were more ductile, supportive of a covalent cross-linking mechanism whereby the entangled hydrophobic chains contribute to wet strength.

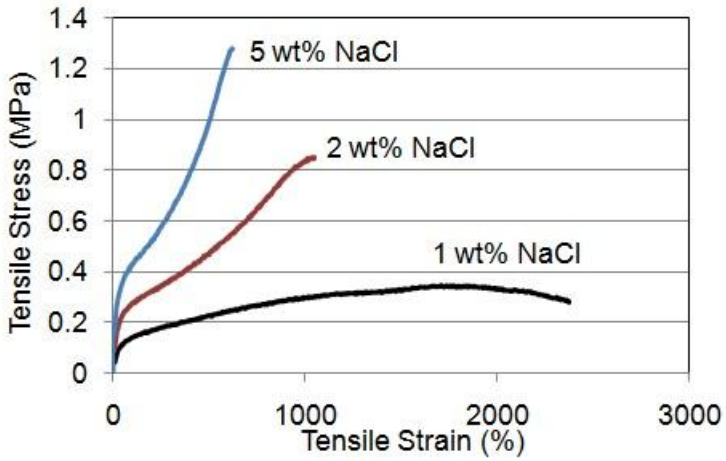

Figure 5.7. Tensile traces of poly(MA_{96}-*co*-$HQUAT_4$)

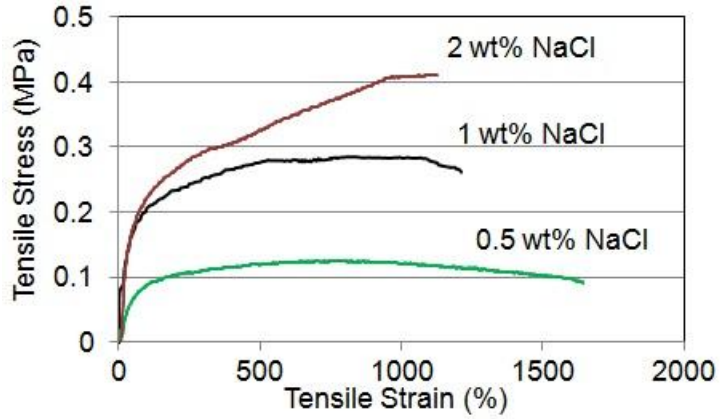

Figure 5.8. Tensile traces of hydrated poly(MA_{90}-*co*-$HQUAT_4$-*co*-$MEOMA_6$) demonstrating the effect of [NaCl]

Table 5.3. Effect of [NaCl] on tensile property for poly(MA_{96}-*co*-$HQUAT_4$) and poly(MA_{90}-*co*-$HQUAT_4$-*co*-$MEOMA_6$) with different degree of hydration

M_n (g/mol)	[NaCl]	Water Uptake	Tensile Strain at Break (%)	Young's Modulus (25 ^oC, MPa)
132K	5 wt%	24%	705±68	0.569±0.065
	2 wt%	38%	1172±148	0.268±0.048
	1 wt%	129%	1708±211	0.115±0.019

M_n (g/mol)	[NaCl]	Water Uptake	Tensile Strain at Break (%)	Young's Modulus (25 ^oC, MPa)
147K	2 wt%	38%	1129±103	0.282±0.018
	1 wt%	43%	1261±168	0.285±0.023
	0.5 wt%	106%	1890±147	0.166±0.010

5.4.5 Solution Rheological Analysis

Steady shear experiments were performed on ionomer solutions with 2 orders of magnitude in concentration. Specific viscosity vs concentration profiles were obtained for poly(MA_{96}-*co*-$HQUAT_4$) (M_n=49 K) in 0.125 wt% and 0.5 wt% NaCl aqueous solutions (Figure 5.9). Various amounts of NaCl were added to the ionomer solutions to determine the influence of charge screening on the solution rheological behavior. In both cases, three concentration regimes can be discriminated that spanned the dilute, semidilute, and concentrated regimes. The specific viscosity in the entire concentration regimes systematically increased with increasing levels of NaCl.

In the dilute regime, the salt screened the surface charges and ionomers adopted a spherical conformation with a hydrophobic core. In the semidilute regimes, the

entanglement concentration (C_e), which is the transition between the unentangled and entangled semidilute regimes and marks the solution concentration at which chains overlap sufficiently to form topologically constrained entanglements, was not observed. The absence of C_e suggests that when polymer chains start to overlap, the viscosity is solely dependent on the number of polymer coils rather than the number of chain entanglements. This is possibly due to the overlap of the electrostatic blobs, which also served to screen mutual charge repulsion. Table 5.4 summarizes the exponents in the dilute, semidilute, and concentrated concentration regimes. It is evident that the slopes in the dilute and concentrated regimes were dependent on NaCl concentration. In the semidilute regimes, the slopes were independent of NaCl concentration and molecular weight.

The addition of NaCl also influenced the transitions between the different concentration regimes. Both C^* and the onset of the concentrated regime (C_D) decreased with the increase of NaCl concentration. Above C_D the concentration dependence of viscosity got more pronounced, which is not in agreement with the scaling relationships for either polyelectrolytes or neutral polymers. The sharp increase of viscosity at high concentrations is concomitant with the apparent gelation above C_D. With increasing salt concentrations, the surface charges were further screened, which enable the spheres to connect with each other and occupied a larger volume in solution.

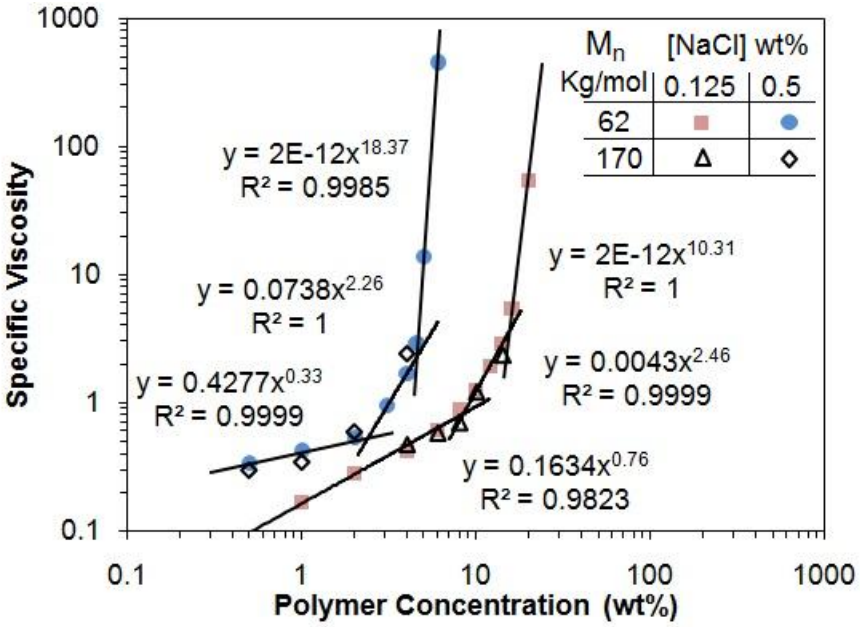

Figure 5.9. Effect of NaCl on ionomer solution behavior.

Table 5.4. Influence of NaCl on scaling exponents and overlap concentration of poly(MA-*co*-HQUAT) solutions

[NaCl] (wt%)	Diluted exponent (C<C*)	Semidilute unentangled exponent (C*<C<C_D)	Concentrated exponent (C >C_D)	C* (wt%)	C_D (wt%)
0.125	0.8	2.5	10	8.5	16
0.5	0.3	2.3	18	2.5	4.5

5.4.6 Solution SAXS

Small-angle X-ray scattering was used to characterize polymers in the dilute concentration regimes. Table 5.5 summarizes the influence of molecular weight and salt concentration on the radius of gyration for ammonium-containing ionomers. The radius of gyration was obtained from fitting the SAXS profiles using Guinier's Law described in the experimental section. The radius of gyration increased as expected with salt concentration, which is consistent with the solution viscosity results due to aggregation of smaller particles at higher salt concentration.

Table 5.5. Radius of gyration of ammonium-containing random copolymers

No.	M_n (g/mol) from LS	[polymer] wt%	[NaCl] aq wt%	Radius of Gyration (nm)
1	49.3K	0.1	0	4.6, 5.6
2		0.1	0.125	5.8
3		0.1	0.25	6.9
4		0.1	0.5	13.7
5		0.5	0.125	5.6
6		0.5	0.5	15.8
7	132K	0.1	0	-
8		0.1	0.125	7.5
9		0.1	0.25	7.9
10		0.1	0.5	15.7
11		0.5	0.125	6.4
12		0.5	0.5	15.7

5.5 Conclusions

The ammonium-containing poly(methyl acrylate)s were successfully synthesized using RAFT polymerization. Swelling ratio of poly(MA-co-HQUAT) increased with increasing ionic content, which enhanced the polymer hydrophilicity and decreased the required salt concentration to trigger solubility. Additionally, swelling ratio was found to be independent of polymer molecular weights. Modifying ionomer hydrophilicity through replacing methyl acrylate with PEG-based acrylate monomers decreased the wet strength. Solution viscosity of ammonium-containing ionomers in water was strongly dependent on both salt concentration and polymer concentration. Furthermore, the absence of C_e was attributed to screening of the repulsive, electrostatic interactions that stabilize the spheres and promoted the aggregation of polymer coils in the semidilute regime. The abrupt gelation in the high salt limit suggested the connectivity transition of polymer aggregates.

5.6 Acknowledgements

The authors acknowledge the financial support from Kimberly-Clark Co.

5.7 References

1. Mathur, A. M.; Drescher, B.; Scranton, A. B.; Klier, J. *Nature* **1998,** 392, 367-370.
2. Zhang, L.; Guo, R.; Yang, M.; Xiqun, J.; Liu, B. *Adv Mater* **2007,** 19, 2988-2992.
3. You, Y. Z.; Zhou, Q. H.; Manickam, D. S.; Wan, L.; Mao, G. Z.; Oupicky, D. *Macromolecules* **2007,** 40, 8617-8624.
4. Harmon, M. E.; Tang, M.; Frank, C. W. *Polymer* **2003,** 44, 4547-4556.
5. Schmaljohann, D. *Adv Drug Delivery Rev* **2006,** 58, 1655-1193.
6. Gil, E.; Hudson, S. *Prog Polym Sci* **2004,** 29, 1173-1222.
7. Schild, H. G. *Prog Polym Sci* **1992,** 17, 163-249.
8. Aoshima, S.; Kanaoka, S. *Adv Polym Sci* **2008,** 210, 169-208.
9. Lutz, J.-F. *J. Polym. Sci., Part A: Polym. Chem.* **2008,** 46, (11), 3459–3470.
10. Lutz, J.-F.; Akdemir, O.; Hoth, A. *J. Am. Chem. Soc.* **2006,** 128, (40), 13046-13047.
11. Lutz, J.-F.; Andrieu, J.; Uzgun, S.; Rudolph, C.; Agarwal, S. *Macromolecules* **2007,** 40, (24), 8540-8543.
12. Lutz, J.-F.; Hoth, A. *Macromolecules* **2006,** 39, (2), 893-896.
13. Magnusson, J. P.; Khan, A.; Pasparakis, G.; Saeed, A. O.; Wang, W.; Alexander, C. *J. Am. Chem. Soc.* **2008,** 130, 10852-10853.

14. Mullner, M.; Schallon, A.; Walther, A.; Freitag, R.; Muller, A. H. E. *Biomacromolecules* **2010,** 11, 390-396.

15. Ma, H.; Hyun, J.; Stiller, P.; Chilkoti, A. *Adv. Mat.* **2004,** 16, 338.

16. Oyane, A.; Ishizone, T.; Uchida, M.; Furukawa, K.; Ushida, T.; Yokoyama, H. *Adv. Mat.* **2005,** 17, 2329.

17. Popescu, D. C.; Lems, R.; Rossi, N. A. A.; Yeoh, C.-T.; Loos, J.; Holder, S. J.; Bouten, C. V. C.; Sommerdijk, N. A. J. M. *Adv. Mat.* **2005,** 17, 2324.

18. Boyer, C.; Whittaker, M.; Luzon, M.; Davis, T. P. *Macromolecules* **2009,** 42, 6917-6926.

19. Boyer, C.; Bulmus, V.; P., D. T.; Ladmiral, V.; Liu, J.; Perrier, S. *Chem Rev* **2009,** 109, 5402-5436.

20. Han, S.; Hagiwara, M.; Ishizone, T. *Macromolecules* **2003,** 36, 8312-8319.

21. Ishizone, T.; Seki, A.; Hagiwara, M.; Han, S.; Yokoyama, H.; Oyane, A.; Deffieux, A.; Carlotti, S. *Macromolecules* **2008,** 41, 2963-2967.

22. Yamamoto, S. I.; Pietrasik, J.; Matyjaszewski, K. *Macromolecules* **2007,** 40, 9348-9353.

23. Roth, P. J.; Jochum, F. D.; Forst, R.; Zentel, R.; Theato, P. *Macromolecules* **2010,** 43, 4638-4645.

24. Criddle, W. J.; Thomas, J. *J. Anal. Appl. Pyrolysis* **1981,** 2, 361.

25. Starks, C. M.; Liotta, C. L.; Halpern, M., *Phase-Transfer Catalysis*. Chapman & Hall: 1994.

26. Lowe, A. B.; McCormick, C. L. *Prog. Polym. Sci.* **2007,** 32, 283-351.

27. McCormick, C. L.; Middleton, J. C.; Cummins, D. F. *Macromolecules* **1992,** 25, 1201.

28. Yeoh, K. W.; Chew, C. H.; Gan, L. M.; Koh, L. L.; Teo, H. H. *J. Macromol. Sci., Chem.* **1989,** A26, 663.

29. Kramer, M. C.; Welch, C. G.; Steger, J. R.; McCormick, C. L. *Macromolecules* **1995,** 28, 5248-5254.

30. Yeoh, K. W.; Chew, C. H.; Gan, L. M.; Koh, L. L.; Ng, S. C. *J. Macromol. Sci., Chem.* **1990,** A27, 711.

31. Tachino, H.; Hara, H.; Hirasawa, E.; Kutsumizu, S.; Tadano, K.; Yano, S. *Macromolecules* **1993,** 26, 752-757.

32. MacKnight, W. J.; Kajiyama, T.; McKenna, L. *Polym. Eng. Sci.* **1968,** 8, 267-271.

Chapter 6: Synthesis and Characterization of Styrenic Nucleobase-Containing Random Copolymers

*Shijing Cheng, Mingqiang Zhang, Ninad Dixit, Robert B. Moore, and Timothy E. Long**

Keywords: nucleobase, adenine, thymine, complementary multiple hydrogen bonding, molecular recognition, supramolecular polymer, thermoplastic elastomer, morphology, self-assembly

6.1 Abstract

The presence of hydrogen bonding enhances polymer melt viscosity and cohesive strength in adhesive applications. In this study, self-complementary thymine and adenine, which are nucleobases in DNA, were introduced to poly(*n*-butyl acrylate) as hydrogen bonding recognition units in order to enhance adhesive properties. The styrenic adenine and thymine monomers were synthesized through N-alkylation of 4-chloromethyl styrene with adenine or thymine. Copolymerization of styrenic adenine or thymine monomers with *n*BA afforded a series of side-chain hydrogen bonding polymers with varied hydrogen bonding content. The polymer complex of adenine and thymine functionalized poly(*n*-butyl acrylate)s revealed higher melt viscosity and a stronger temperature dependence of viscosity than the individual polymers. Time-temperature-superposition and morphological analysis indicated a significant degree of heterogeneity in the random copolymers. Moreover, peel testing measurements were performed to investigate the influence of complementary hydrogen bonding on polymer adhesive performance.

6.2 Introduction

Multiple hydrogen bonding has recently gained attention in the field of macromolecular and supramolecular chemistry due to the pioneering work of Meijer,[1] Stadler,[2] Lehn,[3] and others.[4-6] The strength of these interactions is highly dependent on temperature,[6] solvent,[7-8] humidity,[9] and pH,[10] thus allowing control of properties through a number of environmental parameters.

The hydrogen bonding motif offers unique thermoreversibility and the influence on physical properties is quite evident in melt rheology. For example, Meijer introduced a self-complementary 2-ureido-4[1H]-pyrimidone quadruple hydrogen bonding array at the ends a trifunctional oligomeric poly(propylene glycol-*co*-ethylene glycol) copolymer and a thermoreversible network with film forming capability and elastomeric mechanical properties was observed.[11] The use of multiple hydrogen bonding sites in conjunction with conventional oligomers and polymers offers promise for improved melt processability with equivalent polymer properties at temperatures below hydrogen bond dissociations and also enables potentially recyclable thermoreversible networks. Hydrogen bonding strengths range from 10^2 M^{-1} for DNA nucleobases[12] to 10^7 M^{-1} for self-complementary ureidopyrimidone (UPy) hydrogen bonding groups.[13] The strength of hydrogen bonding associations is further tunable based on structural and geometric parameters as well as molecular design of the hydrogen bonding sites.[14-15] In biological systems, hydrogen bonding plays an essential role in protein folding and in maintaining the structure of DNA and RNA. Introduction of nucleic acid base pairs (adenine, thymine, uracil, guanine, cytosine) into synthetic polymers is achievable through a variety of synthetic methods such as post polymerization,[16] conventional radical

homopolymerization[17] or copolymerization[18] of functionalized (meth)acrylic or vinyl monomers, alternating radical polymerization with maleic anhydrides,[19] living cationic and anionic ring-opening polymerization of cyclic base pair derivatives,[20] nitroxide mediated polymerization (NMP),[21-23] and atom transfer radical polymerization (ATRP).[24] The incorporation of base pairs into synthetic polymers leads to molecular recognition ability,[16-17] metal ligation,[25] photocrosslinking,[16] photoresists,[16] and selective chromatographic media.[17]

In comparison to DNA where the nucleobases are always paired, the isolated nucleobases in synthetic polymers exhibits quite different behavior.[26] Multiple complementary association modes are possible for nucleobases, including the classical Watson-Crick mode[27] which is present in DNA as well as the less commonly observed Hoogsteen association mode.[28] Furthermore, nucleobases exhibit several other weak self-association modes (K_a < 10 M^{-1}), which compete with the complementary association modes. The multiplicative and cooperative effects of the neighboring hydrogen bonding groups in block copolymers lead to strong associations, which reinforce microphase separation.[23] In hydrogen bonding random copolymers, the recognition groups are randomly placed along the polymer backbone, which results in a dramatic difference in morphology and physical properties due to a potential competition between microphase separation and hydrogen bonding intermolecular association. In some cases, microphase separation can occur even for a single hydrogen bonding group at the chain ends (i.e. telechelic functionality).[26]

In recent years, there has been interest exhibited in polymer adhesives containing polar, ionic, or other entities capable of intermolecular association.[29-32] In this study, thymine

and adenine, which are nucleobases in DNA, were utilized as complementary hydrogen bonding units. Adhesive compositions comprising a high molecular weight poly(*n*-butyl acrylate) and a low content of nucleobases motifs are disclosed. The objective of this research is to elucidate the influences of hydrogen bonding association of nucleobase-functionalized acrylic random copolymers for pressure-sensitive adhesive application.

6.3 Experimental

6.3.1 Materials

n-Butyl acrylate (99%) was purchased from Aldrich and purified using an alumina column followed distillation from calcium hydride. AIBN was purchased from Aldrich and used without further purification. 9-(4-vinylbenzyl)adenine (VBA) and 1-(4-vinylbenzyl)thymine (VBT) were synthesized according to the previous literature.[10]

6.3.2 Instrumentation

Size exclusion chromatography (SEC) was performed using a Waters size exclusion chromatograph. The instrument was equipped with an autosampler, three 5 μm PLgel Mixed-C columns, a Waters 2410 refractive index (RI) detector operating at 880 nm, a Wyatt Technologies miniDAWN multi-angle laser light scattering (MALLS) detector operating at 690 nm, and a Viscotek 270 viscosity detector at 40 °C at a flow rate of 1 mL/min in THF. Reported molecular weights are based on absolute measurements using the MALLS detector. ^{1}H NMR spectra were collected in d-DMSO on a Varian 400 MHz spectrometer at 23 °C. Melt rheology measurements were conducted on a TA Instruments G2 Rheometer in parallel-plate geometry with a diameter of 8mm and separation 1mm. Strain amplitude was 1%. Thermal analysis using a TA instruments Differential scanning calorimetry (DSC) determined T_g at a heating rate of 20 °C/min under a nitrogen flush.

Glass transition temperatures were measured as the midpoint of the transition. FTIR spectroscopic analysis was performed using an ASI ReactIR 1000 attenuated total reflectance (ATR) spectrometer. Dynamic light scattering (DLS) measurements were performed with a Malvern Zetasizer Nano S apparatus equipped with a 4.0 mW laser operating at λ =633 nm. All samples were measured at a scattering angle of 173 °C. The data were the mean of three tests. Blends of adenine- and thymine-containing P*n*BA were prepared using solution casting. Chloroform solutions containing a 5 wt% polymer mixture were stirred overnight and cast on a Teflon dish. The solution was allowed to evaporate slowly at room temperature for 1 d. The blend films were then dried at 50 °C for 2 d.

6.3.3 Synthesis of Styrenic Nucleobase-Containing Random Copolymers

General procedure. 9-vinylbenzyl adenine (VBA)[12] (77 mg, 0.31 mmol) and AIBN were weighed into a 100-mL round-bottomed, flask with a magnetic stirbar. The flask was sealed with a rubber septum and purged with N_2 for 20 min. Purified *n*-butyl acrylate (4 mL) and DMSO (30 mL) were syringed into the flask. Finally the reaction mixture was stirred at 60 °C for 24 h. After the polymerization, reaction solution was precipitated into methanol/water mixture.

6.4 Results and Discussion

The copolymerization of styrenic adenine and thymine monomers with *n*BA afforded a series of high molecular weight polymers with varied hydrogen bonding contents (Scheme 6.1). Their molecular weights and thermal properties are summarized in Table 6.1. Both adenine- and thymine-containing polymers exhibited a single T_g, intermediate between that of the parent polymers, indicating the miscibility of these systems. T_g of

adenine- and thymine-containing copolymers with hydrogen bonding content lower than 10 mol% were very close to the T_g of P*n*BA. As illustrated in Figure 6.1, the T_g-composition curves were S-shaped, suggesting the intermolecular interactions involved in such a case were relatively weak. Normally, for hydrogen bonding polymers, T_g always positively deviated from the calculated weight average T_g values due to the reduction of polymer chains mobility upon hydrogen bonding.

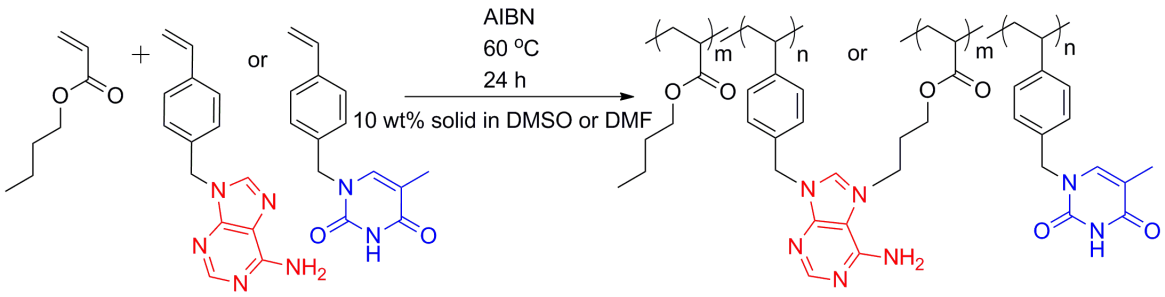

Scheme 6.1. Synthesis of nucleobase-containing random copolymers

Table 6.1. Molecular weights and molecular weight distributions for styrenic nucleobase-containing poly*n*BA

[Adenine] in feed (mol%)	[Adenine] in polymer (mol%)[a]	M_w[b] (g/mol)	M_w/M_n[b]	Yield	T_g (^oC)
3	5	231K	1.57	69%	-45
10	12	241K	1.30	68%	-44
15	15	106K	2.59	65%	NA
20	21	166K	3.74	82%	83
29	33	-	-	71%	95
100	100	-	-	51%	204
[Thymine] in feed (mol%)	[Thymine] in polymer (mol%)[a]	M_w[b] (g/mol)	M_w/M_n[b]	Yield	T_g (^oC)
7	7	166 K	2.16	92%	-46
11	12	191 K	1.83	87%	-45
15	15	105 K	2.84	70%	NA
20	20	135K	2.19	65%	71
28	33	-	-	58%	94
100	100	-	-	67%	168
P*n*BA	0	227 K	2.17	-	-51

-: insoluble in SEC solvent

NA: Broad transition

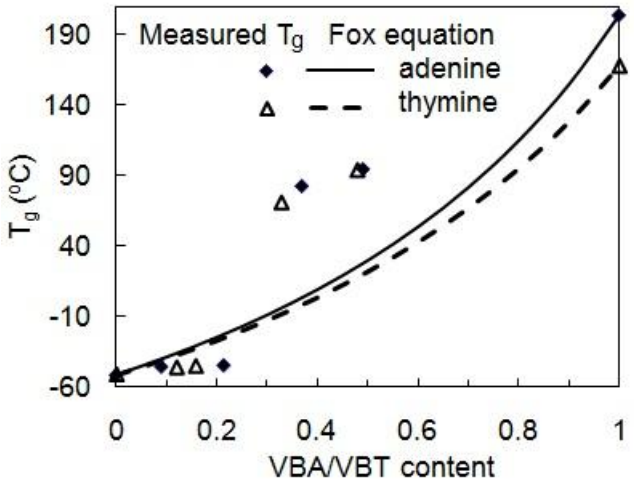

Figure 6.1. Deviation of T_g's of styrenic adenine- and thymine-containing poly(*n*-butyl acrylate)s from the Fox equation.

The role of solvent in the stability of recognition mechanisms was investigated using dynamic light scattering (DLS). Figure 6.2 compares the polymer hydrodynamic diameters in THF, a good solvent for hydrogen bonding formation and in DMF, which is a hydrogen bonding competitive solvent, respectively. In addition, poly(*n*-butyl acrylate) was selected as the reference material without strong hydrogen bonding intermolecular interactions. The intensity DLS results showed that all of the hydrogen bonding copolymers exhibited unimodal size distribution in DMF with the average diameter from 24 to 35 nm. In contrast, the size distribution of nucleobase-containing polymers in THF exhibited bimodal distributions suggesting the presence of larger aggregates. As a comparison, a non-hydrogen bonding polymer analogue, P*n*BA was also included. The average size of P*n*BA in THF was relatively the same as in DMF and exhibited no larger aggregates. This result represented hydrogen bonding association in a non-competitive solvent.

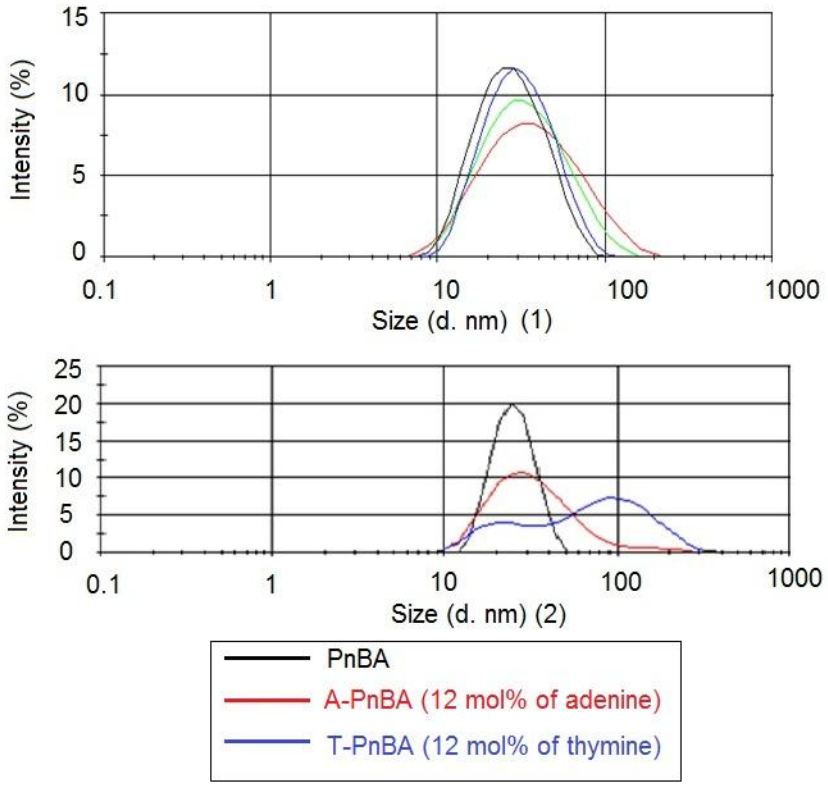

Figure 6.2. Solution aggregation behavior of selected adenine- and thymine-containing poly(*n*-butyl acrylate) with 12 mol% of hydrogen bonding content in (1) DMF and (2) THF

FT-IR analyses at various temperatures were conducted to probe hydrogen bonding dissociation. Infrared spectroscopy (IR) well suited for monitoring supramolecular ordering provides information on the event of loss of molecular order. Supramolecular polymer assembly is temperature dependent and can be restored reversibly upon cooling as long as molecular order persists. Therefore, we performed a variable temperature FT-IR study on the adenine and thymine-containing polymer complex in order to investigate the kinetics of supramolecular ordering. Figure 6.3 shows the scale-expanded FT-IR spectra of the adenine- and thymine-containing polymers. The peaks at 1,643 and 1,600 cm^{-1} were attributed to the N-H bending/scissoring vibration of adenine.[33] The broad

band with a peak maximum at 1,672 cm^{-1} corresponded to the stretching vibration of hydrogen bonded C=O in thymine. When temperature increased from 30 °C to 190 °C the absorbance of hydrogen bonded N-H bending vibration for adenine at 1,643 cm^{-1} decreased upon heating and a new peak emerged at lower wavenumber. Meanwhile, the band at 1,672 cm^{-1} of hydrogen bonded C=O from thymine disappeared, suggesting the disruption of hydrogen bonds between paired thymine and adenine. With careful analysis of the new peak, we found that above 120 °C the peak started to stabilize and the majority of complementary hydrogen bonds were disrupted. In conclusion, the variable temperature FT-IR study further confirmed the hydrogen bonding formation in polymer complex at room temperature and its dissociation upon heating, which resulted in the corresponding peak retrieved to or close to the primary vibration peaks.

Hydrogen bonding reversibility was investigated using heat-cool cycles on the polymer complex of adenine- and thymine-containing polymers (Figure 6.4). Samples were heated from 30 to 120 ^{o}C and equilibrated at each temperature for 5 minutes, and then quench back to 30 ^{o}C (~5 ^{o}C/min). Upon heating, the weak peak at 1643 cm^{-1} shifted about 20 cm^{-1} to the lower wavenumber direction, indicating rapid disruption of hydrogen bonds. In the cooling process, the peak at 1643 cm^{-1} retrieved to its original position, suggesting the reversible formation of hydrogen bonds. However, the heating and cooling traces do not superimpose, suggesting some hysteresis. The strong peak at 1725 cm^{-1} corresponded to the free carbonyl groups broadened upon heating, indicating an increased amount of free C=O groups. This peak did not recover in the cooling process, reflecting some irreversibility of hydrogen bonding. The specific recognition between adenine and thymine are not easily achieved in the bulk state, possibly due to limited diffusion of

pendant groups. Sijbesma et al. also reported a similar behavior of UPy-functionalized polycaprolactones which exhibited different storage moduli in the heat-cool cycles.[34]

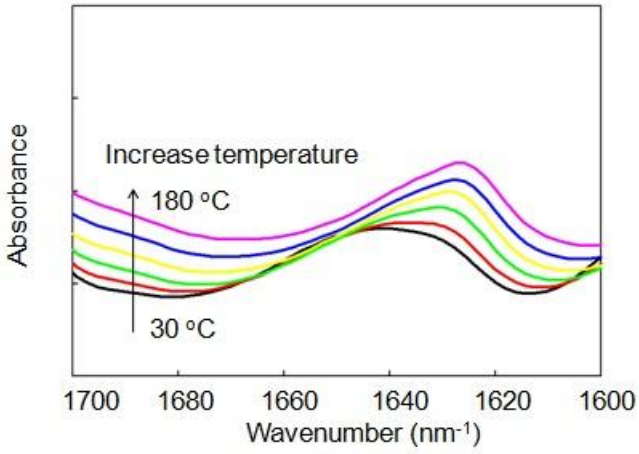

(1)

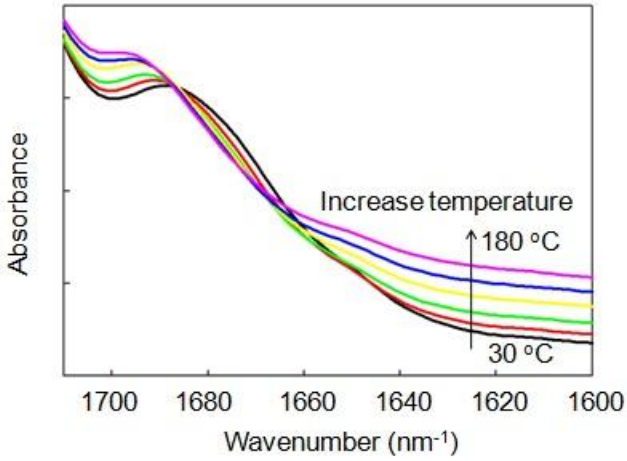

(2)

Figure 6.3. Variable temperature FT-IR spectra of (1) poly(*n*BA-*co*-styrenic adenine) (12 mol% of adenine) and (2) poly(*n*BA-*co*-styrenic thymine) (12 mol% of thymine)

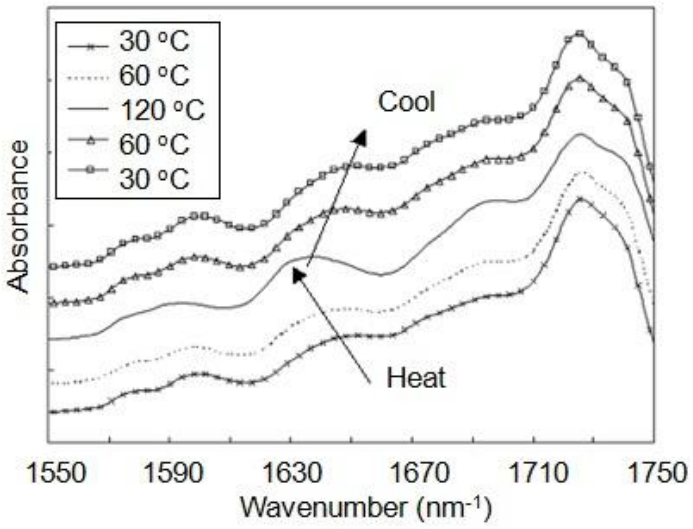

Figure 6.4. Variable temperature FT-IR spectra of the hydrogen bonding complex of adenine- and thymine-containing P*n*BA

Styrenic adenine- and thymine-containing polymers with 12 mol% of nucleobase were tacky at room temperature and did not form films. Their complementary hydrogen bonding enabled film formation at room temperature. Tapping mode AFM was performed on the hydrogen bonding complex as shown in Figure 6.5. The hydrogen bonding complex revealed microphase separation on the scale of 100 nm. The bright regions corresponded to the nucleobase-containing hard domains, which randomly distributed in the soft polymer matrix and did not exhibit any well-defined morphology.

The intramolecular screening effect is a consequence of chain connectivity. The covalent linkage between polymer segments causes the polymer chains bending back on themselves and lead to an increase in the number of same-polymer-chain contacts; thus, the number of interassociation hydrogen bonds per unit volume in the polymer blend will be lower than that in the precursors.[35] Moreover, the spacing between the functional

groups along a polymer chain and the presence of bulky sides groups can also significantly reduce the interassociation hydrogen bonding per unit volume, as a result of a so-called functional group accessibility effect. This effect is also considered to be the origin of steric crowding and shielding. [36]

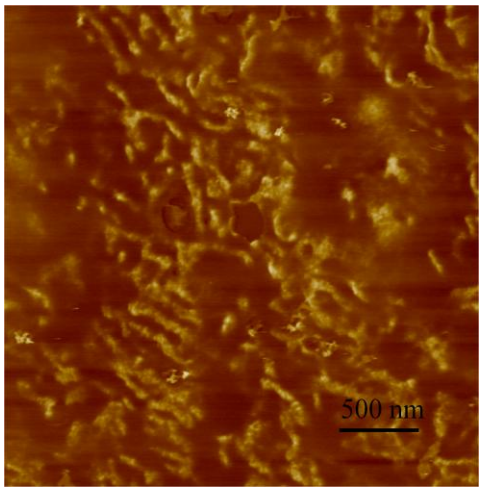

Figure 6.5. AFM image of the hydrogen bonding polymer complex ([A]:[T]=1:1)

The most important molecular parameters determining polymer melt rheology are molecular weight, molecular weight distribution, and the amount of long chain branching. Melt rheological analysis also provided profiles of the complex viscosity versus the temperature for the copolymers. To understand the dissociation of nucleobase pairs in poly(n-butyl acrylate), the melt rheological characterization of adenine- and thymine-functionalized poly(n-butyl acrylate) and their hydrogen bonding blends was performed over a wide temperature range (Figure 6.6). In general, an apparent increase in melt viscosity of the hydrogen bonding complex was observed at all measured temperatures and the complex melt viscosity decreased with the increase of temperature. At 60 ^{o}C, the complex viscosity of the polymer blend was more than 10 times higher than the

precursors. Upon heating, the melt viscosities of all three samples exhibited similar transitions, which decreased dramatically as the temperature approached 70 °C where most hydrogen bonds dissociated. The hydrogen bonding complexes exhibited stronger temperature dependence.

Time-temperature superposition was performed on the adenine- and thymine-containing random copolymers as well (Figure 6.7). Master curves of the storage modulus versus the frequency were referenced to 25 °C, given that the T_g's of these polymers were lower than room temperature. It should also be noted that in the construction of the master curves no vertical shift of the data was needed, demonstrating that the plateau modulus G_N^0 was not a strong function of temperature. The two samples failed to master properly on the low-frequency (high temperature) side; instead they showed pronounced fanning. This failure to obey TTS indicated various relaxation mechanisms in the polymer melt, and phase segregation is likely to be considered as the cause of the failure.

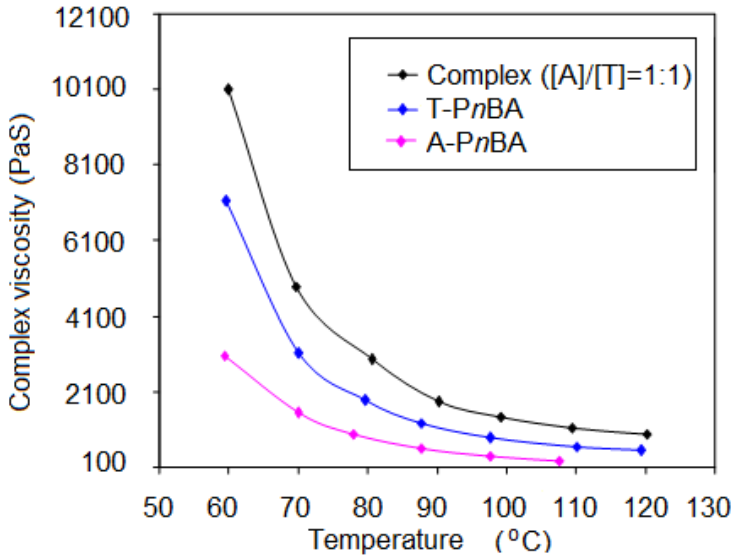

Figure 6.6. Complex melt viscosity as a function of temperature for poly(*n*BA-*co*-styrenic adenine) (15 mol% of adenine) and poly(*n*BA-*co*-styrenic thymine) (15 mol% of thymine)

\

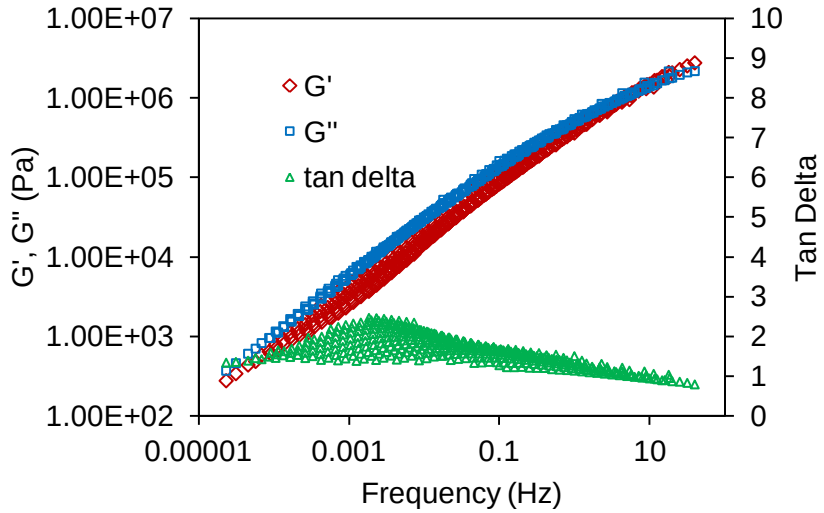

(1)

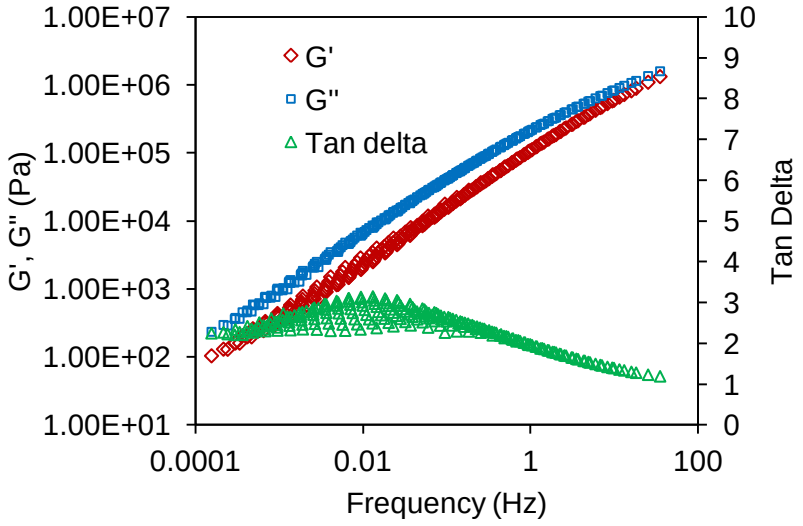

(2)

Figure 6.7. Master curves of (1) poly(*n*BA-*co*-styrenic adenine) (15 mol% of adenine) and (2) poly(*n*BA-*co*-styrenic thymine) (15 mol% of thymine)

Hydrogen bonding associations provide strategies to increase polymer apparent molecular weight to prevent creep and cohesive failure while improving interfacial adhesion.[37] To demonstrate the effectiveness of complementary multiple hydrogen bonding on polymer adhesion, we measured the peel strength (the ability to resist

removal upon peeling). An ASTM-D3300 standard 90° peel testing method was adopted and the results were depicted in Figure 6.8. All polymers with 10 mol% of nucleobase or less failed 100% cohesively. Peel strengths of the styrenic thymine- and adenine-containing copolymers with 7 mol% of thymine and 5 mol% of adenine were 195 g/inch and 125 g/inch, respectively. The peel strength of the hydrogen bonding complex was higher than the precursors and further increased upon annealing. The enhanced wettability is ascribed to the strong association of nucleobases as well as the strong association between nucleobases and the stainless steel surface.

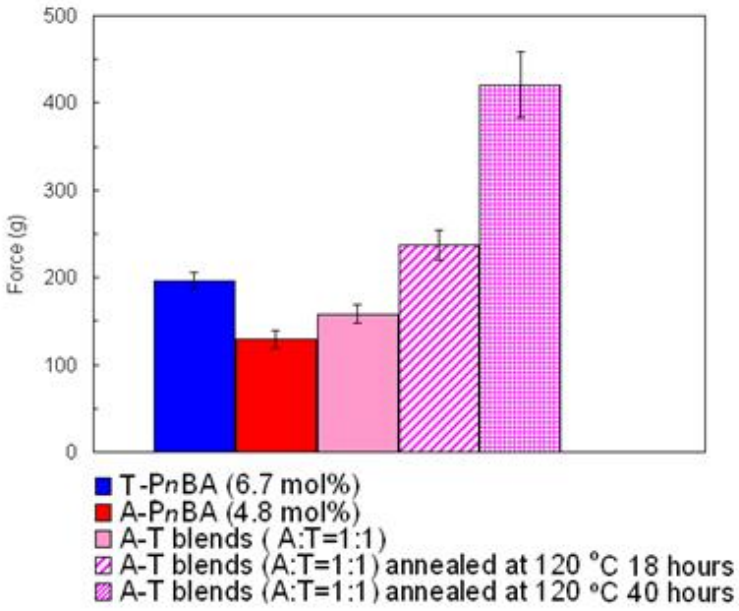

Figure 6.8. Peel strength of poly(*n*BA-*co*-styrenic adenine) and poly(*n*BA-*co*-styrenic thymine)

6.5 Conclusions

P*n*BA containing varied amounts of nucleobases (adenine and thymine) were synthesized. Blending of adenine- and thymine-P*n*BA resulted in higher melt viscosities compared to the corresponding adenine- and thymine-P*n*BA, confirming strong hydrogen

bonding associations between adenine and thymine. Melt rheology and AFM results demonstrated the heterogeneity in the polymer melt due to strong complementary hydrogen bonding. The hydrogen bonding complex demonstrated a stronger temperature dependence of melt viscosity. Moreover, variable-temperature FT-IR studies also demonstrated the thermal reversibility of the hydrogen bonding.

6.6 Acknowledgements

The authors acknowledge the financial support of the Petroleum Research Fund (ACS-PRF 35190-AC7), which is administered by the American Chemical Society.

6.7 References

1. Lange, R. F. M.; Van Gurp, M.; Meijer, E. W. *J. Polym. Sci., Part A Polym. Chem.* **1999,** 37, (19), 3657-3670.
2. Müller, M.; Dardin, A.; Seidel, U.; Balsamo, V.; Ivan, B.; Spiess, H. W.; Stadler, R. J. *Macromolecules* **1996,** 29, 2577-2583.
3. Berl, V.; Schmutz, M.; Krische, M. J.; Khoury, R. G.; Lehn, J.-M. *Chem. Eur. J.* **2002,** 8, 1227-1244.
4. Yamauchi, K.; Lizotte, J. R.; Hercules, D. M.; Vergne, M. J.; Long, T. E. *J. Am. Chem. Soc.* **2002,** 124, (29), 8599-8604.
5. Yamauchi, K.; Long, T. E. *Polym. Mater. Sci. Eng.* **2001,** 85, 465-466.
6. Lutz, J.-F.; Thuenemann, A. F.; Rurack, K. *Macromolecules* **2005,** 38, (20), 8124-8126.
7. Deans, R.; Ilhan, F.; Rotello, V. M. *Macromolecules* **1999,** 32, 4956-4960.

8. Wang, D.; Su, Y.; Jin, C.; Zhu, B.; Pang, Y.; Zhu, L.; Liu, J.; Tu, C.; Yan, D.; Zhu, X. *Biomacromolecules* **2011,** 12, 1370–1379.

9. Soentjens, S. H. M.; Sijbesma, R. P.; van Genderen, M. H. P.; Meijer, E. W. *J. Am. Chem. Soc.* **2000,** 122, (31), 7487-7493.

10. Sotiropoulou, M.; Bokias, G.; Staikos, G. *Macromolecules* **2003,** 36, 1349-1354.

11. Sijbesma, R. P.; Beijer, F. H.; Brunsveld, L.; Folmer, B. J. B.; Hirschberg, J. H. K. K.; Lange, R. F. M.; Lowe, J. K. L.; Meijer, E. W. *Science* **1997,** 278, (5343), 1601-1604.

12. Kyogoku, Y.; Lord, R. C.; Rich, A. *Proc Natl Acad Sci USA* **1967,** 57, 250-257.

13. Brunsveld, L.; Folmer, B. J. B.; Meijer, E. W.; Sijbesma, R. P. *Chem. Rev.* **2001,** 101, (12), 4071-4097.

14. Beijer, F. H.; Sijbesma, R. P.; Kooijman, H.; Spek, A. L.; Meijer, E. W. *J. Am. Chem. Soc.* **1998,** 120, (27), 6761-6769.

15. Beijer, F. H.; Sijbesma, R. P.; Vekemans, J. A. J. M.; Meijer, E. W.; Kooijman, H.; Spek, A. L. *J. Org. Chem.* **1996,** 61, (18), 6371-6380.

16. Ilhan, F.; Galow, T. H.; Gray, M.; Clavier, G.; Rotello, V. M. *J Am Chem Soc* **2000,** 122, 5895-5896.

17. Inaki, Y. *Prog. Polym. Sci.* **1992,** 17, 515-570.

18. Khan, A.; Haddleton, D. M.; Hannon, M. J.; Kukulj, D.; Marsh, A. *Macromolecules* **1999,** 32, 6560.

19. Han, M. J.; Park, S. M.; Park, J. Y.; Yoon, S. H. *Macromolecules* **1992,** 25, 3534-3539.

20. Inaki, Y.; Futagawa, H.; Takemoto, K. *J. Polym. Sci., Part A: Polym. Chem.* **1980,** 18, 2959-2969.

21. Mather, B. D.; Lizotte, J. R.; Long, T. E. *Macromolecules* **2004,** 37, (25), 9331-9337.

22. Mather, B. D.; Baker, M. B.; Beyer, F. L.; Green, M. D.; Berg, M. A. G.; Long, T. E. *Macromolecules* **2007,** 40, (13), 4396-4398.

23. Mather, B. D.; Baker, M. B.; Beyer, F. L.; Berg, M. A. G.; Green, M. D.; Long, T. E. *Macromolecules* **2007,** 40, (19), 6834-6845.

24. Spijker, H. J.; van Delft, F. L.; van Hest, J. C. M. *Macromolecules* **2007,** 40, (1), 12-18.

25. Srivatsan, S. G.; Parvez, M.; Verma, S. *Chem.--Eur. J.* **2002,** 8, (22), 5184-5191.

26. Sivakova, S.; Bohnsack, D. A.; Mackay, M. E.; Suwanmala, P.; Rowan, S. J. *J. Am. Chem. Soc.* **2005,** 127, (51), 18202-18211.

27. Sivakova, S.; Rowan, S. J. *Chem. Soc. Rev.* **2005,** 34, (1), 9-21.

28. Ghosal, G.; Muniyappa, K. *Biochem. Biophys. Res. Commun.* **2006,** 343, 1-7.

29. Courtois, J.; Baroudi, I.; Nouvel, N.; Degrandi, E.; Pensec, S.; Ducouret, G.; Chaneac, C.; Bouteiller, L.; Creton, C. *Adv. Funct. Mater.* **2010,** 20, (11), 1803-1811.

30. Woodward, P.; Merino, D. H.; Hamley, I. W.; Slark, A. T.; Hayes, W. *Aust. J. Chem.* **2009,** 62, (8), 790-793.

31. Alessandri, I. *Small* **2010,** 6, (15), 1679-1685.

32. Gower, M. D.; Shanks, R. A. *Journal of Polymer Science: Part B: Polymer Physics* **2006,** 44, 1237–1252.

33. Toshio Itahara, T.; Uto, T.; Sunose, M.; Ueda, T. *J. Mol. Struct.* **2002,** 616, 213–220.

34. Wietor, J.-L.; Beek, D. J. M. v.; Peters, G. W.; Mendes, E.; Sijbesma, R. P. *Macromolecules* **2011,** 44, 1211–1219.

35. Pehlert, G. J.; Painter, P. C.; Veytsman, B.; Coleman, M. N. *Macromolecules* **1997,** 30, 3671.

36. Pehlert, G. J.; Painter, P. C.; Coleman, M. N. *Macromolecules* **1998,** 31, 8423.

37. Cashion, M. P.; Park, T.; Long, T. E. *The Journal of Adhesion* **2009,** 85, 1-17.

Chapter 7: Nucleobase Self-Assembly in Acrylic Random Copolymers for Adhesive Application

Shijing Cheng, Mingqiang Zhang, Ninad Yogesh Dixit, Robert B. Moore, and Timothy E. Long, to be submitted*

7.1 Abstract

Novel acrylate monomers functionalized with nucleobase pairs (adenine and thymine) were prepared upon *aza*-Michael addition and successfully copolymerized with *n*-butyl acrylate. At a content of 7 mol%, adenine self assembled into needle-like microstructures within amorphous polymer matrices as shown under atomic force microscopy (AFM), small-angle X-ray scattering (SAXS), and wide-angle X-ray diffraction (WAXD); and thymine did not homoaggregate into distinct morphologies even up to 30 mol%. When mixed together, thymine- and adenine-containing random copolymers fused into a thermodynamically stable polymer complex crosslinked through adenine-thymine base pairs. The molar fractions of the nucleobase monomer, nucleobase stacking interactions, and hydrogen bonding were the parameters that principally influence self-assembly. Additionally, the nucleobase-functionalized polyacrylates exhibited specific adhesive and strong cohesive strength.

7.2 Introduction

The use of non-covalent interactions as a tool for the synthesis of well-defined supramolecular structures is one of the main topics in current polymer science.[1-4] The motivation behind the imitation of DNA is to mimic some particular features of this biomacromolecules and to use them for other applicative purposes, e.g. the unique

molecular recognition of complementary nucleobases, the stimuli-responsiveness of multiple hydrogen bonding, and the self-assembly involving cooperative multiple non-covalent interactions. Hydrogen-bonding driven molecular recognition plays a crucial role in the biological functions of biopolymers. The artificial recognition systems containing nucleobase, such as molecularly imprinted polymers[5-6] and nucleobase-templated polymerization[7] also found great potential applications in catalysis, separations, biomedicine, chemo/biosensors, and information storage.

The development of synthetic polymers bearing nucleobase recognition sites is difficult and requires multiple design and lengthy synthesis due to the accessibility for multiple substitutions. Nucleobase units were introduced using post-polymerization modification,[8-9] otherwise protection of the nucleobase monomers is necessary to obtain high conversions.[10-11] Recent developments in controlled metathesis and radical polymerization techniques have enlarged the ability to create well defined polymers with high tolerance to hydrogen bonding and ionic functionalities. During the last decades, several groups reported the preparation of synthetic polymers possessing nucleobases as side groups or chain ends. Sleiman et al. utilized ring-opening metathesis polymerization to synthesize adenine-containing block copolymers, which self assembled into rod morphologies.[12] van Hest et al. synthesized thymine functional block copolymers using atom transfer radical polymerization (ATRP) of thymine methacrylate monomers from a poly(oxyethylene) macroinitiator.[13] Lutz et al. polymerized styrenic nucleobase monomers using ATRP.[14-15] Inaki et al. synthesized a wide range of nucleobase functionalized random and homopolymers and block copolymers using ring-opening cationic and anionic polymerization of acyclic derivatives of the nucleobases.[16] Our

group previously reported the high tolerance of nitroxide mediated polymerization to nucleobase functionalities[17] and prepared styrenic adenine- and thymine-containing ABA triblock copolymers using a novel difunctional alkoxyamine initiator.[18-19] However, like all known bio-receptors, such as DNA, enzyme, and antibodies, and all nucleobase functionalized synthetic polymers for molecular recognition have either relatively rigid structures as guidable scaffolds for nucleobases to anchor or sterically congested polymer backbones,[20] such as vinyl,[21] styrene,[15, 22] and methacrylate.[13-14, 23] Examples of receptors having relatively flexible structures are very few in number.[24-25] The molecular recognition process is highly dependent on both the recognition groups and the spacers that link them. Meijer et al. previously reported a significant decrease in the stability of benzene-1,3,5-tricarboxamides aggregates upon the increase of the polymer backbone polarity.[26]

In the present work, we modified the spacers that link recognition groups and evaluated the influence of structural rigidity on nucleobase self-assembly behavior using AFM and SAXS. The novel acrylic nucleobase monomers were synthesized using a one-step *aza*-Michael addition without any group protection. Michael addition is an efficient and mild reaction that can be employed for introducing highly functional groups, biopolymers (e.g. proteins) or bioactive species (e. g. drugs) into polymers.[27] The prepared monomers were then homopolymerized or copolymerized with *n*-butyl acrylate using conventional free radical polymerization. The hydrogen bonding polymers provided a reversible network with strongly temperature-dependent viscosity and self-healing nature that could be of industrial interest in coating and hot melt applications. Peel strength and shear strength of nucleobase-containing polyacrylates were shown to be

significantly higher than acrylic acid- and 4-vinylpyridine-based polyacrylate analogues at similar hydrogen bonding molar concentration.

7.3 Experimental

7.3.1 Materials

n-Butyl acrylate (*n*BA, 99+%), acrylic acid (AA, 99+%), and 4-vinylpyridine (4VP, 99+%) were purchased from Aldrich and passed through neutral alumina columns before use. α,α'-Azobis(isobutyronitrile) (AIBN, Fluka, 99%) was recrystallized from methanol. 1,4-Butanediol diacrylate (Alfa Aesar, 99%) was used without further purification. Adenine (A, 99%), thymine (T, 99%), triethylamine (TEA, 99%), potassium carbonate (99%), and 2,6-di-*tert*-butyl-4-methylphenol (BHT, 99%) were purchased from Aldrich and used without further purification. Hexane (HPLC grade), chloroform ($CHCl_3$, HPLC), tetrahydrofuran (THF, HPLC grade), *N*,*N*-dimethylsulfoxide (DMSO, HPLC grade) and *N*,*N*-dimethylformamide (DMF, HPLC grade, anhydrous) were purchased from Fisher Scientific and used as received. 9-(4-vinylbenzyl)adenine and 1-(4-vinylbenzyl)thymine were synthesized according to the previous literature.[28]

7.3.2 Instrumentation

^{1}H NMR and ^{13}C NMR spectra were collected in $CDCl_3$ or DMSO-d_6 on a Varian INOVA spectrometer operating at 400 MHz 23 °C. Fast Atom Bombardment Mass Spectrometry (FAB-MS) was conducted in positive ion mode on a JEOL HX110 dual focusing mass spectrometer. Size exclusion chromatography (SEC) was performed using a Waters size exclusion chromatograph. The instrument was equipped with an auto sampler, three 5 μm PLgel Mixed-C columns, a Waters 2410 refractive index (RI) detector operating at 880 nm, a Wyatt Technologies miniDAWN multi-angle laser light

scattering (MALLS) detector operating at 690 nm, and a Viscotek 270 viscosity detector with a flow rate of 1 mL/min at 50 °C in DMF with 0.01 M lithium bromide (LiBr). Reported molecular weights are relative to polystyrene standards.

Differential scanning calorimetry (DSC) was performed under a nitrogen flush of 50 mL/min at a heating rate of 10 °C/min on a TA instruments Q1000TM DSC, which was calibrated using indium (mp = 156.60 °C) and zinc (mp = 419.47 °C) standards. Glass transition temperatures were measured as the midpoint of the transition in the second heating scan. Dynamic mechanical analysis (DMA) was conducted on a TA Instruments Q800 Dynamic Mechanical Analyzer in tension mode at a frequency of 1 Hz, an oscillatory amplitude of 15 μm, and a static force of 0.01 N. The temperature ramp was 3 °C/min. The glass transition temperature (T_g) was determined at the peak maximum of the tanδ curve. All FT-IR experiments were carried out using Varian 670-IR spectrometer (DTGS detector) with Pike Technologies variable temperature GladiATR^{TM} attachment (Diamond crystal). The spectra were collected at 4 cm^{-1} resolution and as an average of 32 scans. The samples were subjected to a temperature ramp of 1 °C /min, starting from 30 °C to 180 °C and FT-IR spectra were collected at every 10 °C beginning from 30 °C.

A Veeco MultiMode scanning probe microscope was used for tapping-mode AFM imaging. Samples were imaged at a set-point ratio of 0.67 with a magnification of 1 μm×1 μm. Veeco's Nanosensor silicon tips having a spring constant of 42 N/m were utilized for imaging. WAXD and SAXS were performed using Rigaku S-Max 3000 pinhole SAXS system. X-ray source was the Cu K_α radiation, and the wavelength was 0.154 nm. For WAXD measurement, the sample-to-detector distance was 80 mm. A Fuji HR-V imaging plate was used to collect the two-dimensional images with an exposure

time of 1 h. The imaging plate was scanned using a RAXIA-Di system, and Rigaku's SAXSGUI software package provided a plot of intensity versus scattering angle, 2θ. For SAXS measurement, silver behenate was used to calibrate the sample to detector distance and the sample-to-detector distance was 1600 mm. SAXSGUI software package was used to obtain scattering intensity, $I(q)$, versus scattering wave vector $q=4\pi\sin(\theta)/\lambda$, where θ was half of the scattering angle and λ was the wavelength of the incident beam. The measured data was corrected for background scattering, sample thickness and transmission. For the variable temperature SAXS and WAXD measurement, samples were heated to the specific temperature and held for 1 h, following with an exposure time of 1 h. Oscillatory shear experiments were performed on a TA AR-G2 rheometer over a broad range of temperatures (0-110 °C) and frequencies (0.1-100 Hz). All measurements were performed using parallel plate geometry, with a diameter of 8 mm and interplate distances of 0.5 mm. A 5 wt% solution of adenine-containing polyacrylate in $CHCl_3$ was mixed with a 5 wt% $CHCl_3$ solution of thymine-containing polyacrylate and stirred for 6-8 h. Then, $CHCl_3$ was left to evaporate slowly at room temperature for 48 h and annealed under reduced pressured at 100 °C for 2 d.Polymers were dissolved in dry $CHCl_3$ and cast into a Teflon® Petri dish, followed by slow evaporation of the solvent and drying the film in vacuo. Discs of 8 mm diameter were punched out for rheometry. All measurements were strain-controlled at a constant nominal strain value within the linear viscoelastic range, determined with strain sweeps. The characteristic viscoelastic functions, storage modulus (G') and loss modulus (G") were measured at different temperatures and frequencies. Master curves were obtained from temperature/frequency sweep measurements using time-temperature superposition (TTS), which is described

with the Williams-Landel-Ferry equation. G" curves were used as the reference curves for TTS. The peel force per unit width was measured in accordance with ASTM-D3300 standard. The test specimens for the adhesive evaluation were prepared with coating a 10 wt% chloroform solution of a nucleobase-containing polymer on a stainless steel plate and a PET rectangular strip of 25 mm width, respectively. Film thickness was controlled using a film casting knife (0.2 mm). The chloroform was subsequently evaporated at 23 °C under vacuum. Residual solvent and voids were not observed in the thin films. The polymer coated PET film was adhered to the complementary polymer coated stainless steel substrate and rolled down once with a 1 kg roll. Adhesive strength was measured at 90° using a Cheminstruments AR-1000 Peel Tester. The cross-head speed was maintained at 12 inch/min, and five measurements were performed on five different specimens to ensure reproducibility. The shear force per unit area was measured in accordance with ASTM-D1002 using an Instron Universal Testing Machine. An untreated glass plate coated with polymer was fixed to the edge of another untreated glass plate so that an area of 6.45 cm^2 (1 in^2) was in contact with the glass. A shear rate of 1 inch/min was used. Instron maximum shear force values were reported as the maximum load and expressed as N/in^2. An average of five measurements was taken.

7.3.3 Synthesis of 4-((3-(Thymin-l-yl)propanoyl)oxy)butyl acrylate

A suspension of thymine (1.00 g; 7.93 mmol) and BHT (60.0 mg) in DMF (20 mL) was treated with triethylamine (0.22 mL, 1.58 mmol) at room temperature. The reaction mixture was stirred under an inert atmosphere (argon) for 1 hr and then treated with 1,4-butanediol diacrylate (3.0 mL, 15.9 mmol). The reaction solution turned clear after stirring at room temperature for 24 h. Then, it was poured into water (150 mL) and

washed with hexane to remove excess 1,4-butanediol diacrylate. The water layer was extracted with dichloromethane (3×20 mL). The combined extracts were dried over $MgSO_4$, filtered, and concentrated in a vacuum evaporator to remove all the solvents. The evaporation residue was separated using flash column chromatography with $CHCl_3$-MeOH (20:1) on silica gel. Evaporation of the total eluent gave a white solid of 1.82 g with an overall yield of 71%, melting at 70 °C. ^{1}H NMR (400 MHz, d_6-DMSO): 1.54-1.68 (m, 4H, $H_{b+b'}$), 1.71 (s, 3H, H_e), 2.66 (t, 2H, J=6.0 Hz, H_c), 3.83 (t, 2H, J=5.2 Hz, H_d), 3.97-4.13 (m, 4H, $H_{a+a'}$), 5.91 (d, 1H, J=11.2 Hz, H_{g1}), 6.14 (dd, 1H, J_1=8.4 Hz, J_2=16.8 Hz, H_h), 6.30 (d, 1H, J=6.8 Hz, H_{g2}), 7.48 (s, 1H, H_f), 11.23 (br, 1H, H_i); ^{13}C NMR (100 MHz, d_6-DMSO): 12.4, 25.1, 33.2, 44.2, 64.1, 64.2, 108.6, 128.8, 131.9, 142.2, 151.2, 164.7, 165.9, 171.2; HRMS (ES+): m/z calcd for [M+H$^+$] 324.13 g/mol, found 324.14 g/mol.

7.3.4 Synthesis of 4-((3-(Adenin-9-yl)propanoyl)oxy)butyl acrylate

A suspension of adenine (1.0 g, 11.9 mmol), BHT (60 mg), K_2CO_3 (40.0 mg, 0.29 mmol) in DMSO (20 mL) was stirred at 50 °C for 1 h and followed with adding 1,4-butanediol diacrylate (3 mL, 15.9 mmol). After the reaction mixture was stirred at 50 °C for 5 h, it was poured into water (150 mL) and washed with hexane to remove excess 1,4-butanediol diacrylate. Then, the water layer was extracted with dichloromethane (3×20 mL). The combined extracts were dried over $MgSO_4$, filtered, and concentrated in a vacuum evaporator to remove all the solvents. The evaporation residue was separated using chromatography with $CHCl_3$-MeOH (20:1) on silica gel. A trace amount of N-7 adduct were eluent first. Evaporation of the remained eluent gave a white solid of 1.30 g with an overall yield of 53%, melting at 117 °C. ^{1}H NMR (400 MHz, d_6-DMSO): 1.45-

1.64 (m, 4H, $H_{b+b'}$), 2.93 (t, 2H, J=6.8 Hz, H_c), 3.95-4.10 (m, 4H, $H_{a+a'}$), 4.35 (t, 2H, J=6.8 Hz, H_d), 5.91 (d, 1H, J=10.4 Hz, H_{g1}), 6.13 (dd, 1H, J_1=10.4 Hz, J_2=17.2 Hz, H_h), 6.29 (d, 1H, J=17.2 Hz, H_{g2}), 7.18 (bs, 2H, H_i), 8.07 (s, 1H, H_e), 8.11 (s, 1H, H_f); ^{13}C NMR (100 MHz, d_6-DMSO): 25.1, 34.0, 64.0, 64.2, 128.7, 131.9, 141.3, 152.8, 156.4, 165.9, 171.1; HRMS (ES+): m/z calcd for [M+H^+] 334.14 g/mol, found 334.15 g/mol.

7.3.5 Synthesis of Acrylic Nucleobase-Containing Random Copolymers and Hydrogen Bonding Analogues

Poly(acrylic adenine-*co*-*n*BA), poly(acrylic thymine-*co*-*n*BA), and poly(AA-*co*-*n*BA) and poly(4VP-*co*-*n*BA) were synthesized using solution free radical polymerization with AIBN as the initiator. A typical synthesis was carried out as follows. Acrylic Adenine (1.0 g, 3.0 mmol) was weighed into a 100-mL round-bottomed flask containing a magnetic stir bar. The flask was sealed with a rubber septum and purged with N_2 for 20 min. Then anhydrous DMSO (35 mL, 10 wt% of solid) was added to the flask to dissolve acrylic adenine monomers. Purified *n*-butyl acrylate (4.0 mL, 28.0 mmol) was syringed into the reaction flask. Lastly, AIBN (10 mg, 0.15 mol%) was dissolved in 5 mL of anhydrous DMSO and flushed with dry nitrogen for 10 min, and was then syringed into the reaction mixture. The reaction flask was placed in an oil bath at 60 °C for 24 h with constant stirring. After polymerization, DMSO was distilled off under reduced pressure. The product was redissolved in THF (25 mL) and precipitated into a methanol and water mixture (800 mL). The final products were dried at 30 °C under reduced pressure (0.5 mm Hg) for 24 h. The product contained 10 mol% acrylic adenine and 90 mol% *n*BA, with a yield of 82%.

7.3.6 Synthesis of Styrenic and Acrylic Nucleobase-Containing Homopolymers

Styrenic and acrylic adenine- and thymine-containing homopolymers were synthesized using conventional free radical polymerization in DMF or DMSO solution with AIBN as the initiator. A representative example of the synthesis was conducted as follows. Acrylic adenine (4.0 g, 12.0 mmol), AIBN (10 mg, 0.6 mmol, 0.25 wt%), and anhydrous DMSO (30 mL) were placed into a 100-mL round-bottomed flask. After the flask was sealed and purged with N_2 for 20 min, it was placed in an oil bath at 60 °C for 24 h with constant stirring. After polymerization, the polymer solution was precipitated into diethyl ether (800 mL). The final products were dried at 30 °C under reduced pressure (0.5 mm Hg) for 24 h. Yield: 90%

7.4 Results and Discussion

7.4.1 Synthesis of Nucleobase Functional Polyacrylates

Synthesis of acrylic nucleobase-containing polymers involved the novel acrylic monomer synthesis using Michael addition and direct radical polymerization of functional acrylic adenine and thymine monomers. Synthesis of nucleobase styrene[28] and methacrylate[13] monomers has been reported in the literature. However, the corresponding homopolymers were glassy at room temperature and insoluble in polar aprotic organic solvents, which strongly disfavored the molecular recognition.[15] We targeted for acrylic nucleobase monomers possessing long alkyl chains, which potentially promote the solubility in a variety of organic solvents. The introduction of nucleobases through regioselective substitution is crucial due to the presence of more than one nucleophillic sites on respective nucleobases. Previously our group successfully attached nucleobase onto polystyrene[9] and poly(D, L-lactide)[29] chain ends through Michael addition. The

base-catalyzed Michael addition is thermodynamically controlled,[30] which affords *N*1-substitubted thymine and *N*9-substituted adenine as the major products (Figure 7.1 and 7.2). The reaction conditions, such as solvent, temperature, and the amount of base catalysts, were optimized and the regioselectivity was achieved in a satisfactory yield. The reaction started heterogeneously and turned clear at the end, due to an enhanced solubility of the final products. Additionally, utilizing excess diacrylates suppressed undesirable difunctionalization.

Conventional free radical copolymerization of acrylic nucleobase monomers with *n*-butyl acrylate was carried out homogeneously in DMF or DMSO, and the polymers were prepared in high yields (Scheme 7.1). The nucleobase concentration in the random copolymer was obtained from the ratio of ^{1}H NMR resonances integration at 7.8-8.0 ppm and 3.6-4.4 ppm (Figure 7.3 and 7.4), which corresponded to the chemical shift of -C*H* (H_f) in nucleobase and -O-CH_2- ($H_{a+a'+a''}$) in both *n*-butyl acrylate and acrylic nucleobase monomers. Table 7.1 lists the monomer feed ratios and the corresponding copolymer compositions. Due to the similar reactivities of *n*BA and the acrylic nucleobase monomers, the copolymer composition matched the feed ratio very well. SEC results revealed broad molecular weight distributions of all samples (PDI>2) possibly due to the non-living character of the polymerization and strong hydrogen bonding.

Scheme 7.1. Michael addition of adenine and thymine with 1,4-butanediol diacrylate

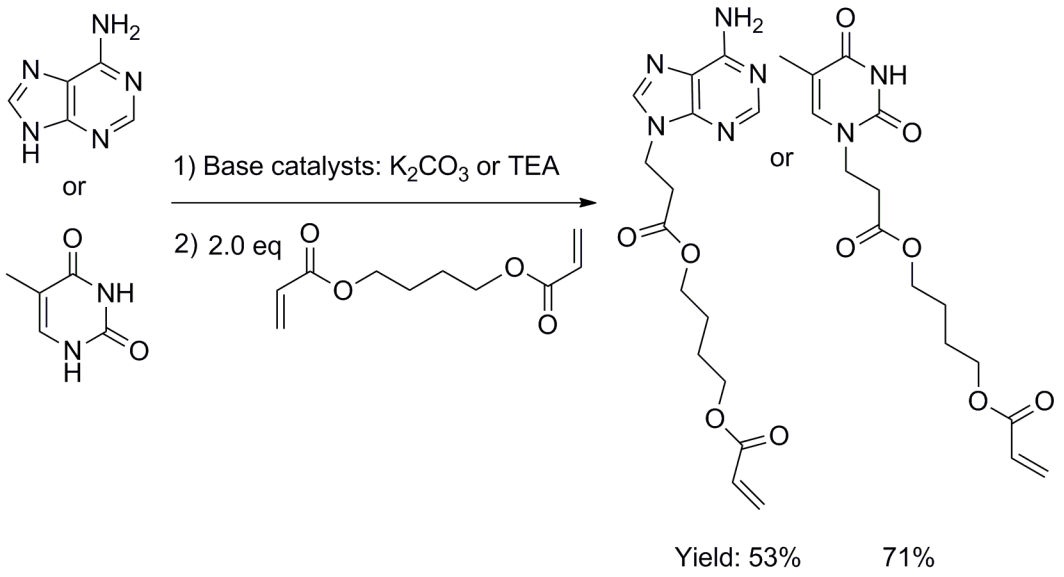

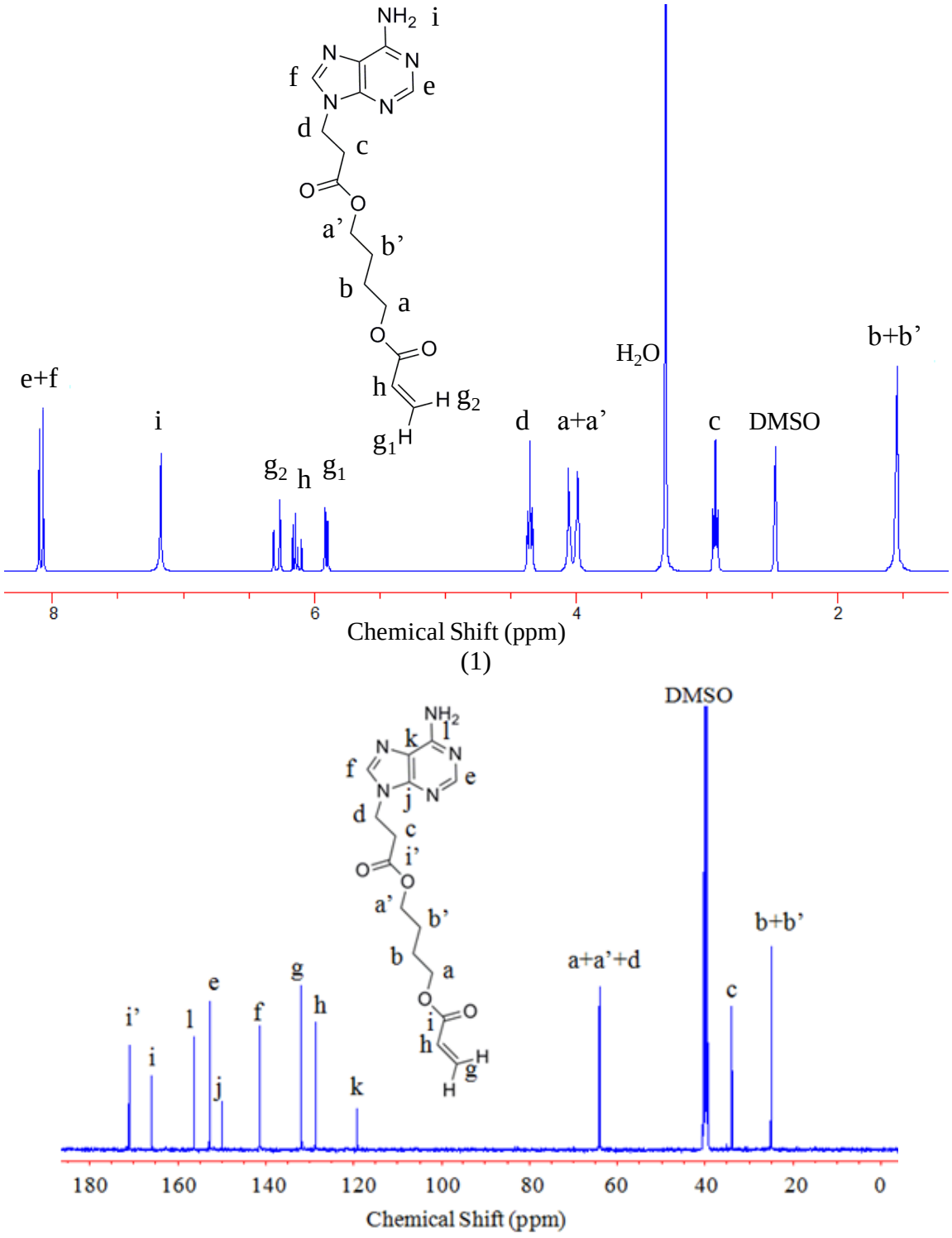

Figure 7.1. ^{1}H NMR (1) and ^{13}C NMR (2) spectra of 4-(3-adenine-9-yl-propanoyloxy)butyl acrylate in d_6-DMSO.

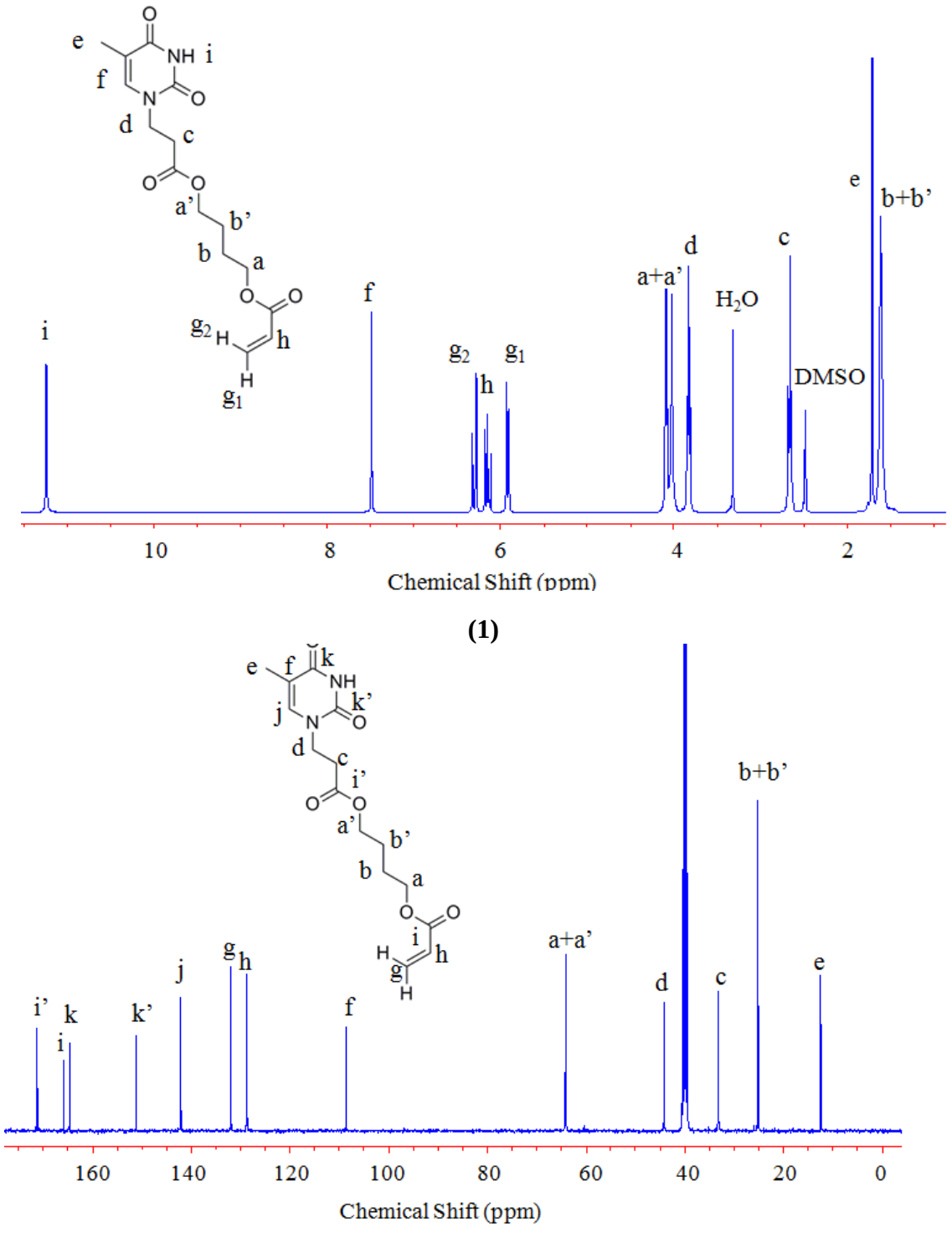

Figure 7.2. ^{1}H NMR (1) and ^{13}C NMR (2) spectra of 4-((3-(thymin-l-yl)propanoyl)oxy)butyl acrylate in d_6-DMSO.

Scheme 7.2. Copolymerization of *n*-butyl acrylate and 4-(3-adenine-9-yl-propanoyloxy)butyl acrylate or 4-((3-(thymin-l-yl)propanoyl)oxy)butyl acrylate

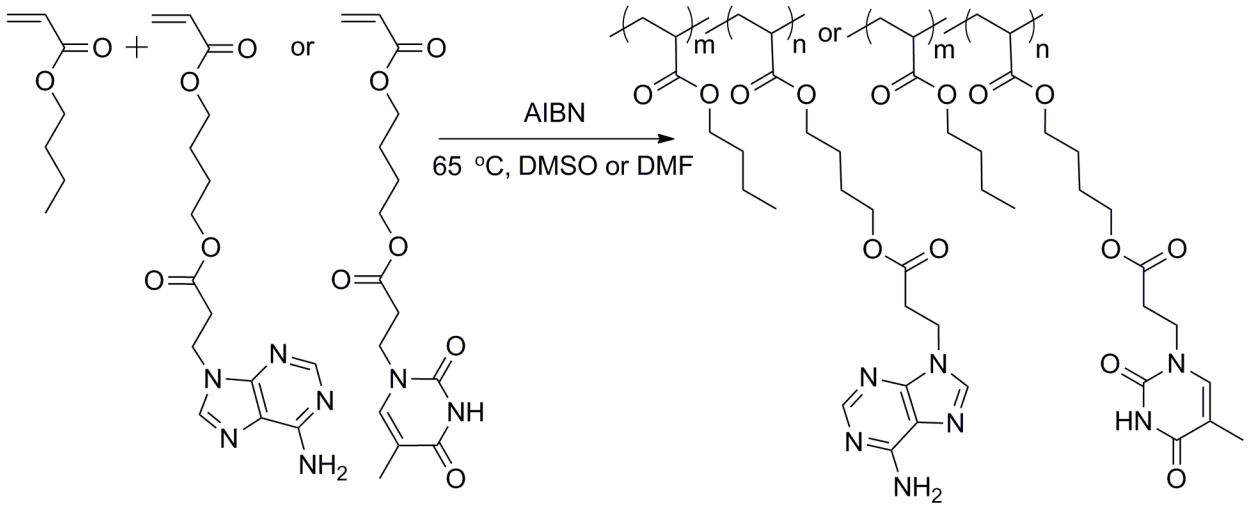

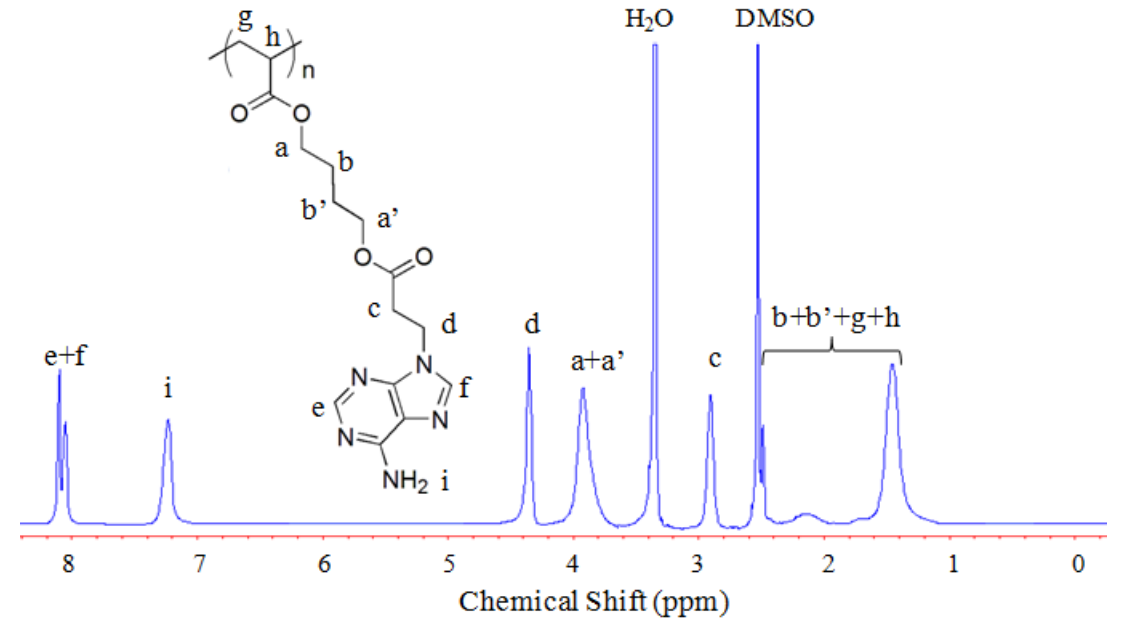

(1)

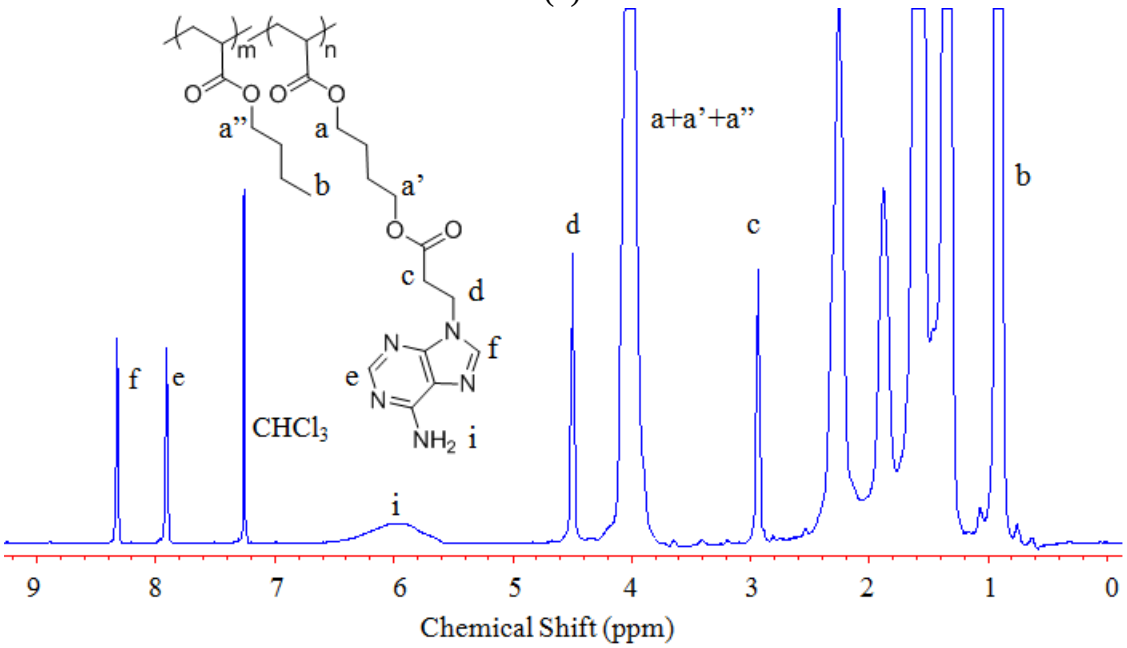

(2)

Figure 7.3. ^{1}H NMR spectrum of acrylated adenine homopolymer **(1)** and poly(acrylated adenine-*co*-*n*BA) **(2)** with 4 mol% of adenine

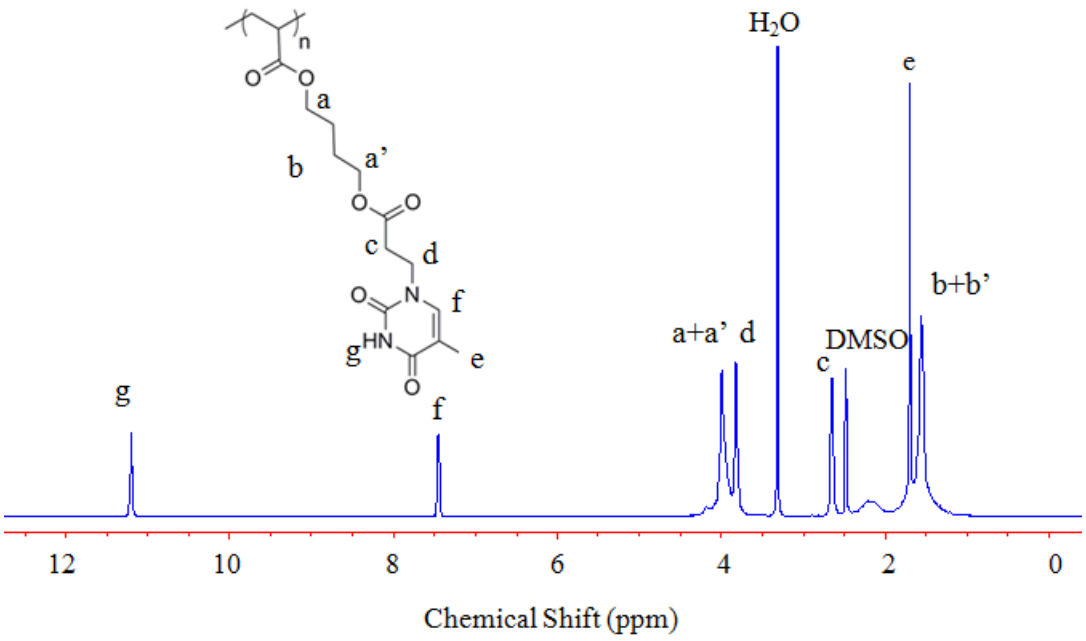

(1)

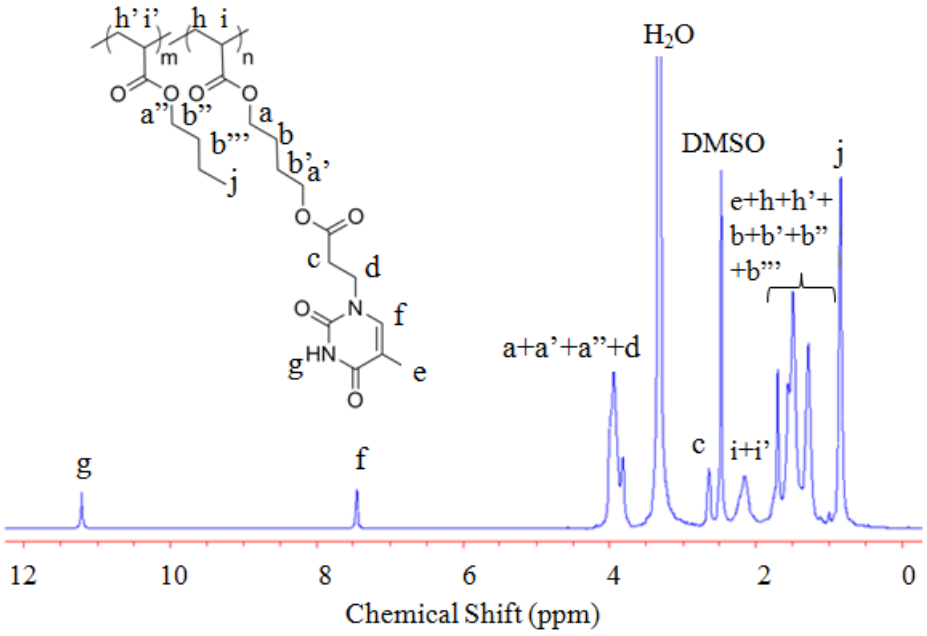

(2)

Figure 7.4. ^{1}H NMR spectrum of acylated thymine homopolymer (1) and poly(acrylated thymine-*co*-*n*BA) with 10 mol% of thymine (2)

Table 7.1. Molecular characterization of adenine- and thymine-containing poly(*n*-butyl acrylate) random copolymers and complementary hydrogen bonding polymer analogues

Sample Name	M_1	$[M_1]$ in feed (mol%)	$[M_1]$ in polymer[a] (mol%)	M_w[b] (g/mol)	M_w/M_n[b]	Yield	T_g (°C)
A-4	Acrylic Adenine	5	4	95K	2.09	86%	-41
A-7	Acrylic Adenine	10	7	125K	1.64	44%	-25
A-16	Acrylic Adenine	19	16	288K	4.47	84%	0
A-100	Acrylic Adenine	100	100	NA	NA	90%	65
T-10	Acrylic Thymine	10	10	122K	3.40	76%	-30
T-18	Acrylic Thymine	18	18	155K	2.40	74%	-14
T-25	Acrylic Thymine	29	25	164K	2.73	80%	1
T-32	Acrylic Thymine	40	32	NA	NA	70%	19
T-100	Acrylic Thymine	100	100	NA	NA	75%	43
StA-100	Styrenic Adenine	100	100	NA	NA	81%	204
StT-100	Styrenic Thymine	100	100	NA	NA	80%	168
VP-10	[4VP]	10	10	70.1 K	2.33	69%	-42
AA-4	[AA]	4	10	64.1 K	1.85	88%	-37

[a] ^{1}H NMR

[b] SEC: 0.01 M LiBr/DMF

NA: Polymers were not soluble

7.4.2 Thermal Transitions

To understand the association of nucleobase pairs, we studied the thermal and dynamic mechanical properties of adenine- and thymine-functionalized poly*n*BA and their complex. DSC curves of acrylic adenine- and thymine-containing copolymers all showed a single T_g, suggesting a random copolymerization of *n*-butyl acrylate and acrylic nucleobase monomers. Figure 7.5 shows the influence of nucleobase content on the T_gs

of the copolymers. A linear increase of T_g was observed with the increase of the mole fraction of adenine and thymine, and it positively deviated from the Fox equation. Such deviation was attributed to the incorporation of strongly associating nucleobase units. The more significant T_g deviation for adenine-containing polymers than that for thymine-containing polymers indicates stronger self-association of adenine than thymine at a similar molar concentration.

The thermodynamic mechanical properties of adenine and thymine acrylate copolymers at small deformations were studied using DMA in tension mode (Figure 7.6). The storage modulus curve (G') of acrylic adenine-containing polymer with 7 mol% of adenine showed a rubber plateau between 5 and 50 °C, followed with a subsequent sharp decrease of modulus and eventually flow at 57 °C. It is immediately clear how significantly the polymer properties change with the addition of even a few mole percent of strongly hydrogen-bonding monomer. With increasing adenine incorporation to 16 mol%, T_g increased; the plateau modulus was two orders of magnitude higher; and the flow temperature increased to 85 °C. This change was attributed to the presence of associated adenine units, which reinforced the polymer matrices as physical crosslinks. Additionally, the tanδ curves in DMA thermograms revealed broad glass transitions spanned 80 °C for A-7 and 60 °C for copolymers with A-16. This slow relaxation is presumably due to the dynamic hydrogen bonds that restricted the mobility of polymer backbone. The broad temperature window also provides a healing window for polymers to reorder. In comparison to adenine, thymine-containing polymers possessing only showed a short and less well-defined rubbery plateau at even higher nucleobase concentration, suggesting less pronounced microphase separation.

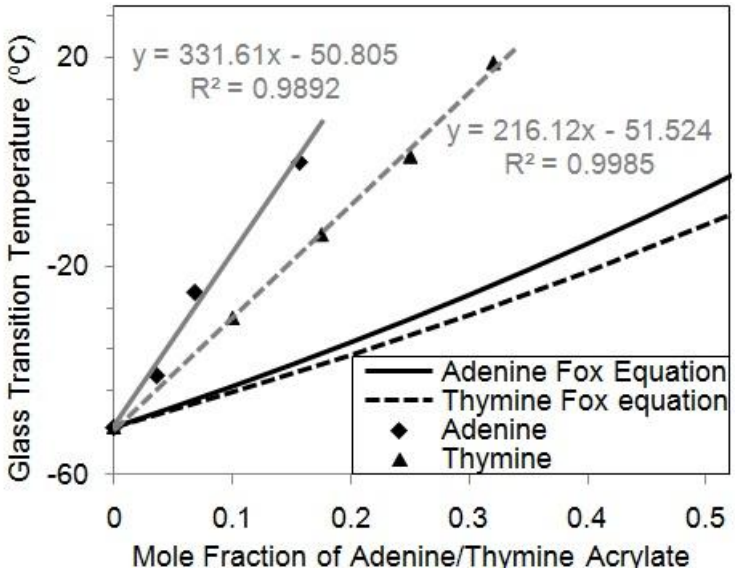

Figure 7.5. Relationship between acrylic thymine contents and T_g

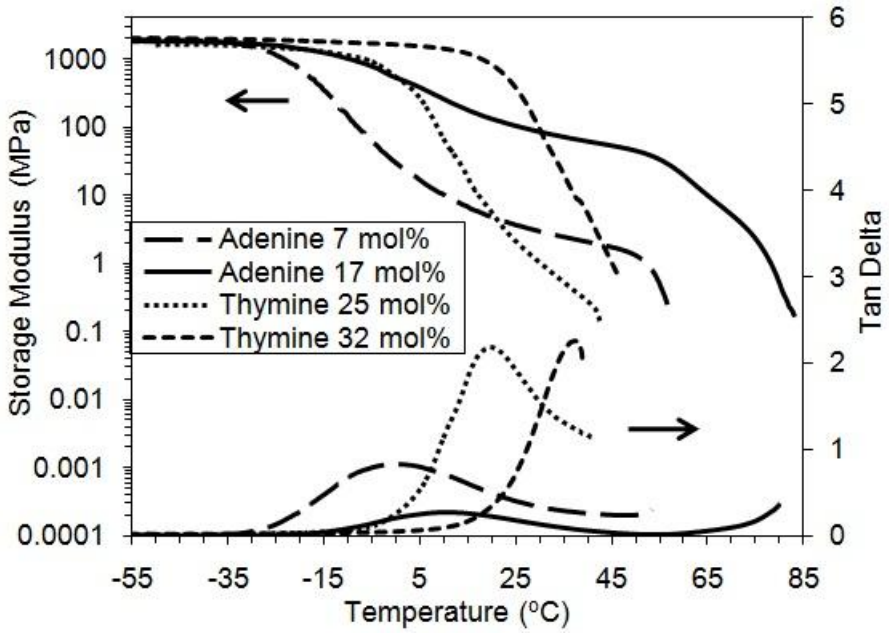

Figure 7.6. DMA traces of poly(*n*BA-*co*-acrylic adenine) with 7 mol% and 17 mol% of acrylic adenine respectively and poly(*n*BA-*co*-acrylic thymine) with 25 mol% of acrylic thymine.

7.4.3 Infrared Spectroscopy

Infrared spectroscopy (IR) well suited for monitoring supramolecular ordering and provides information on the event of loss of molecular order. Supramolecular polymer assembly is temperature dependent and can be restored reversibly upon cooling as long as molecular order persists. Therefore, we performed a variable temperature FT-IR study on the adenine and thymine-containing polymer complex in order to investigate the kinetics of supramolecular ordering. A slow heating and cooling rate of 1 °C/min was used to suppress kinetic (non-equilibrium) effects. Figure 7.7 shows the scale-expanded FT-IR spectra of the adenine- and thymine-acrylate polymer complex with a stoichiometry ratio of [A]:[T]=1:1 at various temperatures. The broad band with a peak maximum at 1,672 cm^{-1} corresponded to the stretching vibration of hydrogen bonded C=O in thymine. The peaks at 1,643 and 1,600 cm^{-1} were attributed to the N-H bending/scissoring vibration of adenine. When temperature increased from 30 °C to 190 °C, the band at 1,672 cm^{-1} disappeared, indicating the dissociation of hydrogen bonded C=O from thymine. Meanwhile, the absorbance of hydrogen bonded N-H bending vibration for adenine at 1,643 cm^{-1} also decreased upon heating, and a new peak emerged at lower wavenumber, suggesting the disruption of hydrogen bonds between paired thymine and adenine. With careful analysis of the new peak, we found that above 120 °C the peak started to stabilize around 1627 cm^{-1}. In this case, the majority of complementary hydrogen bonds were disrupted. In conclusion, the variable temperature FT-IR study further confirmed the hydrogen bonding formation in polymer complex at room temperature and its dissociation upon heating, which resulted in the corresponding peak retrieved to or close to the primary vibration peaks.

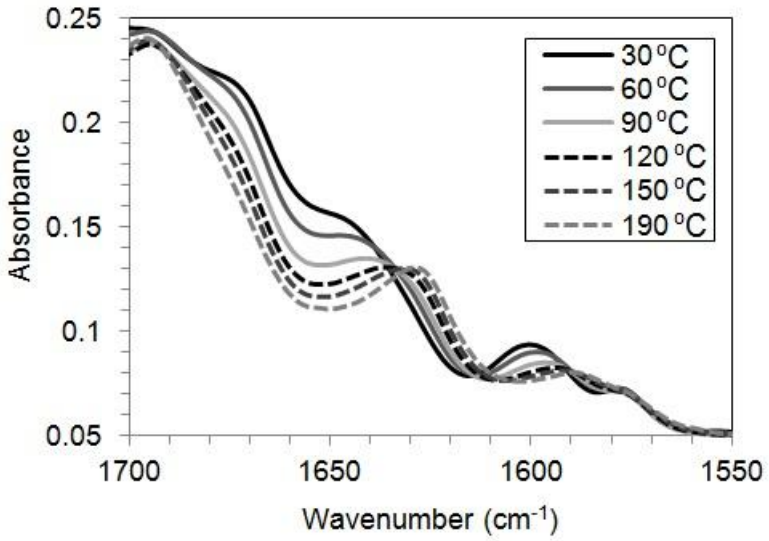

Figure 7.7. Variable temperature FT-IR spectra in the 1600-1700 cm^{-1} region for the complex of poly(*n*BA-*co*-acrylic adenine) and poly(*n*BA-*co*-acrylic thymine)

7.4.4 Morphology

AFM enables imaging of surface texture and morphology of microphase separated structures and is frequently applied to polymer films. AFM micrographs of acrylic adenine-containing random copolymers revealed intriguing surface morphologies as shown in Figure 7.8. Polymers with 7 mol% of adenine were microphase separated into needle-like hard structures. These structures of about 100 nm in length and less than 10 nm in width were randomly oriented in the soft polymer matrix. SAXS results (Figure 7.9) also revealed a broad peak near 0.90 nm^{-1} with a *d* spacing of ca. 7.0 nm, which corresponded to the average distance between needle-like structures observed under AFM. These structures percolated as the adenine content increased from 7 mol% to 16 mol%. The broadness of the SAXS peak also suggested the random orientation of these structures. To further understand the internal structure of the nano-needles, wide-angle X-ray diffraction studies (WAXD) were performed on the annealed film samples (Figure

7.10). The diffraction pattern of the adenine acrylate-containing random copolymers displayed an intense diffraction peak located at 2θ=20°, which was assigned to the local chain packing (amorphous halo) of P*n*BA. The reflection peak at 2θ =12.87° (d =6.87 Å) corresponded to the distance between nucleobase stacks,[24] which were held together with π-π interactions and, from the FT-IR data, adenine-adenine hydrogen bonding. We interpreted these needle-like structures as one-dimensional crystalline stacks of associated adenine units with a parallel arrangement of the rings.

The AFM micrograph of thymine acrylate copolymers did not show any obvious organized nanostructures even up to 32 mol% of thymine. Accordingly, the SAXS profiles of thymine-containing random copolymers only showed broad peaks with very low intensity, implying less pronounced self-association of thymine than adenine. This observation was similar to the self-assembly behavior of adenine- and thymine-terminated telechelic poly(tetrahydrofuran)s.[24] The weak hydrogen bonding self-dimerization constant of adenine and thymine (both less than 10 M^{-1} in $CDCl_3$)[31] suggested that the unique higher order self-assembly of adenine-containing polymers was driven through additional non-covalent interactions, such as π-π stacking, which was more pronounced for adenine than the other pyrimidine or purine derivatives.[32] In general, the extent of stacking decreased as purine-purine>purine-pyrimidine>pyrimidine-pyrimidine.[33] In addition, Hawker and Kramer et al. synthesized random copolymers consisting of *n*BA with quadruple hydrogen bonding side chains based on 2-ureido-4[1H]-pyrimidinone (UPy).[34] Although the UPy groups strongly dimerized, they did not π-π stack into crystalline structures and no microphase separation was observed in this case. Meijer et al. studied the self-assembly process of ureidotriazine

functionalized oligo(*p*-phenylenevinylene), and found that the π-conjugated structures was crucial in guiding hydrogen bonded molecules to further assemble into supramolecular structures.[35]

A comparison study of WAXD was performed on styrenic and acrylic nucleobase-containing homopolymers to further elucidate the significance of structural flexibility on supramolecular self-assembly (Figure 7.11). The diffraction pattern of acrylic adenine homopolymer displayed reflection peaks at 2θ=12.9° (*d*=6.87 Å) and 22.5° (*d*=3.95 Å), which were assigned to associated adenine stacks.[24] Whereas, thymine did not π-π stack strongly and thymine-containing homopolymer did not show distinct reflection peaks. Interestingly, styrenic adenine homopolymer did not reveal reflection peaks either. Although the bulky phenyl rings potentially provided increased aromatic surface, they sterically hindered the well-defined position between adenine-adenine π-π stacks. Moreover, the spacing between the functional groups along a polymer chain and the presence of bulky sides groups can also significantly reduce the associated hydrogen bonding per unit volume, as s result of a so-called functional group accessibility effect. This effect is also considered to be the origin of steric crowding and shielding.[36] Thus, the relatively strong π-π interactions of adenine as well as the good mobility and accessibility introduced from long chain alkyl spacers together resulted in the unique well-defined nanostructures observed in acrylic adenine-containing random copolymers.

Variable temperature X-ray experiments were carried out to further investigate the influence of temperature on adenine self-assembly. Figures 7.12 and 7.13 show the various-temperature SAXS and WAXD profiles of A-16. The intensity of the broad Bragg peak near q= 0.90 nm^{-1} decreased monotonically with temperature until the peak

was barely visible as a shoulder at 80 °C. The same trend was shown in WAXD profiles that the reflection of stacked adenine-adenine decreased in intensity with temperature increase and eventually disappeared above 80 °C, implying the dissociation of the needle-like nano-structures upon heating. From DMA analysis (Figure 7.6), the polymer film started losing mechanical integrity at 80 °C and eventually flew. These results were in agreement with the proposed structural model that these hard needle-like structures composed of π-π stacks of hydrogen bonded adenine which reinforced polymer matrices.

Blending acrylic adenine- and thymine-containing copolymers resulted in a polymer complex with weak microphase separation as shown in AFM (Figure 7.8). The absence of distinctive microphase separation was most likely because the A-T base pairs possessed weaker π-π interactions than A-A[33] and the lack of stereoregularity in polymer backbone. For adenine-containing polymers, adenine intramolecularly π-π packed with the neighboring adenine. This supposition was reinforced with SAXS results of the polymer complexes, which revealed averaged, intermediate Bragg spacings, and no evidence of multiple interdomain spacings (Figure 7.9). As the ratio of [A]/[T] decreased from 4:1 to 2:1, the scattering peak intensity decreased and the polymer complexes became more uniform. Kuo et al. also reported a similar behavior for triazine- and thymine-containing PMMA copolymer mixtures that the degree of homogeneity of the polymer complex was relatively higher than the precursors.[37] Hydrogen bonding suppressed the concentration fluctuations.

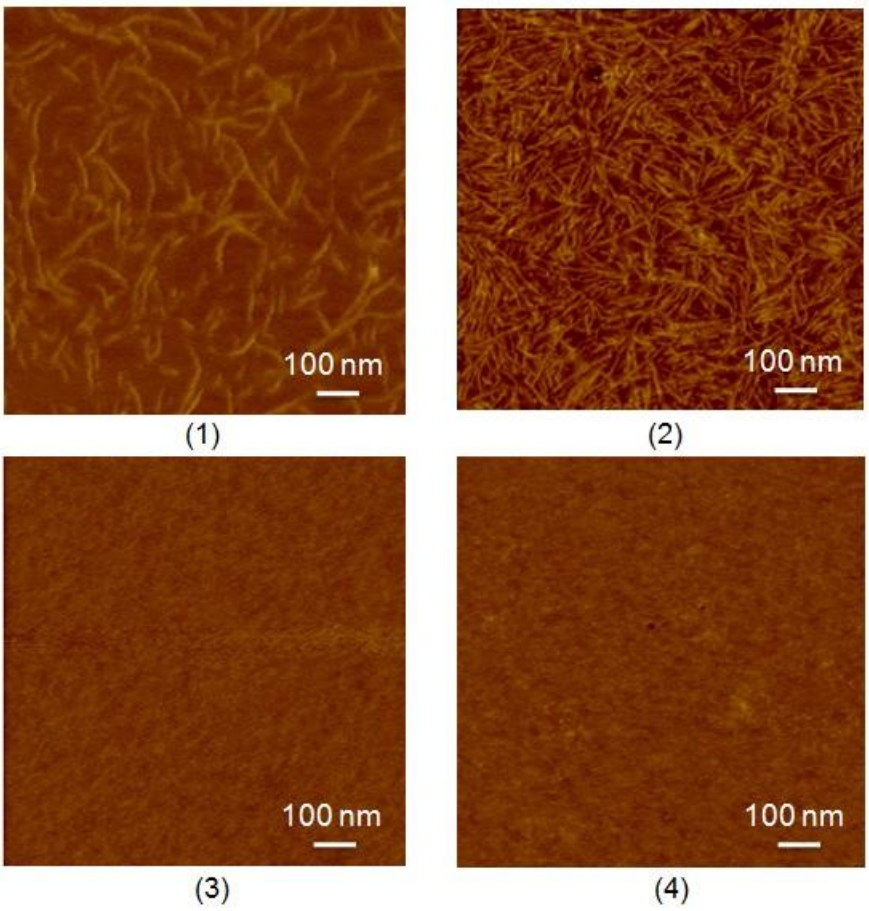

Figure 7.8. Tapping mode AFM phase images of thins films of poly(*n*BA-*co*-acrylic adenine) with (1) 7 mol% and (2) 16 mol% adenine, poly(*n*BA-*co*-acrylic thymine) with (3) 25 mol% and (4) 32 mol% thymine

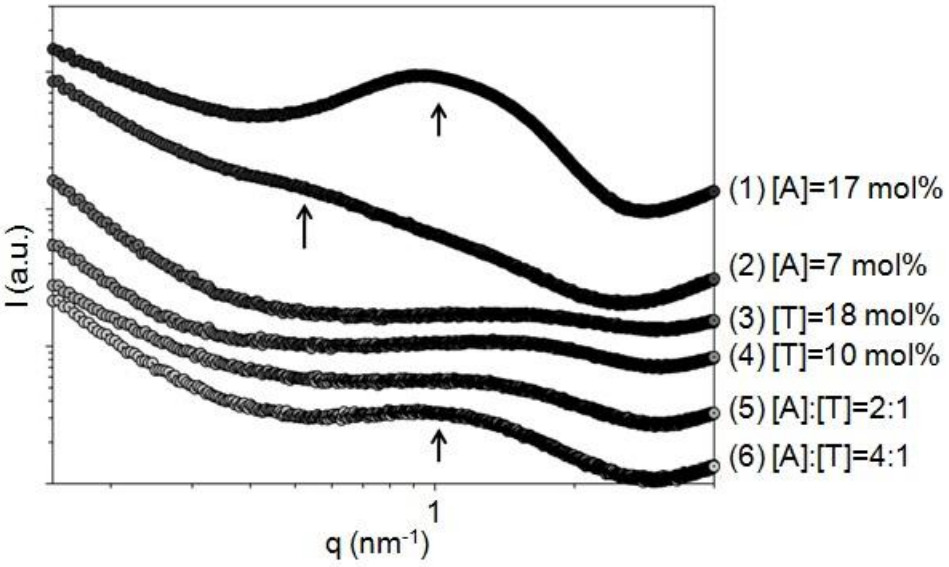

Figure 7.9. SAXS of poly(*n*BA-*co*-acrylic adenine) with (1) 7 mol% and (2) 16 mol% of adenine, poly(*n*BA-*co*-acrylic thymine) with (3) 25 mol% and (4) 32 mol% of thymine, and the polymer complexes of (2) and (3) at [A]/[T]=4 and A]/[T]=2 For sake of clarity, data were shifted by arbitrary factors.

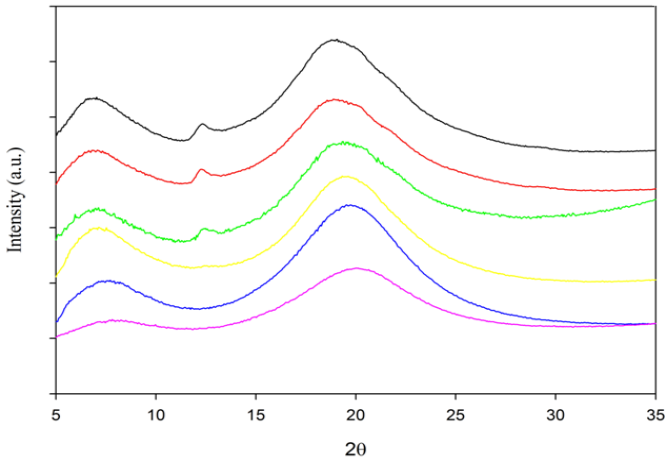

Figure 7.10. Wide angle X-ray (radiation source Cu Kα) diffraction diagram of poly(*n*BA-*co*-acrylated adenine) with 16 mol% (1) and 7 mol% (2) of adenine and poly(*n*BA-*co*-acrylated thymine) with 25 mol% (3) and 32 mol% (4) of thymine. For sake of clarity, data were shifted by arbitrary factors.

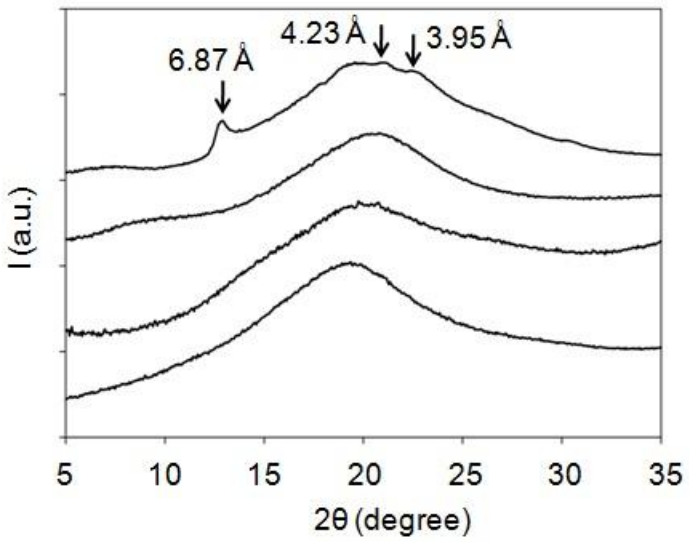

Figure 7.11. X-ray (radiation source Cu K_α) diffraction diagram of (1) acrylic adenine homopolymer, (2) acrylic thymine homopolymer, (3) styrenic adenine homopolymer, and (4) styrenic thymine homopolymer. For sake of clarity, data were shifted by arbitrary factors.

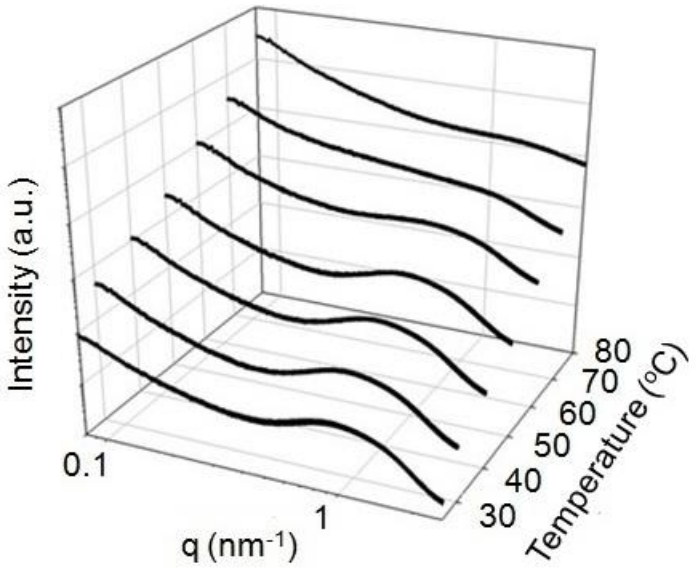

Figure 7.12. Variable temperature SAXS of poly(*n*BA-*co*-acrylated adenine) with 16 mol% of adenine. For sake of clarity, data were shifted by arbitrary factors.

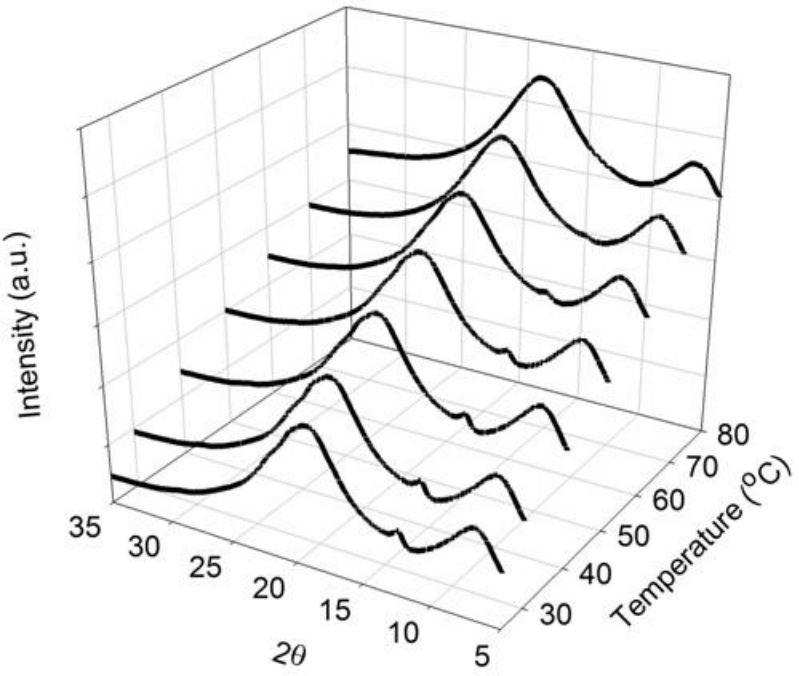

Figure 7.13. Variable temperature WAXD of poly(*n*BA-*co*-acrylated adenine) with 16 mol% of adenine. For sake of clarity, data were shifted by arbitrary factors.

7.4.5 Rheology

Melt rheological characterization was conducted on adenine- and thymine-containing polyacrylates and their complex ([A]:[T]=1:1). Master curves of the storage modulus versus the frequency were referenced to 20 °C, given that the T_g's of these polymers were lower than room temperature (Figure 7.14). It should also be noted that in the construction of the master curves no vertical shift of the data was needed, demonstrating that the plateau modulus G_N^0 was not a strong function of temperature.

The master curve of the hydrogen bonding complex exhibited an increased storage modulus and T_g and extended terminal relaxation time by several orders of magnitude, which was attributed to complementary hydrogen bonding and the formation of a higher apparent molar mass. Even at low frequencies (higher temperatures), the hydrogen

bonding complex exhibited G' 10 times higher than the precursors, indicating that a low level of A-T nucleobase pairs remained even at high temperatures, and this was expected because of the higher association constant of A-T hydrogen bonding than A-A or T-T hydrogen bonding. In comparison with the precursors, the tanδ peak of the polymer complex broadened and shifted to lower frequencies, and the corresponding plateau modulus region was broader, suggesting weaker temperature dependence, possibly because a hydrogen-bonding nucleobase pair would constantly break and reform before finally separating.[34] Although distinct microphase separation driven by π-π interactions occurred in A-7, time-temperature superposition was satisfied in all cases, indicating the governing relaxation process all had similar temperature dependencies. In addition, plotting the shift factors (a_T) versus inverse temperature followed the Williams-Landel-Ferry (WLF) equation-

$$\log a_T = \frac{-c_1^0(T - T_0)}{c_2^0 + (T - T_0)} \qquad (1)$$

Where c_1^0 and c_2^0 are constants and T_0 is the reference temperature. Values of the constants c_1^0 and c_2^0 were determined from the plot of the $-(T-T_0)/\log a_T$ against $T-T_0$; the coefficient c_1^0 was obtained from the reciprocal of the slope, and the coefficient c_2^0 from the intercept. The complexation of adenine and thymine led to an increase in c_1^0 and a significant decrease in c_2^0 (Table 7.2). An important parameter that can be obtained from these fits is the fractional free volume-

$$f_0 = \frac{B}{2.303 c_1^0} \qquad (2)$$

where B is a constant usually assumed to be unity. The fractional free volume decreased for the polymer complex, which suggested that the strong complementary

hydrogen bonding favored an even compact molecular packing. Hawker and Kramer et al. previously reported that TTS was satisfied for UPy-containing polyacrylates, but the shift factors followed an Arrhenius-type behavior since the dissociation of the polymer side-chain hydrogen bonding was a thermally activated process.[34] In our case, for $T_g < T < T_g+100$ °C the kinetic bottleneck for molecular motions was the free-volume availability. The reversibility of complementary hydrogen bonds enabled the polymers to assemble into a more dense, thermodynamically determined network with high plateau modulus.

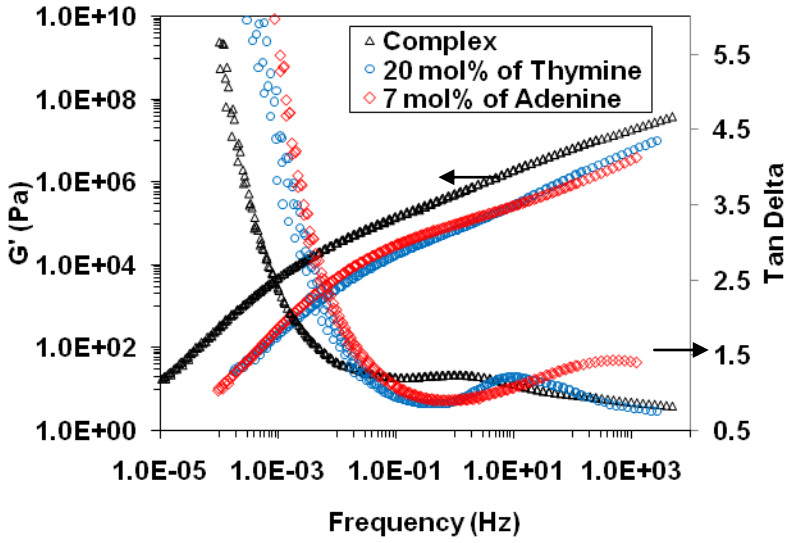

Figure 7.14. Storage and loss modulus master curves of polyacrylates containing 7 mol% of adenine and 25 mol% of thymine respectively and their complex ([A]:[T]=1:1) referenced to 20 °C showing the effect of complementary hydrogen bonding.

Table 7.2. Rheological characterization of adenine- and thymine-containing poly(*n*-butyl acrylate) random copolymers and their complex (T_0=20 °C)

Sample	G_N^0 (MPa)	c_1^0	c_2^0	f_0
Adenine 7 mol%	74	8.1	110	0.054
Thymine 20 mol%	49	7.5	103	0.058
Complex	165	9.1	98	0.048

7.4.6 Adhesive Measurements

Hydrogen bonding associations provide strategies to increase polymer apparent molecular weight to prevent creep and cohesive failure, while improving interfacial adhesion.[38] To demonstrate the effectiveness of complementary multiple hydrogen bonding on polymer adhesion, we measured the peel strength (the ability to resist removal upon peeling) and shear resistance (the ability to resist flow when shear forces are applied). Additionally, a comparison study was performed on acrylic acid (AA) and 4-vinylpyridine (4VP) based polymer analogues with similar molecular weights and hydrogen bonding contents in order to investigate the influence of bond strength on polymer peel strength (Table 7.1). An ASTM-D3300 standard 90° peel testing method was adopted and the results were depicted in Figure 7.15. All polymers with 10 mol% of hydrogen bonding content or less failed 100% cohesively. Peel strength of acrylic thymine- and adenine-containing copolymers with 10 mol% of thymine and 4 mol% of adenine were 11.8 N/inch and 19.1 N/inch, respectively. Whereas, poly(AA-*co*-*n*BA) and poly(4VP-*co*-*n*BA) containing 4 mol% of AA and 10 mol% of VP respectively showed peel strength below 5 N/inch, which was 3 to 4 times lower. The enhanced wettability is possibly due to the strong nucleobase pairing as well as the strong association between

nucleobases and the stainless steel surface in comparison to the association between carboxylic acid (AA) and vinylpyridine (VP). Additionally, peel strength of the adenine and thymine-containing polymer complex was higher than the precursors.

Dynamic shear measurement was performed on an Instron tensile tester to demonstrate the influence of complementary hydrogen bonds occurring between the polymer segments, which potentially provided the cohesion inside the superstructures. As shown in Figure 7.15, shear strength of nucleobase-containing polymers is 3 to 4 times higher than the analogues, suggesting a significant improvement of adhesion at interface. The association of nucleobase led to an increase in apparent molecular weight and network structure formation with increased modulus and T_g. Due to stronger hydrogen bonding, blending adenine- and thymine-containing polymers enhanced the shear strength even more. The optimum combination of cohesive and adhesive strength was achieved which contributed to the highest shear strength in the study.

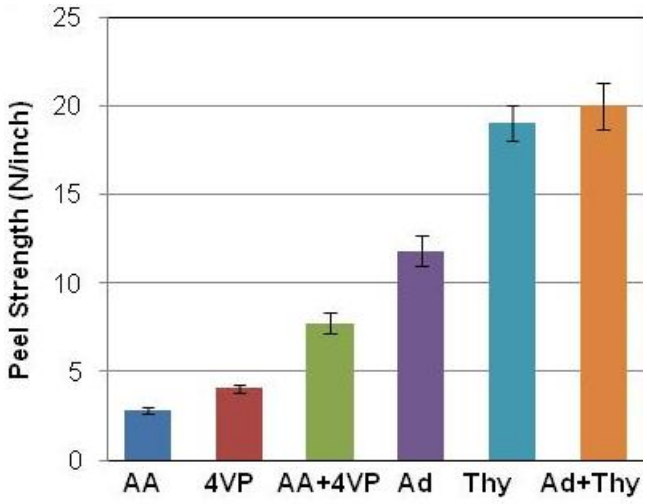

(1)

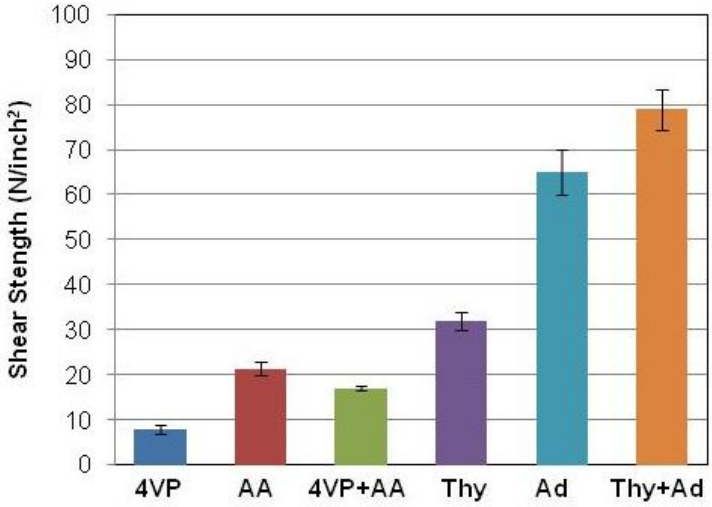

(2)

Figure 7.15. Peel strength and shear strength of poly(*n*BA-*co*-acrylic adenine) and poly(*n*BA-*co*-acrylic thymine) in comparison to AA- and 4VP-based complementary hydrogen bonding polymer analogues

7.5 Conclusions

A novel strategy of combining hydrogen bonding and molecular recognition was developed in low T_g polyacrylates for application as hot-melt pressure sensitive adhesives. P*n*BA were functionalized with novel acrylic adenine and thymine monomers synthesized through Michael addition. Acrylic adenine-containing random copolymers with only 7 mol% of adenine self-assembled into highly ordered needle-like nano-structures, but thymine-containing polymers did not. The different self-assembly behavior was ascribed to the pronounced π-π stacking between adenine units. Time-temperature superposition (TTS) was applied successfully to the storage and loss moduli data and the resulting shift factors were correlated with a significant decrease in free volume of the complex. Additionally, nucleobase-containing complementary hydrogen bonding polymers possessed significantly higher peel and shear strength than the AA- and VP-based polymer analogues. Processing above the hydrogen bonding dissociation temperature presented a methodology to maintain viscosities low for hot melt pressure sensitive adhesives.

7.6 Acknowledgements

The authors acknowledge the financial support of the Petroleum Research Fund (ACS-PRF 35190-AC7), which is administered by the American Chemical Society. Parts of this work were carried out using instruments in the Nanoscale Characterization and Fabrication Laboratory, a Virginia Tech facility operated by the Institute for Critical Technology and Applied Science (ICTAS). We also acknowledge funding from NSF (CHE-0722638) for the acquisition of our Agilent 6220 LC-TOF-MS. This material is partially based upon work supported by the National Science Foundation under Grant No.

DMR-0923107. Additionally, this research was supported in part by the U.S. Army Research Laboratory and the U.S. Army Research Office under contract/grant number W911NF-07-1-0452, Ionic Liquids in Electro-Active Devices Multidisciplinary University Research Initiative (ILEAD MURI).

7.7 References

1. Wojtecki, R. J.; Meador, M. A.; Rowan, S. J. *Nat. Mater.* **2011,** 10, (1), 14-27.
2. Cordier, P.; Tournilhac, F.; Soulie-Ziakovic, C.; Leibler, L. *Nature (London, U. K.)* **2008,** 451, (7181), 977-980.
3. de Greef, T. F. A.; Meijer, E. W. *Nature* **2008,** 453, (7192), 171-173.
4. Sijbesma, R. P.; Beijer, F. H.; Brunsveld, L.; Folmer, B. J. B.; Hirschberg, J. H. K. K.; Lange, R. F. M.; Lowe, J. K. L.; Meijer, E. W. *Science* **1997,** 278, (5343), 1601-1604.
5. Spivak, D.; Gilmore, M. A.; Shea, K. J. *J. Am. Chem. Soc.* **1997,** 119, 4388-4393.
6. Duffy, D. J.; Das, K.; Hsu, S. L.; Penelle, J.; Rotello, V. M.; Stidham, H. D. *J. Am. Chem. Soc.* **2002,** 124, 8290-8296.
7. Lo, P. K.; Sleiman, H. F. *J. Am. Chem. Soc.* **2009,** 131, 4182-4183.
8. Lin, I. H.; Cheng, C.-C.; Yen, Y.-C.; Chang, F.-C. *Macromolecules* **2010,** 43, (3), 1245-1252.
9. Yamauchi, K.; Lizotte, J. R.; Long, T. E. *Macromolecules* **2002,** 35, (23), 8745-8750.
10. Khan, A.; Haddleton, D. M.; Hannon, M. J.; Kukulj, D.; Marsh, A. *Macromolecules* **1999,** 32, 6560.

11. Marsh, A.; Khan, A.; Haddleton, D. M.; Hannon, M. J. *Macromolecules* **1999,** 32, 8725.

12. Bazzi, H. S.; Sleiman, H. F. *Macromolecules* **2002,** 35, (26), 9617-9620.

13. Spijker, H. J.; van Delft, F. L.; van Hest, J. C. M. *Macromolecules* **2007,** 40, (1), 12-18.

14. Lutz, J.-F.; Thuenemann, A. F.; Rurack, K. *Macromolecules* **2005,** 38, (20), 8124-8126.

15. Lutz, J.-F.; Thuenemann, A. F.; Nehring, R. *J. Polym. Sci., Part A Polym. Chem.* **2005,** 43, (20), 4805-4818.

16. Inaki, Y.; Futagawa, H.; Takemoto, K. *J. Polym Sci, Polym. Chem. Ed* **1980,** 18, 2959-2969.

17. Mather, B. D.; Lizotte, J. R.; Long, T. E. *Macromolecules* **2004,** 37, (25), 9331-9337.

18. Mather, B. D.; Baker, M. B.; Beyer, F. L.; Berg, M. A. G.; Green, M. D.; Long, T. E. *Macromolecules* **2007,** 40, (19), 6834-6845.

19. Mather, B. D.; Baker, M. B.; Beyer, F. L.; Green, M. D.; Berg, M. A. G.; Long, T. E. *Macromolecules* **2007,** 40, (13), 4396-4398.

20. Navacchia, M. L.; Favaretto, L.; Treossi, E.; Palermo, V.; Barbarella, G. *Macromol. Rapid Commun.* **2010,** 31, (4), 351-355.

21. Konodo, K.; Iwasaki, H.; Nakatani, K.; Ueda, N.; Takemoto, K.; Imoto, M. *Die Makromolekulare Chemie* **1969,** 125, 42-47.

22. Hurduc, N.; Enea, R.; Scutaru, D.; Sacarescu, L.; Donose, B. C.; Nguyen, A. V. *Journal of Polymer Science, Part A: Polymer Chemistry* **2007,** 45, (18), 4240-4248.

23. Akashi, M.; Takada, H.; Inaki, Y.; Takemoto, K. *J. Polym. Sci., Part A: Polym. Chem.* **1979,** 17, 747-757.

24. Sivakova, S.; Bohnsack, D. A.; Mackay, M. E.; Suwanmala, P.; Rowan Stuart, J. *J. Am. Chem. Soc.* **2005,** 127, 182020-18211.

25. Binder, W. H.; Kunz, M. J.; Kluger, C.; Hayn, G.; Saf, R. *Macromolecules* **2004,** 37, (5), 1749-1759.

26. Mes, T.; Smulders, M. M. J.; Palmans, A. R. A.; Meijer, E. W. *Macromolecules* **2010,** 43, 1981-1991.

27. Mather, B. D.; Viswanathan, K.; Miller, K. M.; Long, T. E. *Prog. Polym. Sci.* **2006,** 31, (5), 487-531.

28. Sedlák, M.; Šimůnek, P.; Antonietti, M. *J. Heterocyclic Chem.* **2003,** 40, 671.

29. Karikari, A. S.; Mather, B. D.; Long, T. E. *Biomacromolecules* **2007,** 8, 302-308.

30. Lira, E. P.; Huffman, C. W. *J. Org. Chem.* **1966,** 31, (7), 2188-2191.

31. Sartorius, J.; Schneider, H.-J. *Chem. Eur. J.* **1996,** 2, 1446 and references cited therein.

32. Sapper, H.; Lohmann, W. *Biophys. Struct. Mechanism* **1978,** 4, 327-335.

33. T'so, P. O. P.; Melvin, I. S.; Olson, A. C. *J. Am. Chem. Soc.* **1963,** 85, 1289–1296.

34. Feldman, K. E.; Kade, M. J.; Meijer, E. W.; Hawker, C. J.; Kramer, E. J. *Macromolecules* **2009,** 42, (22), 9072.

35. Jonkheijm, P.; van der Schoot, P.; Schenning, A. P. H. J.; Meijer, E. W. *Science* **2006,** 313, (5783), 80-83.

36. Pehlert, G. J.; Painter, P. C.; Coleman, M. N. *Macromolecules* **1998,** 31, 8423.

37. Kuo, S.-W.; Tsai, H.-T. *Macromolecules* **2009,** 42, 4701-4711.

38. Cashion, M. P.; Park, T.; Long, T. E. *The Journal of Adhesion* **2009,** 85, 1-17.

Chapter 8: Synergy and Competition between Hydrogen Bonding and Ionic Interaction in Self-Assembly of Supramolecular Polymers

*Shijing Cheng, Mingqiang Zhang, Robert B. Moore, and Timothy E. Long**

8.1 Abstract

In the present work, we introduced ionic interactions through a uracil-containing phosphonium salt (UP^+), which reversibly hydrogen bonded to complementary adenine-containing random copolymers. The presence of phosphonium cations did not influence adenine-uracil hydrogen bonding association, which exhibited an association constant of 113 M^{-1} based on ^1H NMR titration. Introducing UP^+ guest molecules into the adenine-containing polymers increased the polymer glass transition temperatures and reduced the storage modulus, suggesting a screening of adenine-adenine π-π interactions due to adenine-uracil hydrogen bonds. Morphological studies including AFM, small-angle X-ray scattering (SAXS), and wide-angle X-ray diffraction (WAXD) also revealed a reduced degree of microphase separation for the polymer blends in comparison to the pure adenine-containing copolymer.

8.2 Introduction

The introduction of polymer additives to diverse macromolecular architectures using hydrogen bonding interactions has received significant attention for several decades. Earlier researchers reported the reversible attachment of neutral guest molecules for example, non-covalent attachment of mesogens resulted in supramolecular liquid crystalline assemblies.[1] Complementary hydrogen bonding interactions facilitate the

introduction of guest molecules containing recognition units. The reversible attachment of guest molecules to polymers using nucleobase hydrogen bonding has been investigated in both solution[2] and the solid state.[3-5] Rotello et al. have used three-point hydrogen bonding between diacyldiaminopyridines and thymine to attach guest molecules containing flavin[6-7] or POSS to polystyrene.[8]

Hydrogen bonding has only recently been employed in influencing the tacticity of radical polymerizations. Okamoto's[9] and Kamigaito's[10] group has used the hydrogen bonding between bulky fluoroalcohols and esters to influence the tacticity of radical polymerizations of vinyl ester monomers. Hirano et al. reported slight changes in tacticity for poly(*N*-isopropylacrylamide) that was polymerized in the presence of bulky diphosphates which hydrogen bonded to the NH of the monomer.[11] More recently, Kamigaito's group utilized more sophisticated triple hydrogen bonding between diaminopyridine acrylamide monomers and cyclic imide guests to influence tacticity of polymerizations.[12] As expected, the largest cyclic imide guest, naphthalimide, afforded the highest syndiotacticity. In addition, hydrogen bonding guest molecules can also increase the solubility of hydrogen bonding polymers through screening of polymer-polymer self-association, thereby maintaining homogeneity during polymerization reactions.[13]

Our group recently reported on the introduction of phosphonium ionic guest molecules into hydrogen bonding block copolymers.[14] Phosphonium cations have received recent attention in our laboratories[15] due to their higher thermal stabilities relative to ammonium analogs. Earlier evidence indicates that the onset of decomposition of tetraoctylammonium bromide occurs at 170 ºC due to Hofmann elimination, whereas

the analogous phosphonium salt exhibits thermal stability up to 260 ºC.[16-17] In addition, recent reports on phosphonium-containing random copolymers revealed nanoscale ionic aggregation[18] with concomitant thermoplastic elastomeric behavior,[19] and opportunities for stimuli-responsive materials.[20]

In this manuscript, we demonstrate the general concept of reversible ionic site attachment to random copolymers and discuss the synergy and competition of complementary hydrogen bonding in nanostructured random copolymers with guest molecules containing electrostatic interactions. In particular, we examine complementary nucleobase hydrogen bonding between adenine and thymine derivatives.

8.3 Experimental

8.3.1 Materials

n-Butyl acrylate (99%) was purchased from Aldrich and purified using an alumina column and subsequent vacuum distillation from calcium hydride. Trioctylphosphine (90%) and 6-chloromethyluracil (98%) were purchased from Aldrich and used without further purification. 6-(Trioctylphosphonium methyl)uracil chloride (UOP^+) was synthesized according to the previous literature.[14]

8.3.2 Instrumentation

^{1}H NMR and ^{13}C NMR spectra were collected in $CDCl_3$ or DMSO-d_6 on a Varian INOVA spectrometer operating at 400 MHz and 23 °C. FAB-MS was conducted in positive ion mode on a JEOL HX110 Dual Focusing Mass spectrometer. Size exclusion chromatography (SEC) was performed using a Waters size exclusion chromatograph. The instrument was equipped with an auto sampler, three 5 μm PLgel Mixed-C columns, a Waters 2410 refractive index (RI) detector operating at 880 nm, a Wyatt Technologies

miniDAWN multi-angle laser light scattering (MALLS) detector operating at 690 nm, and a Viscotek 270 viscosity detector at 40 °C and a flow rate of 1 mL/min in THF. Reported molecular weights are based on absolute measurements using the MALLS detector.

Differential scanning calorimetry (DSC) was performed under a nitrogen flush of 50 mL/min at a heating rate of 10 °C/min on a TA instruments Q1000TM DSC, which was calibrated using indium (mp = 156.60 °C) and zinc (mp = 419.47 °C) standards. Glass transition temperatures were measured as the midpoint of the transition in the second heating scan. Dynamic mechanical analysis (DMA) was conducted on a TA Instruments Q800 Dynamic Mechanical Analyzer in tension mode at a frequency of 1 Hz, an oscillatory amplitude of 15 μm, and a static force of 0.01 N. The temperature ramp was 3 °C/min. The glass-transition temperature (T_g) was determined at the peak maximum of the tan δ curve.

A Veeco MultiMode scanning probe microscope was used for tapping-mode AFM imaging. Samples were imaged at a set-point ratio of 0.67 at magnifications of 1 um×1 um. Veeco's Nanosensor silicon tips having spring constants of 40 N/m were utilized for imaging. Small angle X-ray scattering (SAXS) data was collected on an Oxford Diffraction XcaliburTM diffractometer equipped with a SapphireTM 3 CCD detector. The data collection routine, unit cell refinement, and data processing were carried out with the program CrysAlis (v1.171, Oxford Diffraction: Wroclaw, Poland, 2004). Wide angle X-ray diffraction (WAXD) was performed using Rigaku S-Max 300 3 pinhole SAXS system. X-ray source is the Cu Kα radiation, and the wavelength is 0.154 nm. The sample-to-detector distance was 80 mm. Fuji HR-V Imaging plate was used to collect the

two- dimensional images, with an exposure time of 1 hour. Imaging plate was scanned using RAXIA-Di system and a plot of intensity versus q was obtained using Rigaku's SAXSGUI software package.

8.3.3 Synthesis of 6-(Tributylphosphonium methyl)uracil chloride (UBP^+)

6-chloromethyluracil (1.0 g, 6.232 mmol) and tributylphosphine (3.25 mL, 2.70 g, 7.29 mmol) were charged to a 100 mL round-bottomed flask containing a magnetic stir bar. Ethanol (40 mL) was added and a condenser was fitted to the flask. The reaction was heated to reflux using an external oil bath for 24 h. Excess solvent was removed using rotary evaporation. The resulting waxy solid was washed with diethyl ether and was dried overnight at room temperature under high vacuum. UBP+ was obtained as a light yellow solid in 92% yield. ^{1}H NMR (400 MHz, DMSO-d6, 25 °C) δ (ppm): 0.86 (t, 9H, J = 6.8 Hz), 1.26 (m, 24H), 1.37 (m, 6H), 1.49 (m, 6H), 2.37 (m, 6H), 3.77 (d, 2H, J = 15 Hz), 5.55 (m, 1H), 11.15 (s, 1H), 11.47 (s, 1H). ^{13}C NMR (101 MHz, DMSO-d6, 25 °C) δ (ppm): 13.96, 17.61, 18.06, 20.52, 22.08, 28.27, 28.8, 30.06, 31.22, 102.08, 145.18, 150.95, 163.37. ^{31}P NMR (162 MHz, DMSO-d6, 25 °C) δ (ppm): 33.68 ppm. FAB MS: m/z = 495.4056 $[M\text{-}Cl]^+$(experimental), m/z = 495.41 (theoretical).

8.4 Results and Discussion

Uracil-containing phosphonium salts, 6-(tributylphosphonium methyl)uracil chloride (UBP^+) and 6-(trioctylphosphonium methyl)uracil chloride (UOP^+) were synthesized in a single step from 6-chloromethyl uracil and trioctylphosphine/tributylphosphine. UBP^+

and UOP^+ exhibited an onset of weight loss at 280 ºC and good solubility in a wide range of common organic solvents.

Quantitative analysis for binding affinity of intermolecular heterocomplexation was otained using ^1H NMR titration experiment to study the competition between complementary hydrogen bonding of adenine-uracil (A-U) and self-association of A-A and U-U. UA blends possibly possessed two major types of hydrogen bonding interactions through the Watson–Crick and the Hoogsteen sites which can form aggregates or base-triples with an appropriate partner and molar ratio of 2:1.[21] Therefore, the poly(acrylic adenine-*co*-*n*BA) was titrated against uracil phosphonium guest molecules and the stoichiometry of poly(acrylic adenine-*co*-*n*BA) to UOP^+ was carefully adjusted.

The association constants for hydrogen-bonded complexes characterized using 400 MHz ^1H NMR at 25 ^oC in $CDCl_3$, which favors hydrogen bonding interactions due to a relatively low dielectric constant. The position of the adenine N-H resonance shifted to higher field (from 5.75 to 5.88 ppm) with the increase of uracil concentration (Figure 8.1). In addition, the resonances of the amido NHs are relatively broader, indicating a faster exchange rate between associated and dissociated A-U complex on the NMR time scale. The curvature of the chemical shift data with increasing adenine concentration was consistent with typical NMR titration experiments in the literature.[22] Fitting this chemical shift data using the Benesi-Hildebrande method produced a double reciprocal plot based on the association of A-U complex as shown in Figure 8.2. The K_a obtained from the slope of the plot is 113 M^{-1}, which is consistent with the values reported previously for

adenine-uracil base pair recognition (ca. 10-100 M^{-1} in $CDCl_3$),[23] demonstrating the non-covalent attachment of UOP^+ in the solution state.

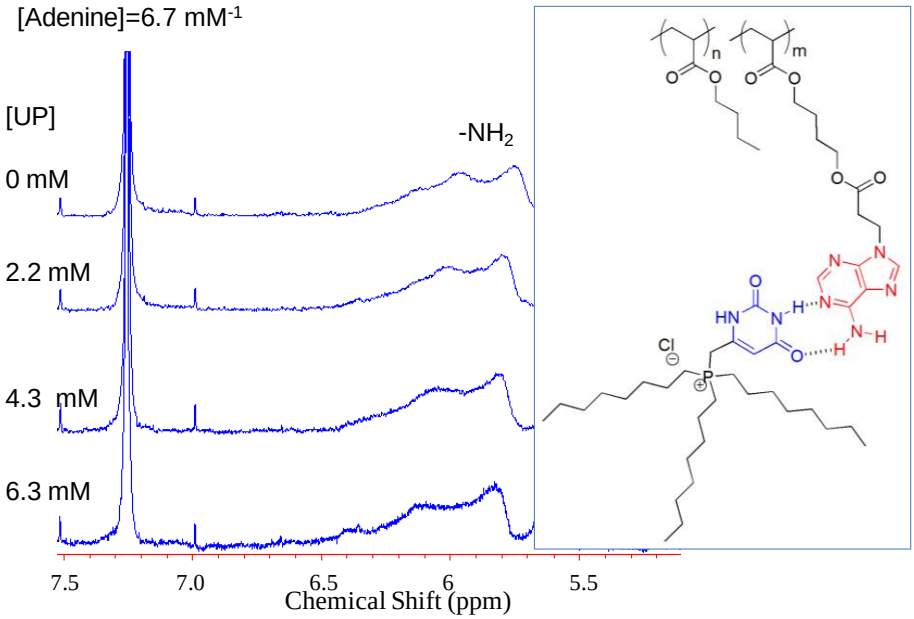

Figure 8.1. ^1H NMR spectra of poly(*n*BA-*co*-Adenine acrylate) containing 3.6 mol% of adenine acrylate with addition of UOP^+ guest molecule in $CDCl_3$. [Adenine]=6.7 mM^{-1}

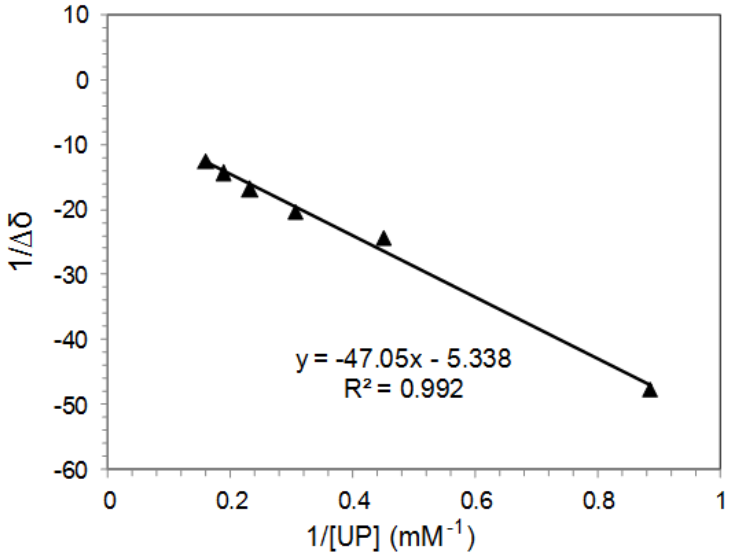

Figure 8.2. Benesi-Hildebrand polts of adenine acrylate-containing polymer and UOP^+ guest molecule association in $CDCl_3$ (3.6 mol% of adenine acrylate, M_w=95K)

In blends of the phosphonium salt with adenine containing random polymers solution-cast from chloroform, crystallization and melting transitions of the phosphonium salt were absent from DSC thermograms (Figure 8.3). Furthermore, the solution-cast films were optically clear. In sharp contrast, solution-cast films of the phosphonium salt with non-functionalized poly(*n*-butyl acrylate) homopolymer were opaque, suggesting macrophase separation and poor mixing of the phosphonium salt and poly(*n*-butyl acrylate).

The addition of UOP^+ present in the samples corresponded to 5 wt% for 0.4 equivalents, and 24 wt% for 1 equivalent. DSC observed a slight increase of glass transition temperature. This increase was clearly observed in DMA described later. The absence of UOP^+ melting peak up to 0.25 equivalents, indicating that there was an interaction existing between the UOP^+ and adenine-containing polymers. This interaction was subsequently satured upon adding a 0.5 equivalents of UOP^+, possibly due to limited amount of accessible adenine, indicating that the stoichiometric self-assembly adopted an important role on steering the specific recognition. The addition of UBP^+ were similar to UOP^+.

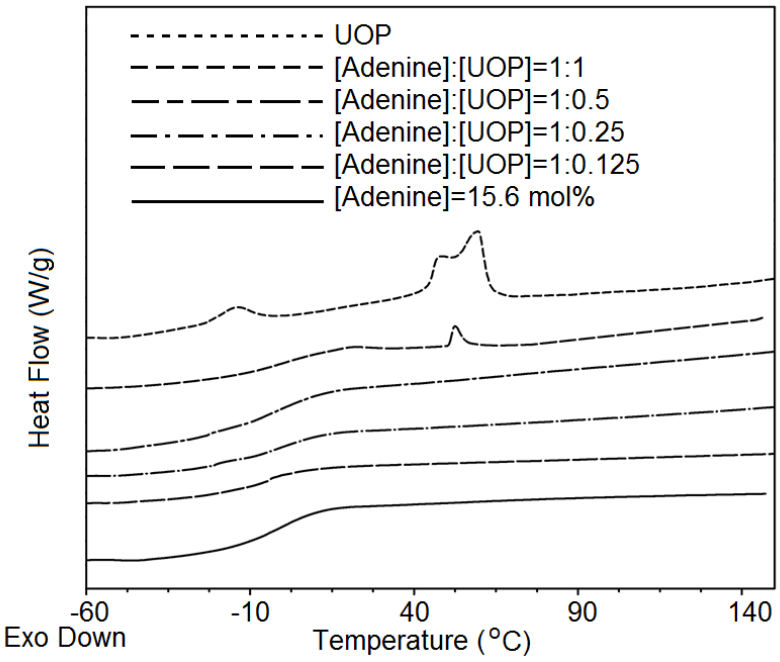

(1)

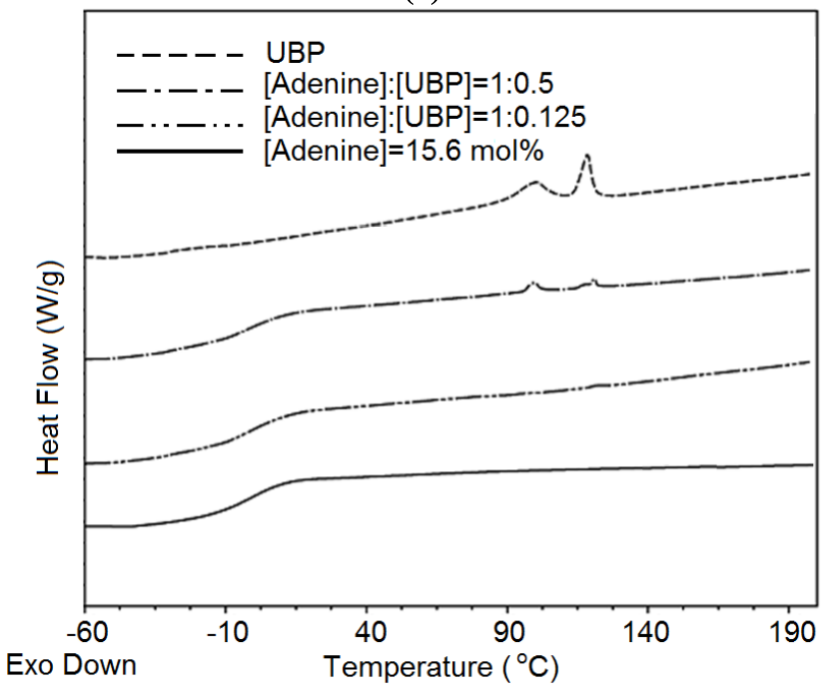

(2)

Figure 8.3. DSC thermograms of the blends of adenine acrylate-containing random copolymers with various contents of UOP^+ and UBP^+ (labeled in the graph). Second heating scan is shown.

Dynamic mechanical (DMA) studies on the blends of adenine copolymer and UOP^+/UBP^+ clearly revealed an increase of glass transition temperature according to the maximum of the tanδ curves, indicating selective incorporation of UOP^+/UBP^+ into the hard phase (Figure 8.4). This is consistent with the DSC analysis and the literature on adenine block copolymer and UOP^+ blends.[14] However, the rubbery plateau shortened and the plateau modulus decreased, which indicated a softening of the hard phase and suggested a screening effect of the adenine-adenine intermolecular hydrogen bonds.

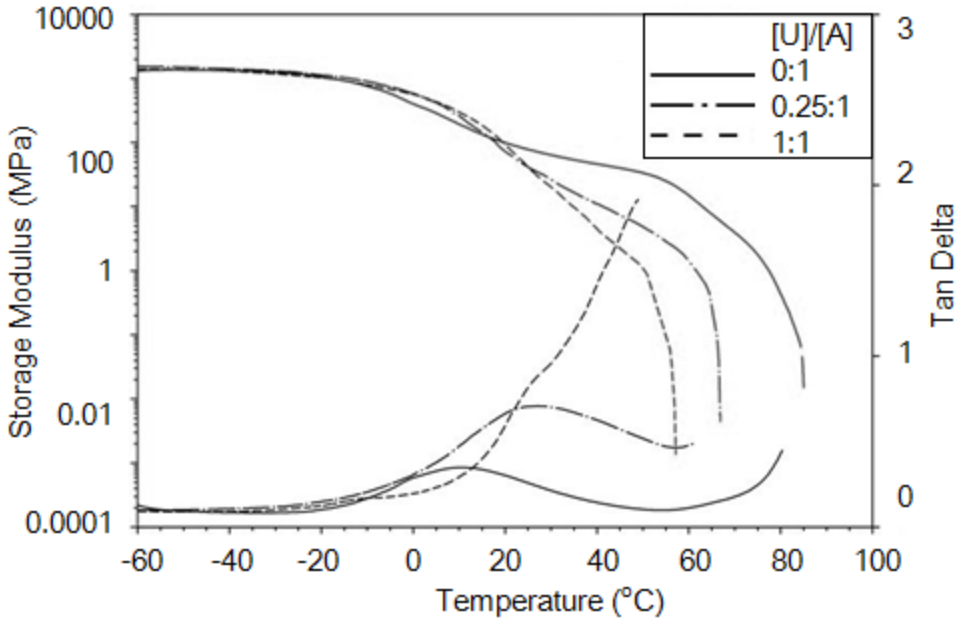

(1)

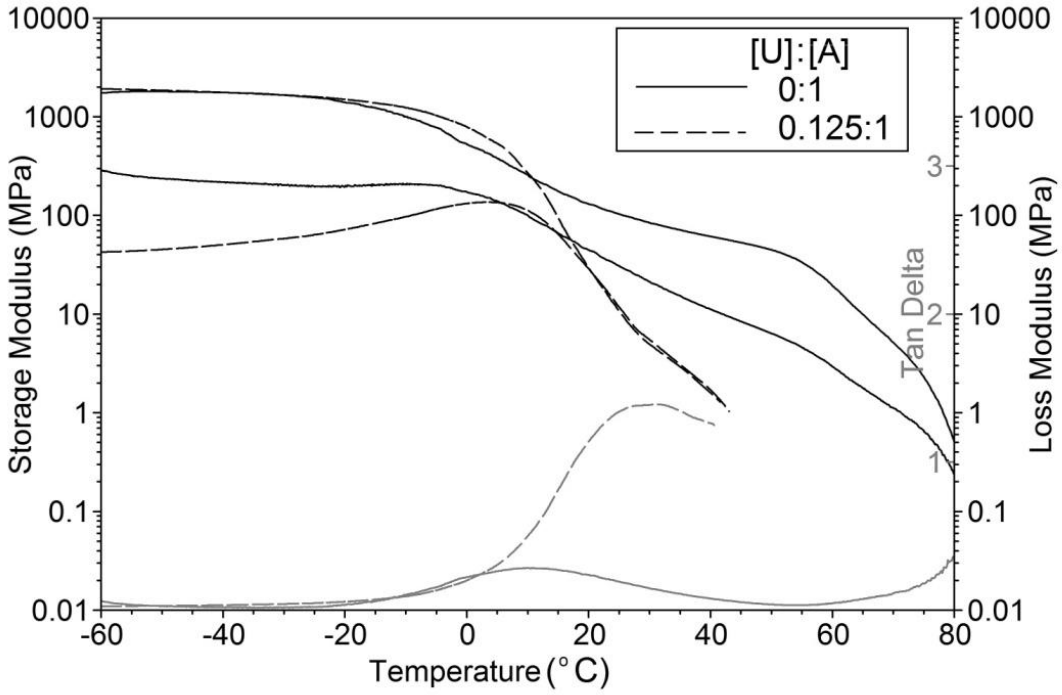

(2)

Figure 8.4. DMA traces of poly(*n*BA-*co*-adenine acrylate) containing 17 mol% of adenine acrylate with various content of (1) UOP^+ and (2) UBP^+

Morphological investigations with atomic force microscopy (AFM) and X-ray scattering were conducted on identical films used for DSC and DMA analyses. AFM images revealed unique needle-like nano structures for acrylic adenine-containing random copolymers (Figure 8.5). Compared with the pure adenine-containing copolymers, the surface textures of the blends with UOP^+ showed less phase contrast and greater hard phase continuity. Increasing the concentration ratio of [A]/[UOP^+] from ¼ to ½ less than stoichiometric levels led to a further decrease of phase contrast and a complete loss of surface textures, suggesting the disruption of the adenine-containing hard phase through selective incorporation of recognition small molecules.

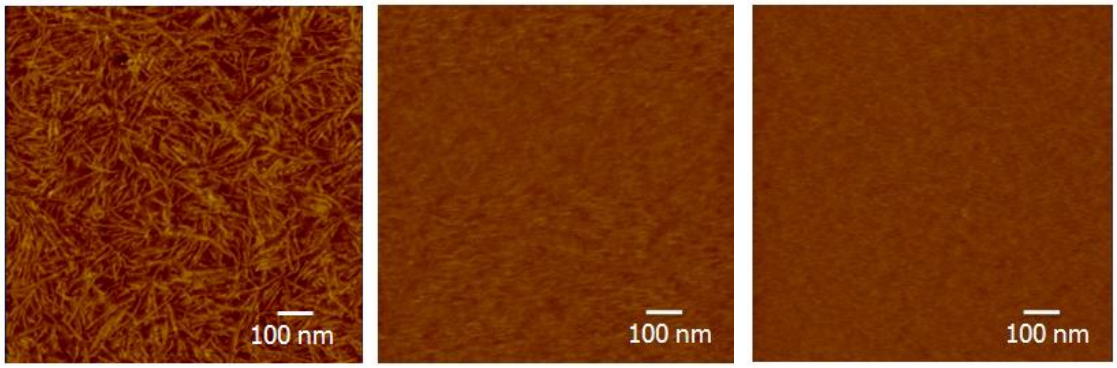

(1) (2) (3)

Figure 8.5. Tapping mode AFM phase images of thins films of poly(*n*BA-*co*-Adenine acrylate) (16 mol% of adenine) blended with various contents of UOP^+ {(1) [A]=16 mol%, (2) [A]/[U]=8:1, (3) [A]/[U]=4:1}

Corresponding SAXS data (Figure 8.6) revealed that the addition of the phosphonium salt resulted in a disruption of partial original morphology and led to a broad peak. Wide-angle X-ray diffraction (WAXD) diffraction pattern (Figure 8.7) of the polymer blends displayed one reflection peak at 13.68º (d=0.65 nm), which is consistent with the presence of π-π stacking interactions between adenine-adenine; generally, such

interactions occur only in stabilized sheets. The d-spacing of 0.65 nm suggested that there were stacks of the nucleobases that were held together through π-π interactions within the needle-like domains.[24-26] This peak persisted even with 0.5 equivalent of UOP^+. At 1 equivalent of UOP^+, the polymer blends exhibited the reflection peaks from UOP^+ crystallines, indicating UOP^+ was over abundant.

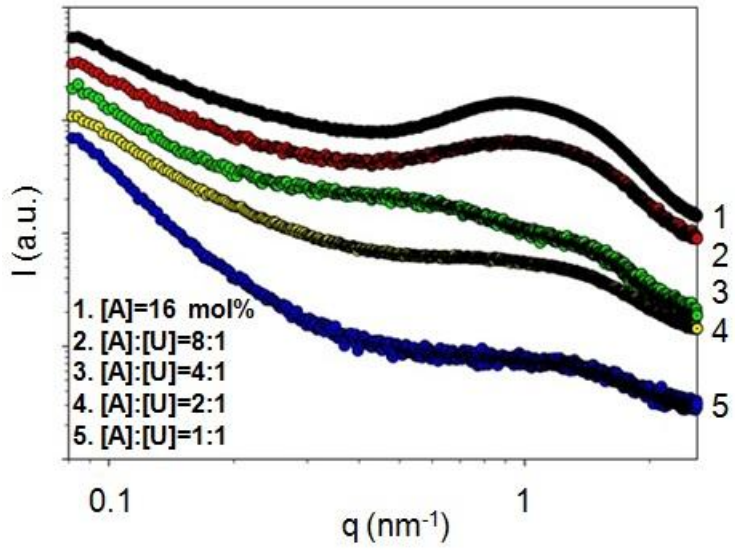

Figure 8.6. SAXS data for Adenine-PBA /UOP^+ complexes in various mole ratios

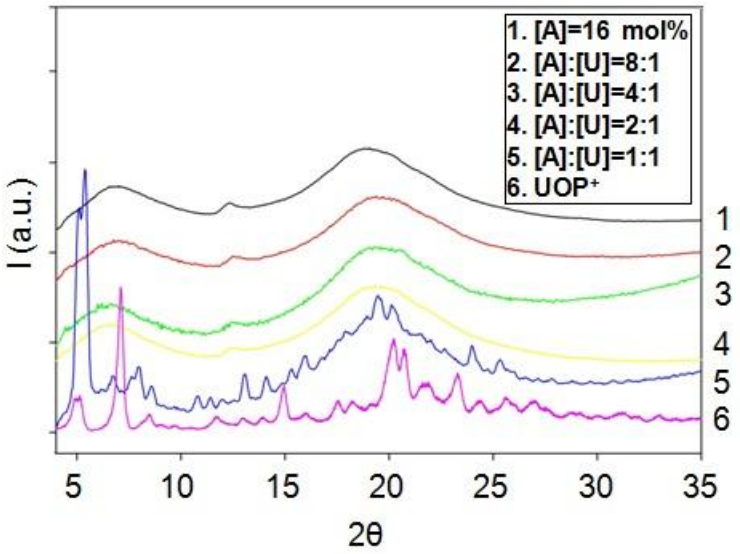

Figure 8.7. WAXD data for Adenine-PBA /UOP^+ complexes in various mole ratios

8.5 Conclusions

In conclusion, this manuscript defines a novel general strategy for the introduction of thermally stable ionic sites to random copolymers through reversible complementary hydrogen bonding. Subsequent blending with unique phosphonium cation containing complementary hydrogen bonding guests was conducted. Influences on surface morphology and mechanical properties were observed.

8.6 Acknowledgements

Acknowledgment is made to the Donors of the American Chemical Society Petroleum Research Fund for partial support of this research. Parts of this work were carried out using instruments in the Nanoscale Characterization and Fabrication Laboratory, a Virginia Tech facility operated by the Institute for Critical Technology and Applied Science (ICTAS). The authors thank Steve McCartney at Virginia Tech ICTAS for his help with AFM imaging. We also acknowledge funding from NSF (CHE-0722638) for the acquisition of our Agilent 6220 LC-TOF-MS. This material is partially based upon work supported by the National Science Foundation under Grant No. DMR-0923107.

8.7 References

1. Kumar, U.; Kato, T.; Fréchet, J. M. J. *J. Am. Chem. Soc.* **1992,** 114, 6630-6639.
2. Thibault, R. J.; Hotchkiss, P. J.; Gray, M.; Rotello, V. M. *J Am Chem Soc* **2003,** 125, 11249-11252.

3. Cheng, C.-C.; Huang, C.-F.; Yen, Y.-C.; Chang, F.-C. *J. Polym. Sci., Part A: Polym. Chem.* **2008,** 46, (19), 6416–6424.

4. Carroll, J. B.; Waddon, A. J.; Nakade, H.; Rotello, V. M. *Macromolecules* **2003,** 36, 6289-6291.

5. Ilhan, F.; Gray, M.; Rotello, V. M. *Macromolecules* **2001,** 34, 2597-2601.

6. Ilhan, F.; Galow, T. H.; Gray, M.; Clavier, G.; Rotello, V. M. *J Am Chem Soc* **2000,** 122, 5895-5896.

7. Subramani, C.; Yesilbag, G.; Jordan, B. J.; Li, X.; Khorasani, A.; Cooke, G.; Sanyal, A.; Rotello, V. M. *Chem Comm* **2010,** 46, 2067-2069.

8. Carroll, J. B.; Waddon, A. J.; Nakade, H.; Rotello, V. M. *Macromolecules* **2003,** 36, 6289-6291.

9. Habaue, S.; Okamoto, Y. *Chem Record* **2000**, 46-52.

10. Koumura, K.; Satoh, K.; Kamigaito, M.; Okamoto, Y. *Macromolecules* **2006,** 39, 4054-4061.

11. Hirano, T.; Kitajima, H.; Seno, M.; Sato, T. *Polymer* **2006,** 47, 539-456.

12. Wan, D.; Satoh, K.; Kamigaito, M. *Macromolecules* **2006,** 39, 6882- 6886.

13. Stubbs, L. P.; Weck, M. *Chem Eur J* **2009,** 9, 992-999.

14. Mather, B. D.; Baker, M. B.; Beyer, F. L.; Green, M. D.; Berg, M. A. G.; Long, T. E. *Macromolecules* **2007,** 40, (13), 4396-4398.

15. Williams, S. R.; Wang, W.; Winey, K. I.; Long, T. E. *Macromolecules* **2008,** 41, (23), 9072-9079.

16. Xie, W.; Xie, R.; Pan, W. P.; Hunter, D.; Koene, B.; Tan, L. S.; Vaia, R. *Chem. Mater.* **2002,** 14, 4837-4845.

17. Burch, R. R.; Manring, L. E. *Macromolecules* **1991,** 24, 1731-1735.

18. Parent, J. S.; Penciu, A.; Guillen-Castellanos, A.; Liskova, A.; Whitney, R. A. *Macromolecules* **2004,** 37, 7477-7483.

19. Arjunan, P.; Wang, H.-C.; Olkusz, J. A., In *Functional Polymers.*, American Chemical Society: Washington DC: 1998; Vol. 704, pp 199-216.

20. Son, S.-Y.; Gong, M.-S. *Sens. Actuators, B* **2002,** B86, (2-3), 168-173.

21. Ghosal, G.; Muniyappa, K. *Biochem. Biophys. Res. Commun.* **2006,** 343, 1-7.

22. Karikari, A. S.; Mather, B. D.; Long, T. E. *Biomacromolecules* **2007,** 8, 302-308.

23. Sivakova, S.; Rowan, S. J. *Chem. Soc. Rev.* **2005,** 34, (1), 9-21.

24. Pedireddi, V. R.; Ranganathan, A.; Ganesh, K. N. *Org Lett* **2001,** 3, 99-102.

25. George, S. J.; Ajayaghosh, A. *Chem Eur J* **2005,** 11, 3217-3227.

26. Sivakova, S.; Bohnsack, D. A.; Mackay, M. E.; Suwanmala, P.; Rowan, S. J. *J. Am. Chem. Soc.* **2005,** 127, (51), 18202-18211.

Chapter 9: Overall Conclusions

Non-covalent interactions including nucleobase hydrogen bonding and ionic interactions were studied in block and random polymers synthesized using controlled radical polymerization techniques such as nitroxide mediated polymerization and reversible addition-fragmentation chain transfer polymerization. Non-covalent interactions were expected to increase the effective molecular weight of the polymeric precursors through intermolecular associations. The influence of non-covalent association on the structure-property relationships of these materials were studied in terms of physical properties (tensile, DMA, rheology) as well as morphological studies (AFM, TEM, SAXS, WAXD).

Side-chain nucleobase association was studied in the form of styrenic and acrylic nucleobase-containing random copolymers. Aza-Michael addition afforded novel adenine- and thymine-containing acrylic monomers with high regio-selectivity and good yields. In comparison to the styrenic nucleobase-containing polymer analogues, acrylic adenine-containing random copolymers revealed unique needle-like microphase separated hard domains of stacked adenines dispersed in a rubbery *n*-butyl acrylate polymer matrix. Complementary hydrogen bonding interactions were observed in adenine- and thymine-functionalized random copolymers blends. In the solid state, the blends exhibited increased plateau modulus as well as higher softening temperatures and evidence of enhanced homogeneity.

In addition, complementary multiple hydrogen bonding were utilized to reversibly attach uracil-functional quaternary phosphonium ionic guest molecules to complementary adenine-functionalized random copolymers. The optically clear, compatible blends

exhibited lower softening temperatures, due to the disruption of adenine-adenine pi-pi stacked hard domains. Phase contrast decreased with the increase of guest molecule concentration and the needle-like nano-structures eventually disappeared, which suggested the selective uptake of uracil phosphonium salts into adenine containing hard domains and the decreased π-π stacking ability of the adenine-uracil base pair.

In another way, the bulky phosphonium cations were incorporated into both random copolymers and triblock copolymers through chain growth polymerization of styrenic phosphonium ionic liquid monomers. The phosphonium cations weakly aggregated in a fashion similar to ammonium-containing random copolymers, revealing both α and β relaxations in DMA and no "ionic" peak in SAXS. The degree of microphase separation and polymer melt flow behavior were highly dependent on the alkyl substituent chain length and the type of counterion.

Chapter 10: Suggested Future Work

10.1 Intramolecular Complementary Hydrogen Bonding for Transient Network Formation

10.1.1 Abstract

Adenine- and thymine-containing polyacrylate terpolymers were synthesized through conventional free radical terpolymerization. DSC and SAXS analyses of the terpolymers exhibited evidence of strong intramolecular hydrogen bonding. The rheological and morphological behavior of the self-complementary hydrogen bonding terpolymers were compared with hydrogen bonding polymer complexes in order to distinguish the influence of intra- and inter-molecular hydrogen bonding. In addition, novel acrylic cytosine-containing monomer was successfully synthesized through *aza*-Michael addition. Cytosine-guanine base pairs with higher association constant would potentially provide polymers with increased binding affinity.

10.1.2 Introduction

Thermoplastic elastomers (TPEs) encompass a broad class of materials that can be processed, for example, by molding or extrusion, at elevated temperatures yet are elastomeric at ambient temperature. Typically such behavior arises through a phase separated microstructure in which “hard” domains are bridged by “soft” rubbery chains; when a stress is applied to the material, the hard domains serve to pin the polymer chains and prevent macroscopic deformation, while the rubbery chains provide elasticity through the connectivity of the network. Transient networks, in which the junctions can

be reversibly broken and re-formed, are interesting from both fundamental and applied standpoints; many reversibly associating polymers have been synthesized for use as rheological property modifiers or physical gels, and numerous theories have been presented to describe their equilibrium and dynamic properties.

Stadler and Freitas studied the rheological behavior of polybutadienes lightly modified with double-hydrogen-bonding phenylurazole groups, finding that even with light substitution along the backbone the storage modulus plateau was broadened and shifted to lower frequencies.[1-2] Rheological properties directly related to the dynamics of the reversible hydrogen bonding. Kramer and Hawker et al. studied the random copolymers consisting of *n*-butyl acrylate backbones with quadruple hydrogen bonding side chains based on 2-ureido-4[1H]-pyrimidinone (UPy), which behaved as thermoplastic elastomers through the strong but reversible association of UPy groups.[3] The average distance between UPy's along the chain influenced polymer physical properties such as plateau modulus, tensile modulus, and relaxation time scale.

In this chapter, we compare the rheological and morphological behavior of intramolecular hydrogen bonding terpolymers with intermolecular hydrogen bonding polymer complex. The close placement of complementary hydrogen bonding motifs in theory would afford a denser polymer network with enhanced mechanical integrity.

10.1.3 Experimental

10.1.3.1 Materials

n-Butyl acrylate (*n*BA, 99+%) was purchased from Aldrich and passed through neutral alumina columns before use. α,α'-Azobis(isobutyronitrile) (AIBN, Fluka, 99%)

was recrystallized from methanol. 1,4-Butanediol diacrylate (Alfa Aesar, 99%) was used without further purification. Acetyl cytosine (C, 99%), triethylamine (TEA, 99%), potassium carbonate (99%), and 2,6-di-*tert*-butyl-4-methylphenol (BHT, 99%) were purchased from Aldrich and used without further purification. Hexane (HPLC grade), chloroform ($CHCl_3$, HPLC), tetrahydrofuran (THF, HPLC grade), *N*,*N*-dimethylsulfoxide (DMSO, HPLC grade) and *N*,*N*-dimethylformamide (DMF, HPLC grade, anhydrous) were purchased from Fisher Scientific and used as received.

10.1.3.2 Instrumentation

^1H NMR and ^{13}C NMR spectra were collected in $CDCl_3$ or DMSO-d_6 on a Varian INOVA spectrometer operating at 400 MHz 23 °C. Fast Atom Bombardment Mass Spectrometry (FAB-MS) was conducted in positive ion mode on a JEOL HX110 dual focusing mass spectrometer. Size exclusion chromatography (SEC) was performed using a Waters size exclusion chromatograph. The instrument was equipped with an auto sampler, three 5 μm PLgel Mixed-C columns, a Waters 2410 refractive index (RI) detector operating at 880 nm, a Wyatt Technologies miniDAWN multi-angle laser light scattering (MALLS) detector operating at 690 nm, and a Viscotek 270 viscosity detector with a flow rate of 1 mL/min at 50 °C in DMF with 0.01 M lithium bromide (LiBr). Reported molecular weights are relative to polystyrene standards.

Differential scanning calorimetry (DSC) was performed under a nitrogen flush of 50 mL/min at a heating rate of 10 °C/min on a TA instruments Q1000TM DSC, which was calibrated using indium (mp = 156.60 °C) and zinc (mp = 419.47 °C) standards. Glass transition temperatures were measured as the midpoint of the transition in the second heating scan.

SAXS was performed using Rigaku S-Max 3000 pinhole SAXS system. X-ray source was the Cu K_α radiation, and the wavelength was 0.154 nm. For SAXS measurement, silver behenate was used to calibrate the sample to detector distance and the sample-to-detector distance was 1600 mm. SAXSGUI software package was used to obtain scattering intensity, $I(q)$, versus scattering wave vector $q=4\pi\sin(\theta)/\lambda$, where θ was half of the scattering angle and λ was the wavelength of the incident beam. The measured data was corrected for background scattering, sample thickness and transmission.

10.1.3.3 Synthesis of Acrylic Cytosine Monomer

A suspension of acetyl cytosine (1.00 g; 6.52 mmol) and BHT (60.0 mg) in DMF (20 mL) was treated with triethylamine (0.22 mL, 1.58 mmol) and K_2CO_3 (50 mg, 0.36 mmol) at room temperature. The reaction mixture was stirred under an inert atmosphere (argon) for 1 hr and then treated with 1,4-butanediol diacrylate (3.0 mL, 15.9 mmol). The reaction solution turned clear after stirring at room temperature for 24 h. Then, it was poured into water (150 mL) and washed with hexane to remove excess 1,4-butanediol diacrylate. The water layer was extracted with dichloromethane (3×20 mL). The combined extracts were dried over $MgSO_4$, filtered, and concentrated in a vacuum evaporator to remove all the solvents. The evaporation residue was separated using flash column chromatography with $CHCl_3$-acetone (1:1) and then $CHCl_3$-MeOH (20:1) on silica gel. Evaporation of the total eluent gave a white solid of 0.45 g with an overall yield of 39%. HRMS (ES+): m/z calcd for $[M+H^+]$ 352.143 g/mol, found 352.148 g/mol.

10.1.4 Results and Discussion

Conventional free radical terpolymerization of acrylic nucleobase monomers with *n*-butyl acrylate was carried out homogeneously in DMF, and the polymers were prepared in high yields (Scheme 10.1). The nucleobase concentration in the random copolymer was obtained from the ratio of ^{1}H NMR resonances integration at 2.8 ppm and 4.5 ppm (Figure 10.1). Table 1 lists the monomer feed ratios and the corresponding terpolymer compositions. Due to the similar reactivities of *n*BA and acrylic nucleobase monomers, the copolymer composition matched the feed ratio very well.

To understand the association of nucleobase pairs, we studied the thermal and dynamic mechanical properties of adenine- and thymine-functionalized poly*n*BA and their hydrogen bonding complex. DSC curves of acrylic adenine- and thymine-containing copolymers all showed a single T_g, suggesting a random copolymerization of *n*-butyl acrylate and acrylic nucleobase monomers. T_g's positively deviated from the Fox equation. Such deviation was attributed to the incorporation of strongly associating nucleobase units.

Scheme 10.1. Synthesis of adenine- and thymine-containing terpolymers

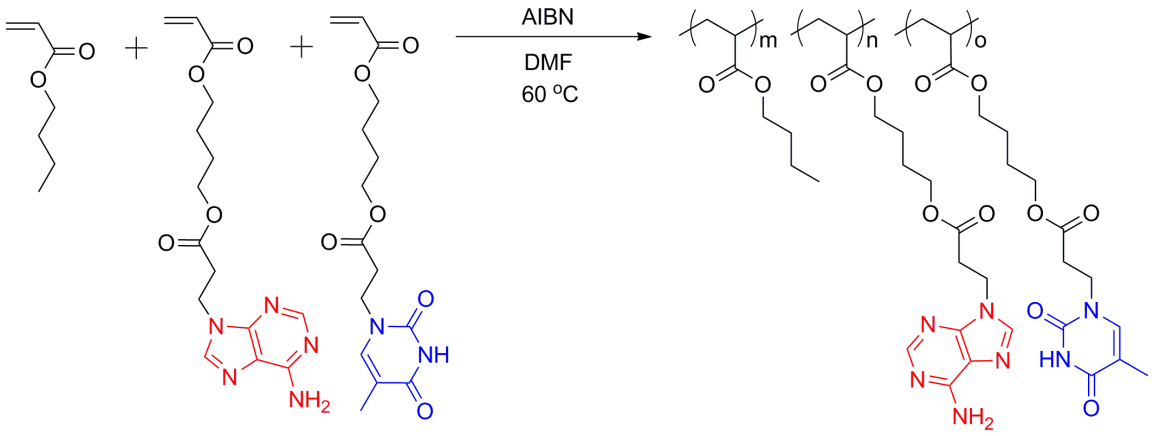

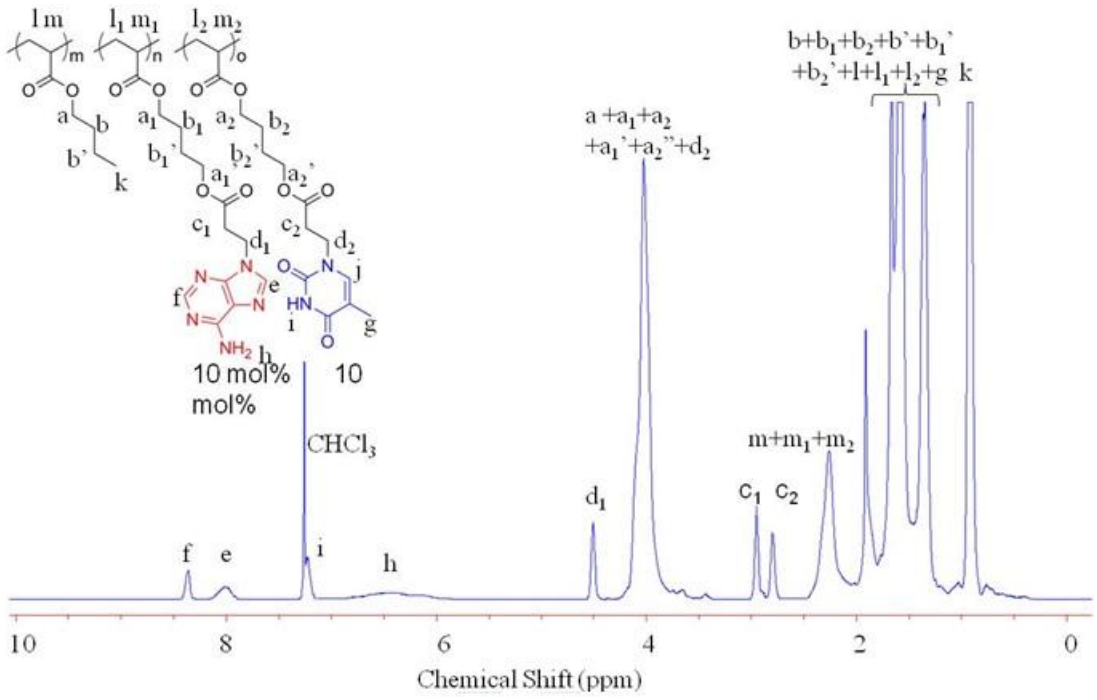

Figure 10.1. ^{1}H NMR spectra of adenine- and thymine-containing terpolymer

Table 10.1 Molecular characterization of adenine- and thymine-containing poly(*n*-butyl acrylate) random terpolymers

[nBA]:[Adenine]:[Thymine] in feed	[Adenine]:[Thymine] in polymer	Yield	T_g (^{o}C)	Fox T_g (^{o}C)
90:5:5	90:5:5	65%	-23	-34
80:5:15	80:5:15	67%	-8	-21
80:10:10	80:10:10	76%	-6	-16
80:15:5	80:15:5	64%	-1	-11

Nucleobase-containing terpolymers exhibited weak microphase separation with a broad SAXS peak present above 1 nm^{-1}. Recalling the SAXS profiles of adenine-

containing random copolymers with 16 mol% of adenine, a distinct peak with high relative intensity exhibited below 1 nm^{-1}. In the terpolymers, the peak shifted to high *q* region and the peak intensity decreased significantly, suggesting enhanced phase miscibility.

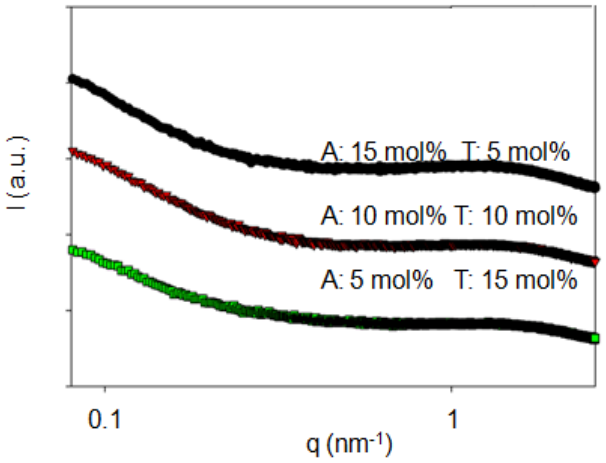

Figure 10.2. SAXS profiles of acrylic adenine- and thymine-containing terpolymers

The introduction of nucleobases through regioselective substitution is crucial due to the presence of more than one nucleophillic sites on respective nucleobases. The base-catalyzed Michael addition is thermodynamically controlled, which affords *N*1-substitubted thymine and *N*9-substituted adenine as the major products.[4] However, reaction of cytosine and guanine is less documented.[5-6] In this study, acrylic cytosine monomer was successfully synthesized through Michael addition with decent yields.

Scheme 10.2 Synthesis of acrylic cytosine monomer

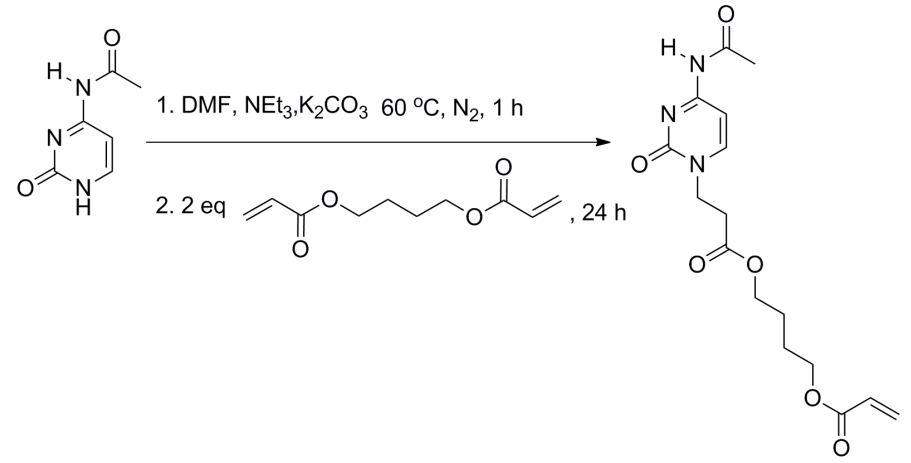

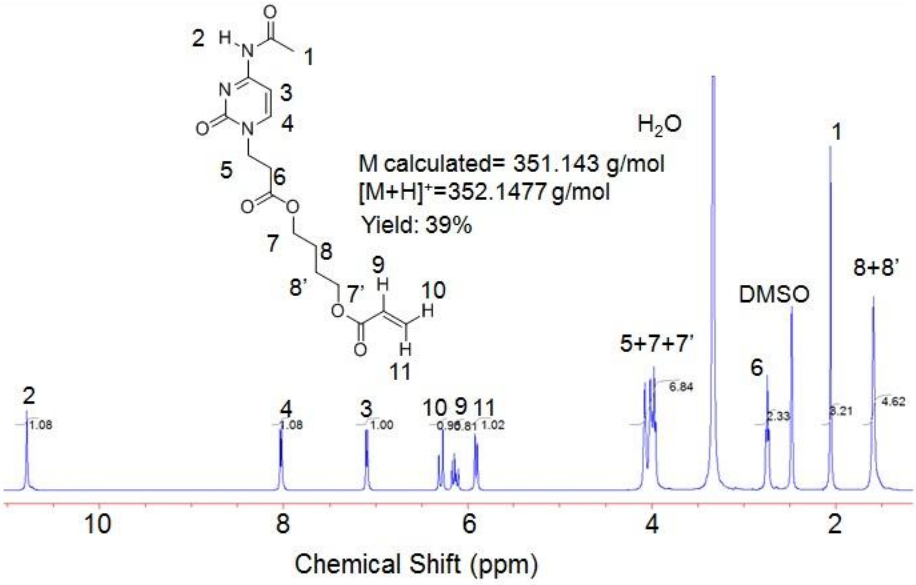

Figure 10.3. ^{1}H NMR spectra of acrylic cytosine-containing monomer

10.1.5 Conclusions

Adenine- and thymine-containing polyacrylate terpolymers were synthesized through conventional free radical terpolymerization. Glass transition temperatures of the nucleobase-containing terpolymers positively deviated from the Fox equation, indicating strong intermolecular/intramolecular hydrogen bonding interactions. SAXS profiles of

the terpolymers exhibited weak microphase separation with d-spacings lower than the hydrogen bonding complex of adenine- and thymine-containing random copolymers. The lowered d-spacings suggested enhanced phase miscibility due to intramolecular hydrogen bonding of adenine-thymine base pairs. In addition, novel acrylic cytosine-containing monomer was successfully synthesized through *aza*-Michael addition. Cytosine-guanine base pairs with higher association constant would potentially provide polymers with increased binding affinity.

10.1.6 Future Work

The next steps in this study are to compare the melt rheology of the terpolymers and the blends at higher temperatures to attempt to observe the dissociation of the hydrogen bonding groups and measure the flow activation energy. Secondly, to synthesize well-defined polymers with narrow molecular weight distribution and controlled molecular weight using controlled radical polymerization to determine the molecular weight influence on hydrogen bonding association.

10.1.7 Acknowledgements

The authors acknowledge the financial support of the Petroleum Research Fund (ACS-PRF 35190-AC7), which is administered by the American Chemical Society. We also acknowledge funding from NSF (CHE-0722638) for the acquisition of our Agilent 6220 LC-TOF-MS. This material is partially based upon work supported by the National Science Foundation under Grant No. DMR-0923107.

10.1.8 References

1. Stadler, R.; Freitas, L. D. *Polym. Bull.* 1986, 15, 173-179.

2. Stadler, R.; Freitas, L. D. *Colloid Polym. Sci.* 1988, 266, 1102-1109.

3. Feldman, K. E.; Kade, M. J.; Meijer, E. W.; Hawker, C. J.; Kramer, E. J. *Macromolecules* 2010, 43, (7), 3576.
4. Lira, E. P.; Huffman, C. W. *J. Org. Chem.* 1966, 31, (7), 2188-2191.
5. Sivakova, S.; Rowan, S. J. *Chem. Soc. Rev.* 2005, 34, (1), 9-21.
6. Spijker, H. J.; van Delft, F. L.; van Hest, J. C. M. *Macromolecules* 2007, 40, (1), 12-18.

10.2 Synthesis and Characterization of Nucleobase-Containing Covalently Crosslinked Networks

As shown in chapter six, the long alkyl spacers afforded structural flexibility for complementary hydrogen bonding formation. The adenine- and thymine-containing acrylic random copolymer exhibited strong temperature dependence on melt viscosity. However, the average distance between hydrogen bonding motifs significantly influenced the relaxation time scale. Covalently crosslinked networks would act as hydrogen bonding scaffolds with lower average distance between recognition units. Additionally, the elastomers containing both covalent and hydrogen bonding crosslinks would store elastic energy on multiple time-scales, giving rise to shape-memory and self-healing properties.

10.3 Synthesis of Complementary Hydrogen Bonding Ionic Liquids

Anion exchange reaction was performed on styrenic phosphonium ionic liquid monomers described in chapter three. Phosphonium ionic liquid monomers bearing large counterions exhibited lowered melting points and enhanced degradation temperatures as

shown in chapter six. Although WAXD and DMA evidenced polymer inhomogeneity and the association of phosphonium cations, polymerization of ILs constrained cationic or anionic centers in repeat units and sacrificed ionic conductivity to some extent in comparison to ILs where both cations and anions are mobile. Recent efforts on overcoming this drawback include incorporating flexible spacers in the monomers between the polymerizable site and ionic functionalities and/or anion-exchange reactions directly on the polymer to enhance counterion mobility. The utilization of molecular recognition to reversibly and selectively attach ionic liquids to targeted polymer backbones would be a promising alternative. The synthesis of uracil phosphonium guest molecules was described in chapter 8. The adenine-uracil pair association constant was found to be independent of the presence of phosphonium cations. In addition, counterion exchange reaction reduced the melting point of phosphonium salts. A series of ionic liquids bearing recognition units (adenine, thymine, cytosine, and guanine) could be synthesized in a similar fashion. A detailed investigation on the structure-property relationship of supramolecular gels swollen with complementary hydrogen bonding ionic liquids would relate their rheological property and conductivity to the thermodynamics of hydrogen bonds.